The Electron–Phonon Interaction in Metals

Nicolas Bock

October 27, 2003

Advisor: Dermot Coffey

A Dissertation submitted to the Faculty of the Graduate School of the State University of New York at Buffalo in partial Fulfillment of the Requirements for the Degree of

Doctor of Philosophy

Department of Physics

Acknowledgments

First and foremost, I would like to thank my thesis advisor, Dr. Dermot Coffey, for his guidance and patience throughout my time as his Ph.D. student. This thesis would not have been possible without him. I would also like to thank Dr. Y. C. Lee, Dr. Francis Gasparini, and Dr. Hong Luo for being on my thesis committee.

I would like to thank Christian Meining, Jungsoo Kim, Mark Kimball, Jens Knöll, and Andrea Fink for their friendship and support while I was working on this thesis.

Finally, I would like to thank Jasmina Demirović and my parents for their never ending love and support.

Abstract

In this thesis we investigate the electron–phonon interaction in metals in the superconducting and normal states. A transformed Hamiltonian is derived in the superconducting state which involves realistic electron and phonon spectra obtained from previously published experimental data on de Haas–van Alphen and neutron scattering experiments. In contrast to previous analyses in which the electronic structure of lead was approximated by a free–electron sphere, the full two–band nature of lead is taken into account in our transformed Hamiltonian. A gap equation is derived and solved numerically on the two bands using previous results by Farnworth and Timusk (Farnworth and Timusk, 1974, 1976) who found the superconducting energy gap to be 1.286 meV and 1.379 meV on the two bands. The quasiparticle self–energy and spectral density function are calculated and comparison with recent ARPES data on lead is made. We find no evidence of α^2F features in our results contrary to claims by Chainani *et al.* (2000).

Using a memory function method we derive expressions for the optical conductivity in the superconducting state and compare with data from Farnworth and Timusk (Farnworth and Timusk, 1976). The two band model we employ results in good agreement with their data, improving on previous theoretical studies by Allen and coworkers (Allen, 1971) who neglected the details of the Fermi surface and approximated it by a free electron sphere.

In the last part we study the normal state and effects of the electron–phonon interaction on thermodynamic properties of sodium at temperatures > 100 K. We find that the leading temperature dependence of the contribution for the interaction between the electronic and lattice degrees of freedom in the entropy goes as T and is different from what previous authors found. Contact is made between our electron–phonon approach which starts out from low temperatures with an electron–ion approach starting from high temperatures (Zwanzig, 1957).

Contents

List of Figures

List of Tables

Chapter 1

Introduction

Many body effects in condensed matter have been one of the active areas of research for many years. Phenomena due to many body effects include superconductivity and magnetism in a wide range of materials and the quantum Hall effect in low dimensional electron/hole gases. These exotic states of matter are principally studied in terms of electronic degrees of freedom in materials. However the coupling of the electronic degrees of freedom to lattice degrees of freedom can play a crucial role. This coupling is usually described by interactions between the electronic excitations and lattice modes, the phonons.

Since the discovery of superconductivity in 1911 by Kammerlingh-Onnes (Kammerlingh-Onnes, 1911) many prominent physicists tried to explain this effect phenomenologically. Examples of early theories include the London two fluid model (London, 1948) for instance. Fröhlich suggested in 1950 (Fröhlich, 1950) that a phonon mediated effective interaction between the electrons is mainly responsible for superconductivity and independent experiments on the isotope effect by Reynolds et al. (Reynolds *et al.*, 1950) and Maxwell (Maxwell, 1950) confirmed this possibility in the same year. Through the Cooper instability of the Fermi surface, Bardeen, Cooper, and Schrieffer (Bardeen *et al.*, 1957a,b) were able in 1957 to derive a microscopic theory that incorporated an effective attractive interaction between electrons as the mechanism of superconductivity. Their simplified model, which captures all

of the qualitative features of the superconducting state, was extended further by Eliashberg with his strong coupling formalism (Eliashberg, 1960a,b). This formalism uses the machinery of field theory to include the details of the phonon spectrum and of the electron–phonon interaction. Later Schrieffer, Wilkins, and Scalapino (Schrieffer *et al.*, 1963) demonstrated how tunneling experiments could be analyzed to extract details of the phonon spectrum from current–voltage characteristics of tunneling junctions. This added further support to the idea that electron–phonon interactions are the mechanism for superconductivity.

Since then superconductivity and superfluidity has been found in many materials. With the discovery of high–T_c materials by Bednorz and Müller in 1986 (Müller and Bednorz, 1987) the field was revived with the possibility of critical temperatures beyond 100 K. The stubbornly low critical temperatures found until their discovery had lead to speculations about an upper limit ≈ 30 K on T_c because of the nature of the electron–phonon mechanism. Consequently there have been numerous proposals for a mechanism for superconductivity in high–temperature superconductors other than the electron–phonon interaction. Most frequently the proposed mechanisms has been magnetic where magnons play the role of phonons. Quantitative calculations of the superconducting properties of these and many other materials is some way off because of the complicated nature of the materials and the disparity between electronic energy scales the superconductivity energy scales.

However the more recent discovery of superconductivity in MgB_2 has lead to detailed models which incorporate both bandstructure and realistic phonon dispersions. These calculations lead to quantitative accurate descriptions of the connections between bandstructure and different superconducting gaps associated with different bands. In this thesis we take a more phenomenological approach to superconductivity in lead which incorporates details of both electronic bandstructure and the phonon spectrum.

The approach we take is somewhat different from the conventional Eliashberg approach which makes the inclusion of the details of bandstructure difficult. The conventional Eliashberg treatment was developed 40 years ago when resources for numerical computations were not up to including material properties to any great extent. In Eliashberg's treatment plau-

sible assumptions and approximations are made which lead to qualitatively correct results and which have provided a framework for investigations of superconductivity for many years. In the approach we adopt here, in which quasiparticle and transport properties are investigated in the superconducting state, it is feasible to investigate which aspects of a material's bandstructure are responsible for superconducting properties. In contrast, the Eliashberg treatment considers averages over states on the Fermi surface which ignores the topology of the Fermi surface. As we will show, the Fermi surface which is principally responsible for the so–called α^2F strong–coupling corrections in Pb is that of the third band which resembles scaffolding rather than a sphere.

In Chapter 2 we will outline in more detail how the crystal Hamiltonian is analyzed and derive an expression for the electron–phonon interaction Hamiltonian. In Chapter 3 we will examine the superconducting state of a two–band system, lead. To this end we will derive a transformed electron–phonon Hamiltonian in the BCS ground state and investigate the effects of quasi–particle interactions with the phonons. We will make contact with ARPES measurements on lead films and bulk lead samples and show how the electron–phonon interaction appears in these. In Chapter 4 we will analyze the phonon assisted contribution to the optical conductivity in superconducting lead samples using a memory function formalism.

The electron–phonon interaction also contributes to thermodynamic properties. In Chapter 5 we will consider the contribution to the entropy of metals at intermediate temperatures. At these temperatures, $\gtrsim$ 100 K, the ion motion is no longer degenerate and so it is possible to treat the lattice degrees of freedom classically as in molecular dynamics or Monte Carlo simulations. However the electrons are still degenerate since $kT \ll \epsilon_F$, and the contribution to the entropy can in principal be calculated either starting from the low temperatures electron–phonon limit or the high temperature electron–ion limit. Previous treatments based on the low temperature Eliashberg expression for the entropy have missed the largest contribution due to the electron–phonon interaction in this region. We calculate this contribution starting from the electron–phonon interaction and show how the principal

temperature dependences can be recovered starting from the electron–ion limit.

The calculations involved in the quantitative descriptions of superconductivity in lead are numerically intensive but provide quantitatively accurate accounts of the role of bandstructure and phonon in this material. This approach can be extended to other more complicated materials in time and may determine the role of different aspects of the high T_c materials in the superconductivity in these materials.

Chapter 2

The Electron–Phonon Interaction

A crystal is a complicated many–body system of electrons and ions whose properties are determined by the Coulomb interaction. Although it is possible to write down the exact Hamiltonian of the system, one can not find the exact solutions to it. Approximate solutions have to be sought and the question of how to formulate and divide up the Hamiltonian becomes very important. We will outline briefly in this Chapter how one can split the crystal Hamiltonian into an electronic part, a lattice part, and interaction terms.

When split in this way, the interaction term represents the interactions of the electrons and the quanta of the lattice vibrations, the phonons. The electron–phonon interaction is expanded in powers of the interaction which involves the single–ion potential of the electrons in the potential of the ions. In general this potential is complicated and involves detailed knowledge of the orbital states of the valence electrons which makes usage of these potentials cumbersome. An additional complication is the fact that the electron wavefunctions are Bloch wavefunctions in the periodic potential of the crystal. As a practical matter we have already assumed at this point that the Coulomb interaction among electrons has been taken care of and have ruled out treating strong correlation effects.

Over the last decades simplifying methods have been developed which make this problem more tractable. The *pseudopotential*–method tries to acomplish two things to this end.

Firstly, the exact single–ion potentials are replaced by simple functions of electron position. One usually distinguishes a core part from a long range part using a screened Coulomb type interaction for the long range part and a simple function for the core part. The true electron wave function is replaced in the formalism by a *pseudowavefunction* which leads to the second important simplification. The pseudowavefunctions are chosen in such a way that they are smooth outside the core and can be approximated well with few plane wave states. We will briefly introduce this important method in the second part of this chapter.

2.1 Derivation

In order to understand the electron–phonon interaction, we will look at the electronic and lattice excitations first. The total Hamiltonian of the crystal can be written as (Wallace, 1998)

$$\mathcal{H} = \mathrm{KE}_I + \mathrm{KE}_e + \Omega_I + \Omega_e + \Omega_{eI}. \tag{2.1.1}$$

The first two terms, KE_I and KE_e, describe the kinetic energy of the ions and the electrons, respectively. The two potential energies, Ω_I and Ω_e, represent the contribution from the interactions among the electrons and the ions, respectively. Finally, the potential energy Ω_{eI} denotes the energy gain of the crystal from interactions between electrons and ions. It should be noted that we will use the following assumptions in our description of the ions: The ions consist of the ion nuclei plus core electrons. We define core electrons as electrons that are sufficiently close to the nucleus such that the resulting "nucleus plus core electrons" associated with one ion do not significantly overlap those of neighboring ions. This allows us to treat the ions as point particles and their potentials as purely radial in nature, since we ignore local charge distribution effects and the orbital nature of the core electrons. We will also be able to write the total potential energy, Ω_I, as a simple sum of single ion potentials.

The total Hamiltonian eq. (2.1.1) will be split into two major parts, the electron and the lattice Hamiltonians. The electron spectrum can be calculated by considering the electronic part of the Hamiltonian,

$$\mathcal{H}_e = \mathrm{KE}_e + \Omega_{eI} + \Omega_e. \tag{2.1.2}$$

The solution to this Hamiltonian depends on the position of the electrons and the position of the ions. It is not obvious to see where one should start with this problem. An argument can be made that the correct way to break up the system into electron and phonon parts is by starting with calculating the phonon spectrum under the assumption that the electrons are unaffected by the lattice vibrations. With this assumption one therefore calculates the electron spectrum first, with the ions in their equilibrium positions. Then the phonon spectrum is calculated with the electrons being in the states calculated in the first step. Lastly, one calculates the corrections to the electronic energies due to the motion of the ions. This is the adiabatic approximation (Born and Huang, 1954).

The justification for the adiabatic approximation is based on the fact that the characteristic phonon energies are much smaller than the characteristic electron energies. The former are of order $\hbar\omega_D$, the Debye frequency, and the latter of the order of ϵ_F, the Fermi energy. Since $\hbar\omega_D \ll \epsilon_F$, only the electron states within the Debye energy around the Fermi surface are affected by the phonons. This is only a small fraction of the total electrons. The effect of the electrons on the phonons however is given by all of the electrons and not just the ones close to the Fermi surface, which means that the few electrons that are affected by the phonons will not cause a major effect to the phonon states. Another way of expression this result is by considering the electron versus the ion masses. Since $\frac{m}{M} \approx \frac{1}{2000}$, where m denotes the electron mass and M the ion mass, the electron distribution instantaneously adjusts to changes in the ion configuration on the time scale of the ion motion. This implies that the adiabatic approximation is good even in the case of systems with very low electron

densities and therefore very small Fermi energies.

In a first pass, we will consider the ions in their equilibrium positions and try to find the electronic states. The Hamiltonian therefore becomes dependent on the ion positions and independent of their motion. We replace the two potential energies in $\mathcal{H}_e$ with self consistent fields that are the same for each electron. This approximation neglects electron–electron interactions beyond the mean field. This allows us to rewrite the Hamiltonian in eq. (2.1.2) as a sum of single electron Hamiltonians,

$$\mathcal{H}_e = \sum_\alpha h(\vec{r}_\alpha) = \sum_\alpha \left\{ \mathrm{ke}_\alpha + \Omega_e(\vec{r}_\alpha) \right\}, \tag{2.1.3}$$

where α enumerates the electrons. Depending on the level of approximation, the potential energy, $\Omega_e(\vec{r}_\alpha)$, will be replaced with combinations of a bare potential and a screening potential (Hartree approximation), and an exchange potential (Hartree–Fock approximation). Electron–electron interaction beyond the particular approximation chosen involve correlation effects and may have to be added at a later stage. The eigenfunctions of the Hamiltonian are the electron wave functions and the electronic energies giving rise to the band structure of the metal.

The remaining terms of the crystal Hamiltonian of eq. (2.1.1) will give us the phonon spectrum. We extract the ionic part from eq. (2.1.1) and get

$$\mathcal{H}_I = \mathrm{KE}_I + \Omega_I + E_G, \tag{2.1.4}$$

where E_G denotes the ground state energy of the electrons. This energy depends on the exact distribution of the ions among which there are the long–range Coulomb interactions which are screened by the electrons. This screening is due to the difference in rapidity in response between the electrons and ions and is the basis for the adiabatic approximation.

In the adiabatic approximation, we assume that the ion motion is slow compared to the electronic system such that the electrons have enough time to relax into their ground state as the ions are moving. The ion Hamiltonian therefore is a function of the ion positions only and does not depend on the electron positions. This procedure requires one to calculate the electronic ground state for any distribution of ions. This is intractable in practice and one usually only calculates the ground state energy with the ions in their equilibrium positions assuming that the electron energies do not change much due to the motion of the ions (Corrections are of order $\mathcal{O}\left(\frac{m}{M}\right)$ and higher).

The lattice Hamiltonian can be written as

$$\mathcal{H}_I = \mathrm{KE}_I + \Omega, \tag{2.1.5}$$

with $\Omega = \Omega_I + E_G$. Conventionally the potential energy Ω is expanded in powers of the ionic displacements. The linear term vanishes since there is no net force on the ions. In the harmonic approximation, only the second order term is kept. Higher order terms will give rise to anharmonic effects in the phonon spectrum and can be included later in form of phonon–phonon interactions, $\mathcal{H}_{pp}$. For low temperatures one expects the lattice vibrations to be small and the harmonic term to be a good approximation to the vibrations. This point of view can break down however at higher temperatures, in crystals with light atoms, solid hydrogen for example, or in polaronic materials due to the very strong electron–latice interactions in these materials, e.g. Table 6.2, Mahan (1990). We are concerned with more generic cases however. We therefore get

$$\mathcal{H}_I = \mathrm{KE}_I + \Omega_0 + \Omega_2. \tag{2.1.6}$$

A Fourier transformation leads to the well known problem of diagonalizing the dynamical matrix. One finds the usual normal modes, which we can write as

$$\vec{U}_{N\nu} = \sum_{\vec{q}\lambda} \sqrt{\frac{\hbar^2}{2N_0 M_\nu \hbar\omega_{\vec{q}\lambda}}} \left(a_{\vec{q}\lambda} + a^\dagger_{-\vec{q}\lambda}\right) e^{i\vec{q}\cdot\vec{R}^0_{N\nu}} \hat{\eta}_{\nu,\vec{q}\lambda}. \tag{2.1.7}$$

In writing eq. (2.1.7) we have split the crystal into N_0 unit cells with a basis, ν numbering the ions within the basis. The position of the ν^{th} ion in the N^{th} cell is given by

$$\vec{R}_{N\nu} = \vec{R}^0_{N\nu} + \vec{U}_{N\nu}, \tag{2.1.8}$$

i.e. the sum of the equilibrium position, $\vec{R}^0$, and the shift from this position, $\vec{U}_{N\nu}$. The sum in eq. (2.1.7) is over the first Brillouin zone. The phonon modes are labelled λ. There are 3ν modes in general. The mass of an ion of type ν is denoted by M_ν, and the frequency of a phonon mode of wave vector $\vec{q}$ and mode λ by $\omega_{\vec{q}\lambda}$. The polarization unit vector is given by $\hat{\eta}_{\nu,\vec{q}\lambda}$, and the phonon creation and annihilation operators by $a_{\vec{q}\lambda}$, and $a^\dagger_{\vec{q}\lambda}$.

So far we discussed the electron states when the ions are in their equilibrium positions and the phonon energies with the electrons always being in their ground state. We now want to consider the interactions between the electrons and the ions which are not included yet into our previous discussion. We turn our attention again to eq. (2.1.1) and reorganize terms. The phonon part was given by

$$\mathcal{H}_I = \text{KE}_I + \Omega_I + E_G = \Phi_0 + \mathcal{H}_p + \mathcal{H}_{pp}. \tag{2.1.9}$$

Φ_0 is the energy of the crystal with its ions in their equilibrium positions and not moving, $\mathcal{H}_p$ is the energy due to lattice vibrations, the phonons, and $\mathcal{H}_{pp}$ as mentioned above. The crystal Hamiltonian therefore can be written as

$$\mathcal{H} = \mathcal{H}_I + \mathcal{H}_e - E_G = \Phi_0 + \mathcal{H}_p + \mathcal{H}_e + \mathcal{H}_{pp} + \mathcal{H}_{ep}, \tag{2.1.10}$$

and it is $\mathcal{H}_{ep}$ which we are interested in. In the ground state, the electrons are within the filled Fermi sea and their distribution is given by a Heaviside function, $\theta(-\epsilon_\alpha + \epsilon_F) = g_\alpha$, a consequence of the one–electron approximation, and we can write

$$\mathcal{H}_e + \mathcal{H}_{ep} - E_G = \sum_\alpha h(\vec{r}_\alpha) - \sum_\alpha g_\alpha \epsilon_\alpha. \tag{2.1.11}$$

As in the case of the ion Hamiltonian, the electronic part will be expanded in powers of the ion displacement from their equilibrium positions. We will only be interested in low orders. The single electron Hamiltonians, $h(\vec{r}_\alpha)$, are given by

$$h(\vec{r}_\alpha) = -\frac{\hbar^2 \nabla_\alpha^2}{2m} + \Omega_e(\vec{r}_\alpha). \tag{2.1.12}$$

Since we assumed that the ions do not overlap and have a potential that is radial, we can write

$$\Omega_e(\vec{r}) = \sum_{N\nu} u(\vec{r} - \vec{R}_{N\nu}) = \sum_{N\nu} u(\left|\vec{r} - \vec{R}^0_{N\nu} - \vec{U}_{N\nu}\right|). \tag{2.1.13}$$

In order to make calculations with the single–ion potential, $u(\vec{r})$, tractable one uses simple models for them. One particularly successful approach is the pseudopotential method, which comes out of the orthogonalized plane wave method, described in more detail later in this chapter. Generally these models distinguish between a "core" part and a region

outside the core. In this method it is assumed that the core part is of very simple form and that the region outside the core can be described by a function which behaves like the Coulomb potential for large distances. These potentials are screened by the Lindhard function (Lindhard, 1954).

We are assuming that the displacement vectors, $\vec{U}$, from the ion's equilibrium position is small, the above expression can be expanded in powers of this displacement.

$$\begin{aligned}\Omega_e(\vec{r}) &= \sum_{N\nu}\left\{u(\vec{r}-\vec{R}^0_{N\nu})+\sum_{i=1}^{3}U^i_{N\nu}\left.\frac{\partial u(\vec{r}-\vec{R}^0_{N\nu}-\vec{U}_{N\nu})}{\partial U^i_{N\nu}}\right|_{\vec{U}_{N\nu}=0}\right.\\ &\left.+\frac{1}{2}\sum_{ij=1}^{3}U^i_{N\nu}U^j_{N\nu}\left.\frac{\partial^2 u(\vec{r}-\vec{R}^0_{N\nu}-\vec{U}_{N\nu})}{\partial U^i_{N\nu}\partial U^j_{N\nu}}\right|_{\vec{U}_{N\nu}=0}+\cdots\right\}.\end{aligned} \tag{2.1.14}$$

The zeroth order term in $\vec{U}_{N\nu}$ is given by

$$\mathcal{H}^{(0)}_{ep}=\sum_{\kappa\vec{Q}}V(\vec{Q})\,c^{\dagger}_{\kappa+\vec{Q}\sigma}c_{\kappa\sigma}, \tag{2.1.15}$$

where we have written the Hamiltonian in the second quantization formalism (e.g. Chapter 6, Feynman, 1972) with the electron creation and annihilation operators, $c^{\dagger}_{\kappa}$, and c_{κ}, respectively. The subscript κ collectively stands for the whole set of quantum numbers needed for the particular problem at hand, not just the electron momentum, $\vec{k}$, but also the electron spin, σ, and a band index, n. The Fourier transform of the single–ion potential is given by,

$$V(\vec{q})=\frac{1}{V_A}\int d^3x\; e^{i\vec{q}\cdot\vec{x}}\;u(\vec{x}), \tag{2.1.16}$$

and V_A is the volume per atom. This term combined with the kinetic energy term will give us the electronic excitations,

$$\mathcal{H}_e = \sum_{\kappa} \frac{\hbar^2 k^2}{2m} c_\kappa^\dagger c_\kappa + \sum_{\kappa\vec{Q}} V(\vec{Q})\, c^\dagger_{\kappa+\vec{Q}\sigma} c_{\kappa\sigma}, \tag{2.1.17}$$

The next order term is given by

$$\mathcal{H}_{ep}^{(1)} = \sum_{\alpha} \sum_{N\nu} \vec{U}_{N\nu} \cdot \vec{\nabla}_{N\nu}\; u(\vec{r}_\alpha - \vec{R}^0_{N\nu} - \vec{U}_{N\nu})\Big|_{\vec{U}_{N\nu}=0}. \tag{2.1.18}$$

In second quantization, this becomes

$$\mathcal{H}_{ep}^{(1)} = \sum_{N\nu} \sum_{\kappa_1\kappa_2} \int d^3r\;\; \langle\kappa_1|\, \vec{U}_{N\nu} \cdot \vec{\nabla}_{N\nu}\; u(\vec{r} - \vec{R}^0_{N\nu} - \vec{U}_{N\nu})\Big|_{\vec{U}_{N\nu}=0} |\vec{r}\rangle\, \langle\vec{r}|\kappa_2\rangle\, c^\dagger_{\kappa_1} c_{\kappa_2}, \tag{2.1.19}$$

where the states κ form a complete set and are assumed to satisfy the Bloch theorem. This means that we can write

$$\langle\vec{r}|\kappa\rangle = \Theta_\kappa(\vec{r}) e^{i\vec{k}\cdot\vec{r}}, \tag{2.1.20}$$

where $\Theta_\kappa(\vec{r}+\vec{R}_{N\nu}) = \Theta_\kappa(\vec{r})$, are periodic in the lattice. Without changing the integrand we can change the variable of the derivative of the pseudopotential to a derivative with respect to $\vec{r}$. The slightly rewritten Hamiltonian then reads

$$\mathcal{H}_{ep}^{(1)} = -\sum_{N\nu} \sum_{\kappa_1\kappa_2} \int d^3r\; \Theta^*_{\kappa_1}(\vec{r}) e^{-i\vec{k}_1\cdot\vec{r}}\; \vec{U}_{N\nu} \cdot \vec{\nabla}_{\vec{r}}\; u(\vec{r} - \vec{R}^0_{N\nu} - \vec{U}_{N\nu})\Big|_{\vec{U}_{N\nu}=0} \Theta_{\kappa_2}(\vec{r}) e^{i\vec{k}_2\cdot\vec{r}}\; c^\dagger_{\kappa_1} c_{\kappa_2}. \tag{2.1.21}$$

We use the definition of the normal modes, eq. (2.1.7), to write

$$\begin{aligned}\mathcal{H}_{ep}^{(1)} &= -\sum_{N\nu}\sum_{\kappa_1\kappa_2}\sum_{\vec{q}\lambda}\int d^3r\,\sqrt{\frac{\hbar^2}{2N_0\,M_\nu\,\hbar\omega_{\vec{q}\lambda}}}\left(a_{\vec{q}\lambda}+a^\dagger_{-\vec{q}\lambda}\right)\\ &\qquad\times e^{i\vec{q}\cdot\vec{R}^0_{N\nu}}\;\Theta^*_{\kappa_1}(\vec{r})e^{-i\vec{k}_1\cdot\vec{r}}\;\hat{\eta}_{\nu,\vec{q}\lambda}\cdot\vec{\nabla}_{\vec{r}}\;u(\vec{r}-\vec{R}^0_{N\nu})\;\Theta_{\kappa_2}e^{i\vec{k}_2\cdot\vec{r}}\;c^\dagger_{\kappa_1}c_{\kappa_2}.\end{aligned}\tag{2.1.22}$$

Since the integration is over all space, we can shift its origin without changing the result. We will therefore use a variable transformation and write for $\vec{x}=\vec{r}-\vec{R}^0_{N\nu}$.

$$\begin{aligned}\mathcal{H}_{ep}^{(1)} &= -\sum_{N\nu}\sum_{\kappa_1\kappa_2}\sum_{\vec{q}\lambda}\sqrt{\frac{\hbar^2}{2N_0\,M_\nu\,\hbar\omega_{\vec{q}\lambda}}}\left(a_{\vec{q}\lambda}+a^\dagger_{-\vec{q}\lambda}\right)\;c^\dagger_{\kappa_1}c_{\kappa_2}\;e^{i\vec{q}\cdot\vec{R}_{N\nu}}\\ &\qquad\times\int d^3x\;\Theta^*_{\kappa_1}(\vec{x})\Theta_{\kappa_2}(\vec{x})e^{i(\vec{k}_2-\vec{k}_1)\cdot\vec{x}}\;\hat{\eta}_{\nu,\vec{q}\lambda}\cdot\vec{\nabla}_{\vec{x}}\;u(\vec{x})\;e^{i(\vec{k}_2-\vec{k}_1)\cdot\vec{R}^0_{N\nu}},\end{aligned}\tag{2.1.23}$$

The sum over ions in the lattice can be transformed into a δ–function,[2.1]

$$\begin{aligned}\mathcal{H}_{ep}^{(1)} &= -\sum_{\kappa_1\kappa_2}\sum_{\vec{q}\lambda}\sqrt{\frac{\hbar^2}{2N_0\,M_\nu\,\hbar\omega_{\vec{q}\lambda}}}\left(a_{\vec{q}\lambda}+a^\dagger_{-\vec{q}\lambda}\right)\;c^\dagger_{\kappa_1}c_{\kappa_2}\;N_0\,\delta_{\vec{q}+\vec{k}_2-\vec{k}_1,\vec{Q}}\\ &\qquad\times\int d^3x\;\Theta^*_{\kappa_1}(\vec{x})\Theta_{\kappa_2}(\vec{x})e^{i(\vec{k}_2-\vec{k}_1)\vec{x}}\;\hat{\eta}_{\nu,\vec{q}\lambda}\cdot\vec{\nabla}_{\vec{r}}\;u(\vec{x}).\end{aligned}\tag{2.1.24}$$

The electron–phonon interaction Hamiltonian in first order is given by

$$\begin{aligned}\mathcal{H}_{ep}^{(1)} &= -\sum_{\kappa}\sum_{\vec{q}\vec{Q}\lambda}\sqrt{\frac{\hbar^2}{2N_0\,M_\nu\,\hbar\omega_{\vec{q}\lambda}}}\left(a_{\vec{q}\lambda}+a^\dagger_{-\vec{q}\lambda}\right)\;c^\dagger_{\kappa+\vec{q}+\vec{Q}}c_{\kappa}\\ &\qquad\times N_0\int d^3x\;\Theta^*_{\kappa+\vec{q}+\vec{Q}}(\vec{x})\Theta_{\kappa}(\vec{x})e^{i(\vec{q}+\vec{Q})\vec{x}}\;\hat{\eta}_{\nu,\vec{q}\lambda}\cdot\vec{\nabla}_{\vec{r}}\;u(\vec{x}),\end{aligned}\tag{2.1.25}$$

[2.1] For a crystal one can define $\sum_{N\nu}e^{i\vec{q}\cdot\vec{R}^0_{N\nu}}=N_0\,\delta_{\vec{q},\vec{Q}}$. $\vec{Q}$ is a reciprocal lattice vector including $\vec{Q}=0$.

Introducing the short–hand notation, $g(\vec{q},\vec{Q},\lambda)$, for the electron–phonon interaction matrix elements, the Hamiltonian is given by

$$\mathcal{H}_{ep}^{(1)} = \sum_{\kappa}\sum_{\vec{q}\vec{Q}\lambda} g(\vec{q},\vec{Q},\lambda)\left(a_{\vec{q}\lambda} + a^{\dagger}_{-\vec{q}\lambda}\right)\; c^{\dagger}_{\kappa+\vec{q}+\vec{Q}} c_{\kappa}, \tag{2.1.26}$$

where

$$g(\vec{q},\vec{Q},\lambda) = -\sqrt{\frac{\hbar^2}{2N_0\, M_\nu\, \hbar\omega_{\vec{q}\lambda}}}\; N_0 \int d^3x\; \Theta^{*}_{\kappa+\vec{q}+\vec{Q}}(\vec{x})\,\Theta_{\kappa}(\vec{x})\, e^{i(\vec{q}+\vec{Q})\cdot\vec{x}}\; \hat{\eta}_{\nu,\vec{q}\lambda}\cdot\vec{\nabla}_{\vec{r}}\; u(\vec{x}). \tag{2.1.27}$$

In the case of plane waves for the electronic states, the periodic part of the Bloch functions, $\Theta_{\kappa}(\vec{x}) \propto e^{i\vec{k}\cdot\vec{r}}$, is set to a constant, $1/\sqrt{V}$, where V is the volume of the crystal, the matrix elements can be calculated. Integration by parts leads to

$$g(\vec{q},\vec{Q},\lambda) = -i\sqrt{\frac{\hbar^2}{2N_0\, M_\nu\, \hbar\omega_{\vec{q}\lambda}}}\; \hat{\eta}_{\nu,\vec{q}\lambda}\cdot\left(\vec{q}+\vec{Q}\right) V(\vec{q}+\vec{Q}). \tag{2.1.28}$$

The second order electron–phonon Hamiltonian can be derived in a very similar fashion, and we will only state the final result here.

$$\mathcal{H}_{ep}^{(2)} = \frac{1}{2}\sum_{\kappa}\sum_{\vec{q}\vec{q}'\vec{Q}}\sum_{\lambda\lambda'} h(\vec{q},\vec{q}',\vec{Q},\lambda,\lambda')\left(a_{\vec{q}\lambda} + a^{\dagger}_{\vec{q}\lambda}\right)\left(a_{\vec{q}'\lambda'} + a^{\dagger}_{\vec{q}'\lambda'}\right)\; c^{\dagger}_{\kappa+\vec{q}+\vec{q}'+\vec{Q}} c_{\kappa}, \tag{2.1.29}$$

where

$$h(\vec{q},\vec{q}',\vec{Q},\lambda,\lambda') = -\frac{\hbar^2}{2N_0\,M_\nu\sqrt{\hbar\omega_{\vec{q}\lambda}\,\hbar\omega_{\vec{q}'\lambda'}}}\sum_{ij}\eta^i_{\nu,\vec{q}\lambda}\eta^j_{\nu,\vec{q}'\lambda'} \times N_0\int d^3x\;\Theta^*_{\kappa+\vec{q}+\vec{q}'+\vec{Q}}(\vec{x})\,\Theta_\kappa(\vec{x})\,e^{i(\vec{q}+\vec{q}'+\vec{Q})\vec{x}}\;\frac{\partial^2 u(\vec{r})}{\partial r_i\,\partial r_j}. \tag{2.1.30}$$

With a plane wave basis for the electronic states, the above expression can be further simplified and one finds

$$h(\vec{q},\vec{q}',\vec{Q},\lambda,\lambda') = -\frac{\hbar^2\left[\hat{\eta}_{\nu,\vec{q}\lambda}\cdot\left(\vec{q}+\vec{q}'+\vec{Q}\right)\right]\left[\hat{\eta}_{\nu,\vec{q}'\lambda'}\cdot\left(\vec{q}+\vec{q}'+\vec{Q}\right)\right]}{2N_0\,M_\nu\sqrt{\hbar\omega_{\vec{q}\lambda}\,\hbar\omega_{\vec{q}'\lambda'}}}V(\vec{q}+\vec{q}'+\vec{Q}). \tag{2.1.31}$$

As mentioned before, models are needed for the single–ion potentials used in the electron–phonon matrix elements. We are going to describe now how to derive models for the electron–phonon interaction using the pseudopotentials and orthogonalized plane waves.

2.2 The Orthogonalized Plane Wave Method (OPW)

2.2.1 Introduction

The orthogonalized plane wave method (OPW) is based on the assumption that one can completely separate the core states from the conduction–band states. The core states are considered localized and adjacent cores do not overlap. It is further assumed that the large positive kinetic energy associated with the strong oscillations of the wave function of the valence electrons in the core region cancels large parts of the strong negative core potential (Herring, 1940; Phillips and Kleinman, 1959). These assumptions lead to the replacement of the core potential with a "Pseudopotential", which is the sum of the core potential with the kinetic energy of the conduction–band wave function. Furthermore, since the

introduction of the pseudopotential eliminates the need for a strongly oscillating valence–band wave function in the core region, the conduction–band wave functions can now be expanded in terms of plane wave states which are orthogonal to the core states, simplifying the calculating of eigenvalues and eigenstates of the crystal Hamiltonian. OPW therefore offers a nice explanation as to why the plane wave approximation is so successful in so many metals such as the alkali and polyvalent metals. The method was used by a number of workers with great success, to name only a few, Harrison (Harrison, 1960) calculated the band structure of Aluminum and Anderson and Gold (Anderson and Gold, 1965) the band structure of Lead.

2.2.2 Derivation

In order to approximate the valence–band electron wave functions, one could imagine an approach in which these are expanded in a basis that consists of ordinary plane waves, and then only retain the first few terms of such an expansion. This expansion suffers from the fundamental problem that one needs a large number of terms, since the valence–band wave functions oscillate strongly around the core region. Herring (Herring, 1940) pointed out that the convergence behavior of this kind of expansion could be improved upon if one were to use basis functions that are orthogonalized to the core states.

In particular it was noted by Phillips and Kleinman (Phillips and Kleinman, 1959) that there will be strong cancellations between the large contributions from the core potential and the large kinetic energies associated with rapid oscillations of the orthogonalized plane wave states. This means that one can use plane wave states in the expansion and move the remaining difference into a "pseudopotential" that perturbs the wave functions.

Following Phillips and Kleinman (Phillips and Kleinman, 1959) (see also Jones (Jones, 1975), Harrison (Harrison, 1966), and Tinkham (Tinkham, 1964) for further reference) let $\left|\psi_{\vec{k}}\right\rangle$ denote a conduction–band electron and $|\psi_\alpha\rangle$ a core electron wave function, remembering that it was assumed that one could separate the electronic wave function of the

crystal in this fashion. We will make the approximation of a self–consistent field, i.e. we will assume that the total Hamiltonian of the crystal electrons can be split into a sum of single–electron Hamiltonians, where each electron is in a self–consistently calculated field created by all the ions and the other electrons, ignoring correlations between the electrons beyond this mean–field approximation. The Schrödinger equation for both wave functions can then be written as

$$\{\mathrm{KE} + \Omega(\vec{r})\} \left|\psi_{\vec{k}}\right\rangle = \epsilon_{\vec{k}} \left|\psi_{\vec{k}}\right\rangle \tag{2.2.1}$$

$$\{\mathrm{KE} + \Omega(\vec{r})\} \left|\psi_{\alpha}\right\rangle = \epsilon_{\alpha} \left|\psi_{\alpha}\right\rangle . \tag{2.2.2}$$

In order to solve these two equations, one could expand out the wave functions in terms of some known set of functions which would lead to a set of coupled equations, one for each expansion term, and the problem is then transformed into the problem of diagonalizing a matrix in a reduced basis. If one chooses a set of states that resembles the true wave function well already in low orders, then the reduced basis will be small and the matrix is of low dimensionality, simplifying the calculation. Let us define an OPW state as

$$\left|\mathrm{OPW}_{\vec{k}}\right\rangle = \left|\vec{k}\right\rangle - \sum_{\alpha} \left|\psi_{\alpha}\right\rangle \left\langle\psi_{\alpha}\middle|\vec{k}\right\rangle = (1 - \mathcal{P}) \left|\vec{k}\right\rangle , \tag{2.2.3}$$

where $\left|\vec{k}\right\rangle$ denotes a properly normalized plane wave state, i.e. $\left\langle\vec{r}\middle|\vec{k}\right\rangle = (1/V)e^{i\vec{k}\vec{r}}$, and $\left|\psi_{\alpha}\right\rangle$ a normalized core state. The operator $\mathcal{P}$ is the projection operator onto the core state wave functions,

$$\mathcal{P} = \sum_{\alpha} \left|\psi_{\alpha}\right\rangle \left\langle\psi_{\alpha}\right| . \tag{2.2.4}$$

Thus, the states $\left|\mathrm{OPW}_{\vec{k}}\right\rangle$ are orthogonal to the core states. The states $\left|\mathrm{OPW}_{\vec{k}}\right\rangle$ therefore just comprise a new basis of the conduction–band states and one can expand a conduction–band wave function in terms of this OPW basis.

$$\left|\psi_{\vec{k}}\right\rangle = \sum_{\vec{k}'} a_{\vec{k}'}(1-\mathcal{P})\left|\vec{k}'\right\rangle = (1-\mathcal{P})\left|\varphi_{\vec{k}'}\right\rangle, \tag{2.2.5}$$

where $\left|\varphi_{\vec{k}}\right\rangle$ denotes the *pseudo wave function*, which is given by

$$\left|\varphi_{\vec{k}}\right\rangle = \sum_{\vec{k}'} a_{\vec{k}'}\left|\vec{k}'\right\rangle, \tag{2.2.6}$$

and the $a_{\vec{k}'}$ are expansion coefficients. When we use the pseudo wave function in eq. (2.2.1) for the band electron Hamiltonian, we get

$$\{\mathrm{KE}+\Omega(\vec{r})\}(1-\mathcal{P})\left|\varphi_{\vec{k}}\right\rangle = \epsilon_{\vec{k}}(1-\mathcal{P})\left|\varphi_{\vec{k}}\right\rangle. \tag{2.2.7}$$

After rearranging terms we get

$$\left\{\mathrm{KE}+\Omega(\vec{r})+(\epsilon_{\vec{k}}-[\mathrm{KE}+\Omega])\mathcal{P}\right\}\left|\varphi_{\vec{k}}\right\rangle = \{\mathrm{KE}+u\}\left|\varphi_{\vec{k}}\right\rangle = \epsilon_{\vec{k}}\left|\varphi_{\vec{k}}\right\rangle. \tag{2.2.8}$$

This expression is merely a rearrangement of terms and is not an approximation. We will call

$$\Omega(\vec{r})+(\epsilon_{\vec{k}}-[\mathrm{KE}+\Omega(\vec{r})])\mathcal{P} = u(\vec{r}) \tag{2.2.9}$$

the *pseudopotential*. This operator is very difficult to deal with as it stands since the energy eigenvalues we are looking for are part of the operator, which means that eq. (2.2.9) is only an implicit definition of the pseudopotential and needs to be solved self–consistently. The projection operator $\mathcal{P}$ will mix in core wavefunctions, and we can add arbitrary combinations of core wave functions to the pseudo wave function without changing anything in the energy eigenvalues. The conduction band electron wave functions are therefore not unique. This is because the energy eigenvalues of the form $\epsilon = \frac{\hbar^2 k^2}{2m}$ can be satsified by different sets of eigenstates. The question of uniqueness was studied by (Austin *et al.*, 1962) in which it was concluded that one can construct a pseudopotential with unique solutions for the wave functions by generalizing the expression in eq. (2.2.9).

As Phillips and Kleinman (Phillips and Kleinman, 1959) argue, u is small compared to the kinetic energy term and can therefore be regarded as a perturbation. In leading order the solution of eq. (2.2.8) is given by the kinetic energy alone, and the pseudowavefunctions are plane wave states. We will adopt this approximation in this thesis.

2.3 Electron–Ion Pseudopotential

We will want to calculate the matrix elements of the pseudopotential between two electronic states,

$$\left\langle \vec{k}+\vec{q}\middle| u \middle|\vec{k}\right\rangle . \tag{2.3.1}$$

The non–locality of the pseudopotential operator u manifests itself in form of the $\vec{k}$ dependence of the matrix elements. As it turns out however (Harrison, 1966,Chapter 8-6), this dependence can be dropped, introducing only a small error. It is therefore common to use the local pseudopotential approximation in which the operator u is approximated

by a function of position of the electron relative to the ion core. In other words, we will replace the single ion potentials that appear in eq. (2.1.13) with the pseudopotential, $u(\vec{r})$. Different models have been used in the past for the pseudopotential. Heine and Abarenkov (Heine and Abarenkov, 1964, 1965) introduced a method in which the core potential is fit to experimental data. The method therefore is not ab initio, but uses experimental data at a very early stage of the calculation. In this model, the ionic potential is split into two regions. Outside a spherical region of radius R_c around the ion, the potential is simply given by the Coulomb potential between a charge Ze of the ion and an electron, i.e.

$$\Omega_2(\vec{r}) = -\frac{Ze^2}{r}. \tag{2.3.2}$$

Inside this spherical region however, the potential is expressed as an expansion in terms of angular momentum eigenstates. This expansion is chosen such that the eigenstates inside the core match the eigenstates outside the core at the spherical region boundary, $r = R_c$. The total potential then reads

$$\Omega(\vec{r}) = \begin{cases} -\sum_l A_l(E) P_l & \text{for } r < R_c \\ -\frac{Ze^2}{r} & \text{otherwise,} \end{cases} \tag{2.3.3}$$

where the P_l are projection operators onto angular momentum eigenstates with angular momentum l, and the A_l are the expansion coefficients which generally depend on the energy of the eigenstates. The expansion series inside the core is cut off beyond $l = 2$ for practicality reasons. Animalu and Heine (Animalu and Heine, 1965) calculated pseudopotentials for 25 elements using this method.

Assuming simple expressions for the core part of the potential, three noteworthy models have been developed based on the Heine–Abarenkov approach. The first is based on the work of Harrison. He assumes the core part to be a $1s$–like state, i.e.

$$\Omega_{Ha}(\vec{r}) = \begin{cases} -\frac{Ze^2}{r} + \Omega_c(r) & \text{for } r < R_c \\ -\frac{Ze^2}{r} & \text{otherwise,} \end{cases} \tag{2.3.4}$$

where $\Omega_c(r)$ of the form of a $1s$ electron density, i.e. $\Omega_c(r) \propto e^{-r/\rho}$, where ρ is a parameter. The Fourier transform of the Coulomb part of this potential is given by

$$\Omega_{Ha}(q) = \frac{1}{V}\left[-\frac{4\pi Ze^2}{q^2} + \frac{\beta}{(1+q^2\rho^2)^2}\right], \tag{2.3.5}$$

where β is the proportionality factor which will be set to a value such that the pseudopotential fits the experimental data. The second model is due to Heine and Abarenkov who assumed that the core part is given by a square well of depth Ω_0,

$$\Omega_{HA}(\vec{r}) = \begin{cases} -\Omega_0 & \text{for } r < R_c \\ -\frac{Ze^2}{r} & \text{otherwise.} \end{cases} \tag{2.3.6}$$

The Fourier transform of this potential is given by

$$\Omega_{HA}(q) = -\frac{4\pi}{Vq^2}\left\{\left(Ze^2 - \Omega_0 R_c\right)\cos(qR_c) + \frac{\Omega_0 \sin(qR_c)}{q}\right\}. \tag{2.3.7}$$

A simplification of this model was used by Ashcroft, who set the core potential Ω_0 to zero. The Fourier transform of this potential is given by

$$\Omega_A(q) = -\frac{4\pi Ze^2}{Vq^2}\cos(qR_c). \tag{2.3.8}$$

Table 2.1: Parameters used in the Ashcroft and Harrison pseudopotential models

Ashcroft Pseudopotential (Lead)	
p_F	1.57 Å^{-1}
R_c	0.57 Å

Harrison Pseudopotential (Sodium)	
p_F	0.90 Å^{-1}
β	37 Ry $a_0^3 = 74.57$ eV Å^3
a_0	0.53 Å
ρ	$\frac{1}{2}a_0$

Figure 2.1: Comparison of different pseudopotentials.

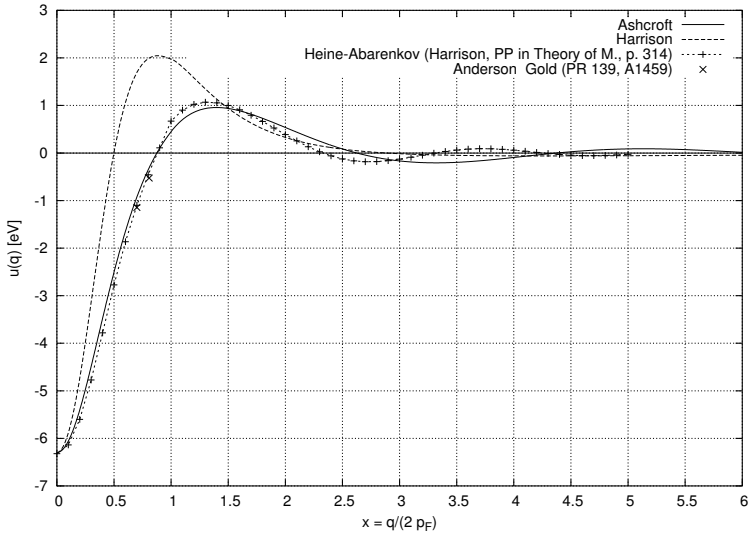

It should be emphasized that none of the above potentials are screened. They represent the bare ion potential.

We use the Lindhard function for screening of the pseudopotentials,

$$u(x) = \frac{1}{2} + \frac{1-x^2}{4x} \log\left|\frac{1+x}{1-x}\right|, \tag{2.3.9}$$

where the parameter $x = q/(2\,p_F)$.

In this thesis we are using two different pseudopotential models. In Chapters 3 and 4 we

use the Ashcroft pseudopotential and in Chapter 5 we use the Harrison pseudopotential. A plot of the two pseudopotentials is shown in Fig. 2.1. The parameters for those two models are given in table 2.1. The pseudopotentials have a similar functional dependence on the dimensionless parameter $x = q/(2p_F)$. The Harrison pseudopotential however exhibits an earlier x–axis crossing than the other two which makes this pseudopotential cut off at lower q than the other ones.

Chapter 3

Superconductivity in a Two–Band System: Single Particle Properties

Quantitative investigations of superconductivity in real multiband systems have only developed in recent years with the availability of the necessary computational resources. Interest in this area is driven by experiment. Recently it was discovered that the long–known compound MgB_2 becomes a superconductor at temperatures below $T_c = 39$ K. This value of T_c is comparable to that of $LaSrCuO_4$, the first of the cuprate superconductors to be discovered. This discovery initiated a number of theoretical and experimental studies on the nature of the superconducting state in this material. MgB_2 shows a significant isotope effect, a tell–tale sign of the involvement of phonons in the process (Bud'ko *et al.*, 2001). Several tunneling experiments found very different values for the superconducting gap (Rubio-Bollinger *et al.*, 2001; Schmidt *et al.*, 2001), which led Liu et al. (Liu *et al.*, 2001) to suggest that the superconducting state of MgB_2 exhibits multiple gaps. First principle calculations (Kortus *et al.*, 2001) found essentially two distinct conduction bands, and it is this two–band nature of the MgB_2 system that is responsible for two different gaps. Here we use a more phenomenological approach to a simpler material which has been known to be a superconductor for a long time.

Lead becomes a superconductor below a temperature of $T_c = 7.2$ K. It is an example of a strong–coupling superconductor which was first described accurately by Eliashberg (Eliashberg, 1960a,b). He generalized BCS theory to the case where signatures of the electron–phonon interaction can appear in measured quantities. In this treatment and in many subsequent studies, it was assumed that the shape of the Fermi surface has no impact on superconducting properties and that it can be approximated by a free electron spherical surface. De Haas–van Alphen measurements and a subsequent analysis of these by Anderson and Gold (Anderson and Gold, 1965) show that in lead the lowest lying band is completely inside the Fermi surface, and that the second and third bands both cut across the Fermi energy, whereas the fourth band lies completely above the Fermi see. Consequently, lead is more accurately described by a two–band model instead of a free electron one–band model. Complicating this further, the topological structure of the third electron–like band is quite intricate and it can be expected that a more realistic description of the electronic band structure might lead to effects similar to the ones found in MgB_2, namely a splitting of the superconducting energy gap into two distinct values.

In the subsequent analysis, we first derive a model Hamiltonian by starting with the usual electron–phonon Hamiltonian and transforming it with the Bogoliubov–Valatin transformation (Bogoliubov, 1958; Bogoliubov *et al.*, 1959; Valatin, 1958) into the BCS quasiparticle operator basis. We then calculate the quasiparticle propagators $\mathcal{G}_\gamma(\vec{k}, E)$ and $\mathcal{F}_\gamma(\vec{k}, E)$ following the notation of Abrikosov, Gorkov, and Dzyaloshinskii (Abrikosov *et al.*, 1963) and derive a gap equation by introducing the condition that the off–diagonal on–shell self–energy (due to the $\mathcal{F}_\gamma(\vec{k}, E)$ quasiparticle propagator) vanishes. Due to the reasons pointed out above we use realistic models for the electron– and phonon–spectra based on the model proposed by Anderson and Gold (Anderson and Gold, 1965) and by Cowley (Cowley, 1974a). We then calculate the single–particle self–energies associated with these propagators and their spectral density and make contact with recent photoemission measurements on lead samples. In the following chapter we will apply our model to higher order correlation functions and the analysis of strong–coupling effects seen in optical conductivity.

3.1 Lead — Phonons

Solid lead has the face centered cubic crystal structure with a lattice constant, $a = 4.95\,\text{Å}$. In our calculations, models were used for the electron and phonon dispersion relations. The phonon dispersion is accurately described with a force constant model (Cowley, 1974a). This model is fit to experimental neutron scattering data from (Stedman *et al.*, 1967). Starting from the dynamical matrix[3.1],

$$D(\vec{k}) = \sum_{N\nu} D(\vec{R}^0_{N\nu}) e^{-i\vec{k}\cdot\vec{R}^0_{N\nu}}, \tag{3.1.1}$$

where the matrix $D(\vec{R})$ is defined as a second order derivative in the ion potentials,

$$D_{ij}(\vec{R}_{N\nu} - \vec{R}'_{M\mu}) = \left.\frac{\partial^2 \Omega_I}{\partial U^i_{N\nu} \partial U^j_{M\mu}}\right|_{\vec{U}=0}, \tag{3.1.2}$$

Cowley replaced the matrix elements in $D(\vec{k})$ with fitting parameters and split the dynamical matrix into contributions over "stars", lattice points on a sphere in momentum space of given radius. The dynamical matrix can be written as

$$D(\vec{k}) = \sum_i \sum_{\vec{R}_{(i)}} D(\vec{R}_{(i)}) e^{-i\vec{k}\cdot\vec{R}_{(i)}}, \tag{3.1.3}$$

where the $\vec{R}_{(i)}$ stand for the i^{th} nearest neighbors. Starting with nearest neighbors only, he then successively fit this model to the experimental data. As he notes, the root mean square deviation from the experiment improved only very slowly beyond the 6^{th} nearest neighbors.

[3.1] Due to the symmetry of the dynamical matrix, $D(\vec{R}^0_{N\nu}) = D(-\vec{R}^0_{N\nu})$, some authors write the Fourier transform as $D(\vec{k}) = \sum_{N\nu} D(\vec{R}^0_{N\nu}) e^{i\vec{k}\cdot\vec{R}^0_{N\nu}}$

Figure 3.1: Pb phonon dispersion calculated from force constant model (Cowley, 1974a). Shown are the three acoustic branches along different directions in the Brillouin zone.

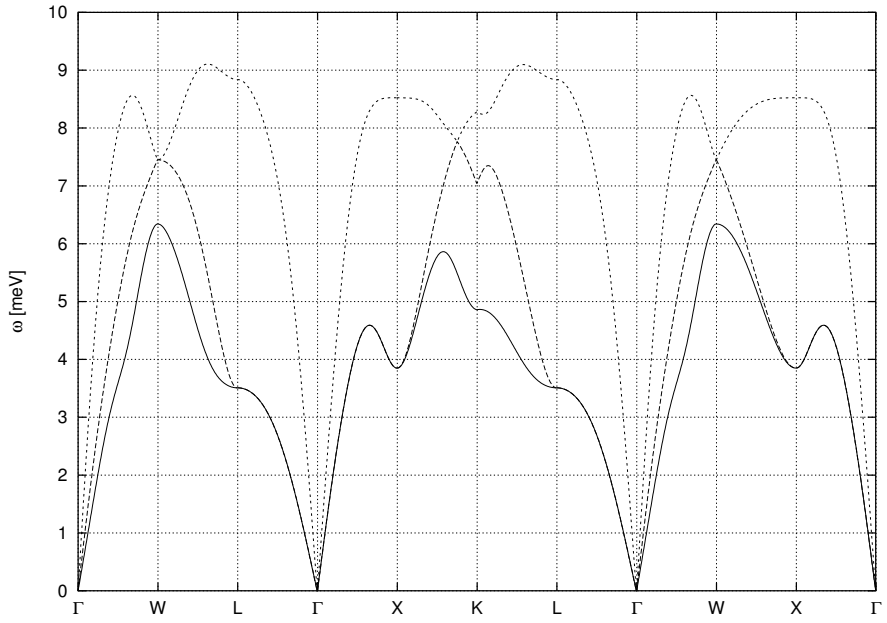

He therefore terminated this procedure after inclusion of the 8^{th} nearest neighbor sites. Using his fitting parameters, we calculate the phonon energies and polarization vectors by solving the following eigenvalue problem,

$$M\omega^2\vec{\eta} = D(\vec{k})\vec{\eta}. \tag{3.1.4}$$

Fig. 3.1 shows the phonon dispersion along some selected directions. For reference, the points shown in Fig. 3.1 are also shown relative to the whole Brillouin zone in Fig. 3.3. Their coordinates are shown in Table 3.1.

Table 3.1: Notation for high–symmetry points in the Brillouin zone

Γ	$(2\pi)/a\,(0,0,0)$	W	$(2\pi)/a\,(1,1/2,0)$
L	$(2\pi)/a\,(1/2,1/2,1/2)$	X	$(2\pi)/a\,(1,0,0)$
K	$(2\pi)/a\,(3/4,3/4,0)$	U	$(2\pi)/a\,(1/4,1/4,1)$

3.2 Lead — Electrons

The electron dispersion is taken from the work of Anderson and Gold (Anderson and Gold, 1965). Their model is based on the orthogonalized plane wave method which is fit to de Haas–van Alphen data of the Fermi surface. The Fermi energy, ϵ_F, the Fourier components of the pseudopotential, V_{111}, and V_{200}, and a spin–orbit coupling parameter, λ, are regarded as fitting parameters. The fitting procedure starts by extracting the cross sectional area of the Fermi surface from the de Haas–van Alphen periods using the Onsager–Lifshitz–Kosevich relation,

$$A_0 = \frac{2\pi e}{c\hbar P}, \tag{3.2.1}$$

where P is the measured period. The model is given by a single–electron Hamiltonian,

$$\mathcal{H} = -\frac{\hbar^2\nabla^2}{2m} + \Omega_{ps}(\vec{r}), \tag{3.2.2}$$

where Ω_{ps} is the pseudopotential. The pseudo wavefunction which is the eigenfunction of the Hamiltonian of eq. (3.2.2) is periodic in the crystal due to Bloch's theorem, which implies that we can expand it in terms of reciprocal lattice vectors,

$$\begin{aligned} \left|\varphi_{\vec{k}}\right\rangle &= u_{\vec{k}}(\vec{r})\ e^{i\vec{k}\cdot\vec{r}} \\ &= \sum_{\vec{K}} u_{\vec{k},\vec{K}}\ e^{i(\vec{k}+\vec{K})\cdot\vec{r}}. \end{aligned} \tag{3.2.3}$$

The $u_{\vec{k},\vec{K}}$ are expansion coefficients to be determined later and the $\vec{K}$ denote reciprocal lattice vectors. Since the pseudopotential itself is periodic in the crystal, it too can be expanded in terms of reciprocal lattice vectors. The Schrödinger equation splits into reciprocal lattice vector components,

$$\frac{\hbar^2(\vec{k}+\vec{K})^2}{2m}\ u_{\vec{k},\vec{K}} + \sum_{\vec{K}'}\ u_{\vec{k},\vec{K}'}\ \Omega_{ps}(\vec{k}+\vec{K}') = \xi_{\vec{k}}\ u_{\vec{k},\vec{K}}. \tag{3.2.4}$$

Anderson and Gold found that only a few reciprocal lattice vectors suffice in eq. (3.2.4) in order to fit the experimental Fermi surface data. In order to enhance the accuracy of their description they included spin–orbit coupling introducing an additional parameter λ characterizing the strength of that interaction. The procedure leads to a complex 8x8 matrix. Its 4 doubly degenerate eigenvalues yield the energies of the first four bands, and its eigenvectors the expansion coefficients in the place wave basis. The matrix is given by

$$\begin{pmatrix} A & B \\ -B & A^* \end{pmatrix}, \tag{3.2.5}$$

where the two sub–matrices, A, and B, are given by

$$A = \begin{pmatrix} U_0 + V_{200} + 2V_{111} & \frac{i(U_4-U_3)}{4} & \frac{U_1+U_2-U_3-U_4}{4} & \frac{i(U_4-U_3)}{4} \\ -\frac{i(U_4-U_3)}{4} & U_0 - V_{200} + \frac{\lambda}{2} & \frac{i(U_4-U_3)}{4} & -\frac{U_1+U_2-U_3-U_4}{4} \\ \frac{U_1+U_2-U_3-U_4}{4} & -\frac{i(U_4-U_3)}{4} & U_0 + V_{200} - 2V_{111} & -\frac{i(U_4-U_3)}{4} - \frac{\lambda}{\sqrt{2}} \\ -\frac{i(U_4-U_3)}{4} & -\frac{U_1+U_2-U_3-U_4}{4} & \frac{i(U_4-U_3)}{4} - \frac{\lambda}{\sqrt{2}} & U_0 - V_{200} - \frac{\lambda}{2} \end{pmatrix}, \tag{3.2.6}$$

and

$$B = \frac{U_2 - U_1}{4} \begin{pmatrix} 0 & 1 & 0 & -1 \\ -1 & 0 & -1 & 0 \\ 0 & 1 & 0 & -1 \\ 1 & 0 & 1 & 0 \end{pmatrix}. \tag{3.2.7}$$

The labeling of the matrix elements refers to the reciprocal lattice vector $\vec{Q}$ involved. Anderson and Gold describe a method in which the Brillouin zone is divided into 24 regions and different sets of $\vec{Q}_i$ are used in each region. Inside the region shown in Fig. 3.3 for example, one uses in units of $2\pi/a$, $\vec{Q}_{i=1,2,3,4} \in \{0, (0,0,2), (1,1,1), (1,-1,1)\}$. The matrix element V_{111} then corresponds to $\Omega_{ps}(\vec{Q} - \vec{Q}') = V_{\vec{Q}_1 - \vec{Q}_3} = V_{111}$.

The kinetic energy terms are given by

$$U_{i=1,2,3,4} = \frac{\hbar^2}{2m} \left| \vec{k} + \vec{Q}_i \right|^2 \tag{3.2.8}$$

$$U_0 = \frac{\hbar^2}{2m} \sum_{i=1}^{4} \frac{U_i}{4}. \tag{3.2.9}$$

The four adjustable parameters of the model are used with the following values,

$$\begin{aligned} \epsilon_F &= 9.765 \text{ eV} \\ V_{111} &= -1.142 \text{ eV} \\ V_{200} &= -0.530 \text{ eV} \\ \lambda &= 1.306 \text{ eV}. \end{aligned} \tag{3.2.10}$$

Figure 3.2: Pb electron dispersion calculated using the model by Anderson and Gold (1965). Shown are the first four bands.

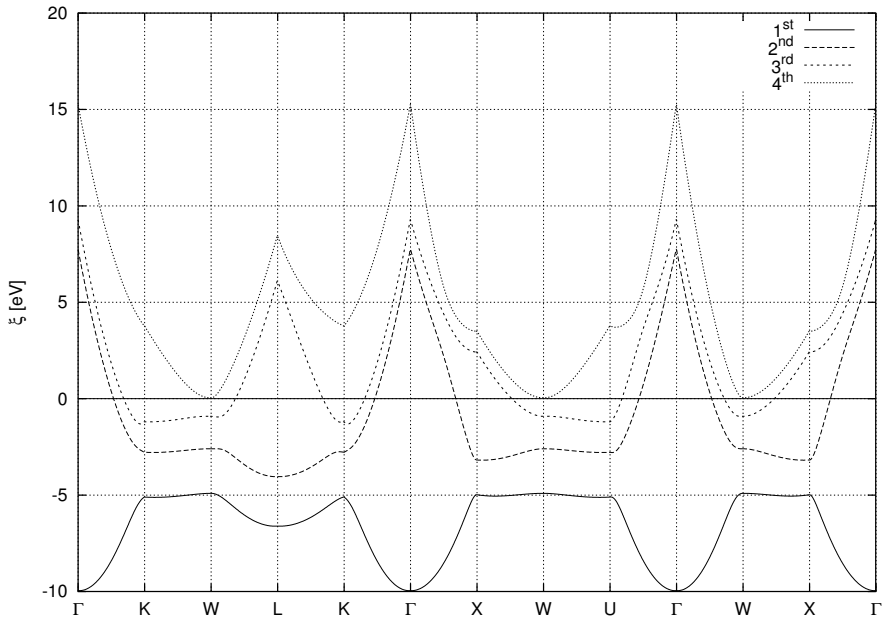

Here we are interested in the low energy properties, i.e. states that are close to the Fermi surface. Only the second and the third band cross the Fermi surface. From Anderson and Gold's data, the calculated band structure is shown in Fig. 3.2. On the scale of the figure it appears as if the fourth band actually touches the Fermi surface. This is not true however, at closest approach, the band is still ≈ 50 meV above the Fermi surface and remains empty at superconducting temperatures.

A representation of the two bands and the Brillouin zone, taken from Anderson and Gold's paper, and calculated using their parameters, are shown in Figs. 3.3, and 3.4. We can compare our rendering of the two bands with an empty lattice calculation (e.g., Fig. 9.9 Ashcroft and Mermin, 1976). In the empty lattice the fourth band is occupied and the zones show sharp edges. Due to electron–electron interactions however, electron states are pushed from the fourth into the lower lying bands so as to empty it and the edges of the second and third bands are smoothened.

Figure 3.3: From Anderson and Gold (1965): A representation of the Brillouin zone in Pb.

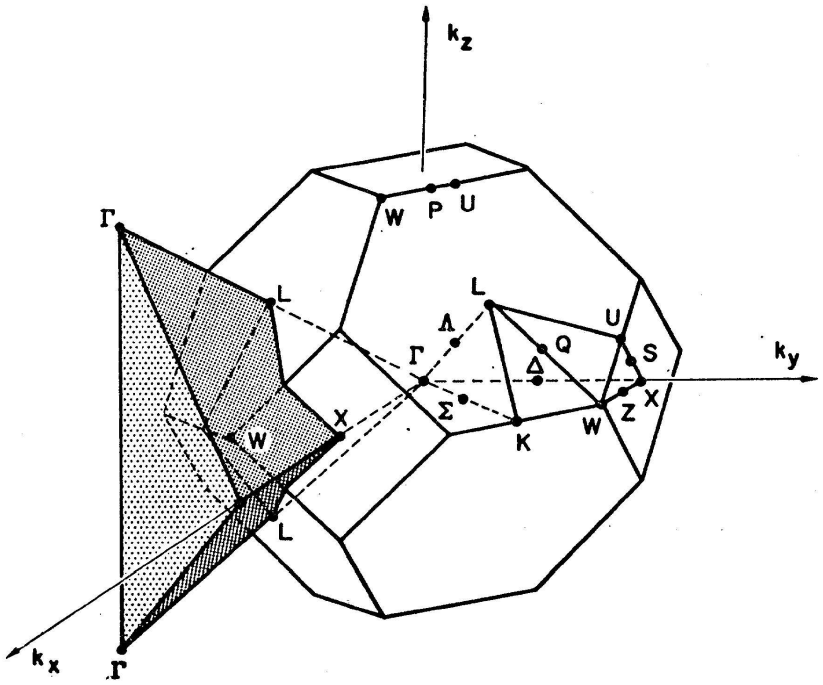

Figure 3.4: A rendering of the second band and third bands in Pb.

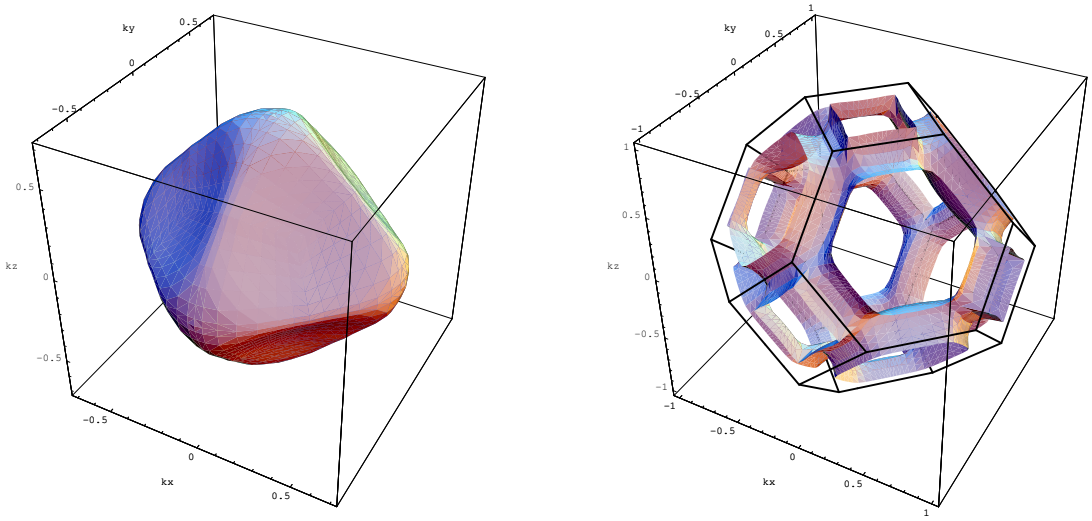

Although diagonalizing the Anderson and Gold 8x8 matrix is computationally not very challenging in itself, we will need to calculate these many times since we will integrate over the electron momentum. It turns out that using a diagonalization routine directly is computationally not feasible. We therefore had to simplify the model.

As pointed out earlier, we will require two of the four bands only. The second band is close to spherical which led us to set the Fermi momentum in that band to a constant. The dispersion around the Fermi surface was linearized,

$$\xi_{\vec{k}}^{(2)} = \hbar v_F^{(2)} \left(\left| \vec{k} \right| - k_F \right). \tag{3.2.11}$$

The Fermi velocity was calculated using the Anderson and Gold matrix and averaged over the entire surface. We found a value of $v_F^{(2)} = -1.367 \times 10^6$ m s^{-1}. The second band is hole–like, which is why the Fermi velocity is negative.

The third band is more complicated. As shown in the right panel of Fig. 3.4, the Fermi surface consists of "pipes" around the edges of the Brillouin zone. This shape naturally suggests the use of cylindrical coordinates. We therefore split the third band into 36 pipes and used a separate parametrization for each pipe. We will denote the height on the cylinder with z^i and the polar angle with β^i. The direction $\beta^i = 0$ is taken to be a direction that lies within a face of the Brillouin zone. The superscript i stands for one of the 36 pipes. Since the thickness of the Fermi surface depends strongly on β but only weakly on z we assumed that there is no z–dependence and only a β–dependence. In fact one can classify the 36 pipes into two groups or types, type I being pipes around edges between two hexagonal faces and type II pipes between a hexagonal face and a square face. The β–dependence was fit to a 6^{th} order polynomial,

$$p_F^n = \begin{cases} a_0^n + a_1^n \beta + a_2^n \beta^2 + a_3^n \beta^3 + a_4^n \beta^4 + a_5^n \beta^5 & \beta < \hat{\beta}^n/2 \\ b_0^n + b_1^n \beta + b_2^n \beta^2 + b_3^n \beta^3 + b_4^n \beta^4 + b_5^n \beta^5 & \text{otherwise,} \end{cases} \tag{3.2.12}$$

Table 3.2: The 3$^{\rm rd}$–band fitting parameters for p_F.

a_1^I	0.2450 Å^{-1}	a_1^{II}	0.2447 Å^{-1}
a_2^I	0.0437 Å^{-1}	a_2^{II}	-0.0684 Å^{-1}
a_3^I	0.3788 Å^{-1}	a_3^{II}	0.1045 Å^{-1}
a_4^I	-1.0422 Å^{-1}	a_4^{II}	-0.0585 Å^{-1}
a_5^I	1.7359 Å^{-1}	a_5^{II}	0.0589 Å^{-1}
a_6^I	-0.9432 Å^{-1}	a_6^{II}	-0.0389 Å^{-1}
b_1^I	-6.4407 Å^{-1}	b_1^{II}	-2.4316 Å^{-1}
b_2^I	24.3407 Å^{-1}	b_2^{II}	8.2812 Å^{-1}
b_3^I	-33.3615 Å^{-1}	b_3^{II}	-9.9951 Å^{-1}
b_4^I	22.2081 Å^{-1}	b_4^{II}	5.9131 Å^{-1}
b_5^I	-7.2748 Å^{-1}	b_5^{II}	-1.7337 Å^{-1}
b_6^I	0.9432 Å^{-1}	b_6^{II}	0.2024 Å^{-1}

where n denotes the two types of pipes and is either I or II. The parameters used in our calculations are listed in table 3.2 and a plot of the Fermi momentum in the two types of pipes is shown in Fig. 3.5.

The angle $\hat{\beta}$ denotes the angle subtended by the two faces of the Brillouin zone touching at a particular edge. We used the values,

$$\begin{aligned} \hat{\beta}^I &= 1.91 \text{ rad} \\ \hat{\beta}^{II} &= 2.19 \text{ rad.} \end{aligned} \tag{3.2.13}$$

The dispersion was linearized and the Fermi velocity we calculated for both types is $v_F^{(3)} = 1.055 \times 10^6$ m s^{-1}. The third band is electron–like.

Figure 3.5: The Fermi momentum as a function of angle β for the two types of third band pipes.

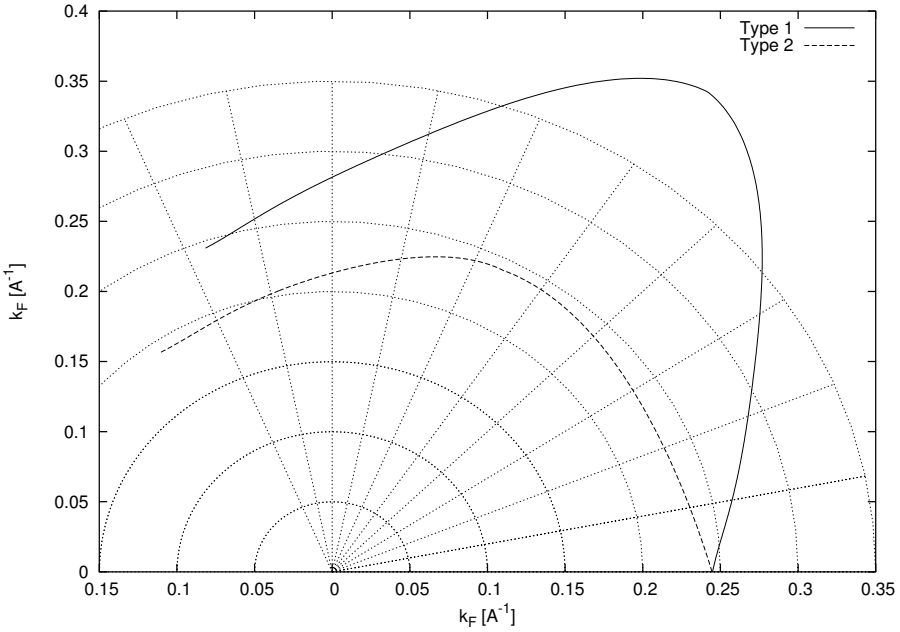

As another test of our model we calculated the volume of the second and third bands and found good agreement with the results of Anderson and Gold. We find 0.360 holes/atom in the second band and 0.467 electrons/atom for the third band. Anderson and Gold quote values of 0.375 holes/atom and 0.393 electrons/atom for the second and third bands respectively. Their results are therefore 4% larger in the second band and 16% smaller in the third band.

3.3 The Superconducting State

3.3.1 The Transformed Hamiltonian

In the following we will derive an expression for the single particle properties starting from the usual electron–phonon Hamiltonian,

$$\mathcal{H} = \sum_{\vec{k}\sigma} \xi_{\vec{k}}\ c^{\dagger}_{\vec{k}\sigma} c_{\vec{k}\sigma} + \sum_{\vec{k}\sigma} \sum_{\vec{q}\vec{Q}\lambda} g(\vec{q},\vec{Q},\lambda)(a_{\vec{q}\lambda} + a^{\dagger}_{\vec{q}\lambda}) c^{\dagger}_{\vec{k}+\vec{q}+\vec{Q}\sigma} c_{\vec{k}\sigma}, \tag{3.3.1}$$

where the electronic energies, $\xi_{\vec{k}}$, are given by the analysis of Anderson and Gold. σ denotes the electron spin. In case of a multi–band band structure, we should sum over the bands also. In order to simplify the notation, we will not explicitly mention this sum over bands at this point. It can be added back into the problem at a later stage. We apply the Bogoliubov transformation to the electron operators to rewrite the Hamiltonian in terms of the quasiparticle operators. These transformations are given by

$$c_{\vec{k}\uparrow} = u_{\vec{k}} \gamma_{\vec{k}\uparrow} + v^{*}_{-\vec{k}} \gamma^{\dagger}_{-\vec{k}\downarrow} \tag{3.3.2}$$

$$c_{-\vec{k}\downarrow} = u_{-\vec{k}} \gamma_{-\vec{k}\downarrow} - v^{*}_{\vec{k}} \gamma^{\dagger}_{\vec{k}\uparrow}. \tag{3.3.3}$$

The coherence factors satisfy the following relations,

$$\begin{aligned} E_{\vec{k}} &= \sqrt{\left|\Delta_{\vec{k}}\right|^2 + \xi^2_{\vec{k}}} \\ \left|u_{\vec{k}}\right|^2 &= \frac{1}{2}\left(1 + \frac{\xi_{\vec{k}}}{E_{\vec{k}}}\right) \\ \left|v_{\vec{k}}\right|^2 &= \frac{1}{2}\left(1 - \frac{\xi_{\vec{k}}}{E_{\vec{k}}}\right) \\ u_{\vec{k}} v_{\vec{k}} &= \frac{\Delta_{\vec{k}}}{2E_{\vec{k}}}. \end{aligned} \tag{3.3.4}$$

The total Hamiltonian, transformed into the BCS ground state, is given by

$$\mathcal{H} = \mathcal{H}_0 + \mathcal{V}_A + \mathcal{V}^{\dagger}_A + \mathcal{V}_B + \mathcal{V}_C + \mathcal{V}_D + \mathcal{V}^{\dagger}_D. \tag{3.3.5}$$

The unperturbed part of the Hamiltonian is given by

$$\mathcal{H}_0 = \sum_{\vec{k}\sigma} \left\{ E_{\vec{k}} \gamma^\dagger_{\vec{k}\sigma} \gamma_{\vec{k}\sigma} + \left| v_{\vec{k}} \right|^2 \xi_{\vec{k}} \right\}. \tag{3.3.6}$$

The first three perturbation terms are given by a term which destroys or creates a pair of quasi–particles,

$$\mathcal{V}_A = \sum_{\vec{k}} \frac{\xi_{\vec{k}} \Delta_{\vec{k}}}{E_{\vec{k}}} \; \gamma_{-\vec{k}\downarrow} \gamma_{\vec{k}\uparrow}, \tag{3.3.7}$$

and a term that will renormalize the quasi–particle energy,

$$\mathcal{V}_B = \sum_{\vec{k}\sigma} \frac{-\left| \Delta_{\vec{k}} \right|^2}{E_{\vec{k}}} \gamma^\dagger_{\vec{k}\sigma} \gamma_{\vec{k}\sigma}. \tag{3.3.8}$$

The electron–phonon part generates the last two terms. The first one, $\mathcal{V}_C$,

$$\mathcal{V}_C = \sum_{\vec{k}\sigma} \sum_{\vec{q}\vec{Q}\lambda} g(\vec{q}, \vec{Q}, \lambda) A_{\vec{q}\lambda} \left[u_{\vec{k}} u^*_{\vec{k}+\vec{q}+\vec{Q}} - v_{\vec{k}} v^*_{\vec{k}+\vec{q}+\vec{Q}} \right] \gamma^\dagger_{\vec{k}+\vec{q}+\vec{Q}\sigma} \gamma_{\vec{k}\sigma}, \tag{3.3.9}$$

allows for scattering of a quasiparticle on a phonon. The second term, $\mathcal{V}_D$,

$$\mathcal{V}_D = \sum_{\vec{k}} \sum_{\vec{q}\vec{Q}\lambda} g(-\vec{q}, -\vec{Q}, \lambda) A^\dagger_{\vec{q}\lambda} \left[u_{\vec{k}} v_{\vec{k}+\vec{q}+\vec{Q}} + v_{\vec{k}} u_{\vec{k}+\vec{q}+\vec{Q}} \right] \gamma_{-\vec{k}\downarrow} \gamma_{\vec{k}+\vec{q}+\vec{Q}\uparrow}, \tag{3.3.10}$$

creates or destroys pairs of quasi–particles via the emission or absorption of a phonon. In the above, the linear combination of phonon creation and destruction operators, $a_{\vec{q}\lambda} + a^\dagger_{\vec{q}\lambda}$, was written simply as $A_{\vec{q}\lambda}$.

3.3.2 Greens Functions in the BCS Ground State

In the ground state in which the single–particle states are created and destroyed by $c_\kappa^\dagger$ and c_κ, the electron Greens function[3.2] is,

$$\mathcal{G}(\vec{k}\sigma, \tau_2 - \tau_1) = -\left\langle T_\tau \left[c_{\vec{k}\sigma}(\tau_2) c^\dagger_{\vec{k}\sigma}(\tau_1) \right] \right\rangle . \tag{3.3.11}$$

In the mean field $\gamma_{\vec{k}\sigma}$ basis which we use to describe the superconducting ground state, there are three quasiparticle Greens functions,

$$\mathcal{G}_\gamma(\vec{k}\sigma, \tau_2 - \tau_1) = -\left\langle T_\tau \left[\gamma_{\vec{k}\sigma}(\tau_2) \gamma^\dagger_{\vec{k}\sigma}(\tau_1) \right] \right\rangle \tag{3.3.12}$$

$$\mathcal{F}_\gamma(\vec{k}, \tau_2 - \tau_1) = -\left\langle T_\tau \left[\gamma_{\vec{k}\uparrow}(\tau_2) \gamma_{-\vec{k}\downarrow}(\tau_1) \right] \right\rangle \tag{3.3.13}$$

$$\mathcal{F}^\dagger_\gamma(\vec{k}, \tau_2 - \tau_1) = -\left\langle T_\tau \left[\gamma^\dagger_{-\vec{k}\downarrow}(\tau_2) \gamma^\dagger_{\vec{k}\uparrow}(\tau_1) \right] \right\rangle . \tag{3.3.14}$$

These are related to the electron Greens function

$$\begin{aligned} \mathcal{G}(\vec{k}\uparrow, \tau_2 - \tau_1) &= \left|u_{\vec{k}}\right|^2 \mathcal{G}_\gamma(\vec{k}\uparrow, \tau_2 - \tau_1) - \left|v_{\vec{k}}\right|^2 \mathcal{G}_\gamma(-\vec{k}\downarrow, \tau_1 - \tau_2) \\ &\quad + u_{\vec{k}} v_{\vec{k}} \mathcal{F}_\gamma(\vec{k}, \tau_2 - \tau_1) + u^*_{\vec{k}} v^*_{\vec{k}} \mathcal{F}^\dagger_\gamma(\vec{k}, \tau_2 - \tau_1), \end{aligned} \tag{3.3.15}$$

Since the Matsubara frequencies are quasi–periodic, one can use the following Fourier transformations,

$$\mathcal{G}(\vec{k}\sigma, \tau_2 - \tau_1) = \frac{1}{\hbar\beta} \sum_{ik_n} e^{-ik_n(\tau_2 - \tau_1)} \mathcal{G}(\vec{k}\sigma, ik_n) \tag{3.3.16}$$

$$\int_0^{\hbar\beta} d\tau \; e^{-ik_n\tau} = \hbar\beta \delta_{ik_n, 0}, \tag{3.3.17}$$

[3.2] We will use the finite temperature formalism and take the limit $T \to 0$ later.

where $\beta = \frac{1}{k_B T}$. The discrete Matsubara frequencies are defined as

$$ik_n = \begin{cases} \frac{(2n+1)\pi}{\hbar\beta} & \text{for Fermions} \\ \frac{2n\,\pi}{\hbar\beta} & \text{for Bosons} \end{cases} \tag{3.3.18}$$

The Fourier transform of the electron Greens function in terms of the quasiparticle propagators is given by

$$\mathcal{G}(\vec{k}\uparrow, ik_n) = \left|u_{\vec{k}}\right|^2 \mathcal{G}_\gamma(\vec{k}\uparrow, ik_n) - \left|v_{\vec{k}}\right|^2 \mathcal{G}_\gamma(-\vec{k}\downarrow, -ik_n) + u_{\vec{k}} v_{\vec{k}} \mathcal{F}_\gamma(\vec{k}, ik_n) + u^*_{\vec{k}} v^*_{\vec{k}} \mathcal{F}^\dagger_\gamma(\vec{k}, ik_n), \tag{3.3.19}$$

where $\mathcal{F}_\gamma(\vec{k}, ik_n) = \mathcal{F}^\dagger_\gamma(\vec{k}, -ik_n)$. In the absence of the interaction terms, $\mathcal{V}_{A-D}$, in the Hamiltonian, $\mathcal{F}_\gamma(\vec{k}, \tau_2 - \tau_1) = \mathcal{F}^\dagger_\gamma(\vec{k}, \tau_2 - \tau_1) \equiv 0$. The interaction terms lead to self energies for both $\mathcal{G}_\gamma$ and $\mathcal{F}_\gamma$ propagators which can be calculated perturbatively. We define the gap function by the requirement that the real part of the on–shell retarded self–energy $\Sigma^{ret}_{\gamma^\dagger\gamma^\dagger}(\vec{k}, E_{\vec{k}})$ vanishes, $\Re\left(\Sigma^{ret}_{\gamma^\dagger\gamma^\dagger}(\vec{k}, E_{\vec{k}})\right) \equiv 0$. This self–energy is given by (cf. eq. (C.55) from Appendix C),

$$\hbar\Sigma^{ret}_{\gamma^\dagger\gamma^\dagger}(\vec{k}, E) = -\frac{\xi_{\vec{k}}\Delta_{\vec{k}}}{E_{\vec{k}}} - \frac{1}{\hbar}\frac{\xi_{\vec{k}}}{E_{\vec{k}}} \sum_{\vec{q}\vec{Q}\lambda} \left|g(\vec{q}, \vec{Q}, \lambda)\right|^2 \frac{\Delta_{\vec{k}+\vec{q}+\vec{Q}}}{2E_{\vec{k}+\vec{q}+\vec{Q}}} \left[\hbar\, g^{ret}(E) + \hbar\, g^{ret}(-E)\right], \tag{3.3.20}$$

where

$$\hbar\, g^{ret}(\pm E) = \frac{n_{\vec{q}\lambda} + f_{\vec{k}+\vec{q}+\vec{Q}}}{\pm\hbar^{-1}E + \omega_{\vec{q}\lambda} - \hbar^{-1}E_{\vec{k}+\vec{q}+\vec{Q}} \pm i\delta} + \frac{1 + n_{\vec{q}\lambda} - f_{\vec{k}+\vec{q}+\vec{Q}}}{\pm\hbar^{-1}E - \omega_{\vec{q}\lambda} - \hbar^{-1}E_{\vec{k}+\vec{q}+\vec{Q}} \pm i\delta}, \tag{3.3.21}$$

from eq. (C.57). We will take the zero temperature limit of the thermal functions. The electronic distribution, $f_{\vec{k}}$, vanishes exponentially with temperature and terms involving $\sum_{\vec{q}\lambda} n_{\vec{q}\lambda}$ also go to zero with T. The gap equation is therefore given by

$$\Delta_{\vec{k}} = -\sum_{\vec{q}\vec{Q}\lambda} \left| g(\vec{q},\vec{Q},\lambda) \right|^2 \frac{\Delta_{\vec{k}+\vec{q}+\vec{Q}}}{2E_{\vec{k}+\vec{q}+\vec{Q}}} \mathcal{P}\left[\frac{1}{E_{\vec{k}} - \hbar\omega_{\vec{q}\lambda} - E_{\vec{k}+\vec{q}+\vec{Q}}} - \frac{1}{E_{\vec{k}} + \hbar\omega_{\vec{q}\lambda} + E_{\vec{k}+\vec{q}+\vec{Q}}} \right]. \tag{3.3.22}$$

Through a rearrangement of the thermal factors, $g^{ret}(E)$, we find

$$\begin{aligned} \Im\left(\hbar\Sigma^{ret}_{\gamma^\dagger\gamma^\dagger}(\vec{k},E)\right) &= \pi\frac{\xi_{\vec{k}}}{E_{\vec{k}}} \sum_{\vec{q}\vec{Q}\lambda} \left| g(\vec{q},\vec{Q},\lambda) \right|^2 \frac{\Delta_{\vec{k}+\vec{q}+\vec{Q}}}{2E_{\vec{k}+\vec{q}+\vec{Q}}} \\ &\quad \times \left[\delta\left(E - \hbar\omega_{\vec{q}\lambda} - E_{\vec{k}+\vec{q}+\vec{Q}}\right) - \delta\left(E + \hbar\omega_{\vec{q}\lambda} + E_{\vec{k}+\vec{q}+\vec{Q}}\right) \right], \end{aligned} \tag{3.3.23}$$

and

$$\begin{aligned} \Re\left(\hbar\Sigma^{ret}_{\gamma^\dagger\gamma^\dagger}(\vec{k},E)\right) &= -\frac{\xi_{\vec{k}}}{E_{\vec{k}}} \sum_{\vec{q}\vec{Q}\lambda} \left| g(\vec{q},\vec{Q},\lambda) \right|^2 \frac{\Delta_{\vec{k}+\vec{q}+\vec{Q}}}{2E_{\vec{k}+\vec{q}+\vec{Q}}} \left[\frac{1}{E - \hbar\omega_{\vec{q}\lambda} - E_{\vec{k}+\vec{q}+\vec{Q}}} \right. \\ &\quad \left. - \frac{1}{E + \hbar\omega_{\vec{q}\lambda} + E_{\vec{k}+\vec{q}+\vec{Q}}} - \frac{1}{E_{\vec{k}} - \hbar\omega_{\vec{q}\lambda} - E_{\vec{k}+\vec{q}+\vec{Q}}} + \frac{1}{E_{\vec{k}} + \hbar\omega_{\vec{q}\lambda} + E_{\vec{k}+\vec{q}+\vec{Q}}} \right]. \end{aligned} \tag{3.3.24}$$

The imaginary part is odd in E and the real part even. We also analytically continue the self–energy of $\mathcal{G}_\gamma(\vec{k}\sigma, ik_n)$ to the real energy axis. With eq. (C.52) we get

$$\begin{aligned} \hbar\Sigma^{ret}_{\gamma\gamma^\dagger}(\vec{k},E) &= -\frac{\Delta^2_{\vec{k}}}{E_{\vec{k}}} + \frac{1}{2}\sum_{\vec{q}\vec{Q}\lambda} \left| g(\vec{q},\vec{Q},\lambda) \right|^2 \left(g^{ret}(E) - g^{ret}(-E) \right) \\ &\quad - \frac{\Delta_{\vec{k}}}{E_{\vec{k}}} \sum_{\vec{q}\vec{Q}\lambda} \left| g(\vec{q},\vec{Q},\lambda) \right|^2 \frac{\Delta_{\vec{k}+\vec{q}+\vec{Q}}}{2E_{\vec{k}+\vec{q}+\vec{Q}}} \left(g^{ret}(E) + g^{ret}(-E) \right). \end{aligned} \tag{3.3.25}$$

In the zero temperature limit we can split off the on–shell piece in the real part of the last term and find that it cancels the first term once the expression for $\Delta_{\vec{k}}$ is used. The self–energy $\Sigma^{ret}_{\gamma\gamma^\dagger}(\vec{k},E)$ can therefore be written as

$$\Im\left(\hbar\Sigma^{ret}_{\gamma\gamma^\dagger}(\vec{k},E)\right) = -\frac{\pi}{2}\sum_{\vec{q}\vec{Q}\lambda}\left|g(\vec{q},\vec{Q},\lambda)\right|^2\left[\delta\left(E-\hbar\omega_{\vec{q}\lambda}-E_{\vec{k}+\vec{q}+\vec{Q}}\right)+\delta\left(E+\hbar\omega_{\vec{q}\lambda}+E_{\vec{k}+\vec{q}+\vec{Q}}\right)\right]$$
$$+\pi\,\frac{\Delta_{\vec{k}}}{E_{\vec{k}}}\sum_{\vec{q}\vec{Q}\lambda}\left|g(\vec{q},\vec{Q},\lambda)\right|^2\frac{\Delta_{\vec{k}+\vec{q}+\vec{Q}}}{2E_{\vec{k}+\vec{q}+\vec{Q}}}\left[\delta\left(E-\hbar\omega_{\vec{q}\lambda}-E_{\vec{k}+\vec{q}+\vec{Q}}\right)-\delta\left(E+\hbar\omega_{\vec{q}\lambda}+E_{\vec{k}+\vec{q}+\vec{Q}}\right)\right],$$

(3.3.26)

and

$$\Re\left(\hbar\Sigma^{ret}_{\gamma\gamma^\dagger}(\vec{k},E)\right) = \frac{1}{2}\sum_{\vec{q}\vec{Q}\lambda}\left|g(\vec{q},\vec{Q},\lambda)\right|^2\left[\frac{1}{E-\hbar\omega_{\vec{q}\lambda}-E_{\vec{k}+\vec{q}+\vec{Q}}}+\frac{1}{E+\hbar\omega_{\vec{q}\lambda}+E_{\vec{k}+\vec{q}+\vec{Q}}}\right]$$
$$-\frac{\Delta_{\vec{k}}}{E_{\vec{k}}}\sum_{\vec{q}\vec{Q}\lambda}\left|g(\vec{q},\vec{Q},\lambda)\right|^2\frac{\Delta_{\vec{k}+\vec{q}+\vec{Q}}}{2E_{\vec{k}+\vec{q}+\vec{Q}}}\left[\frac{1}{E-\hbar\omega_{\vec{q}\lambda}-E_{\vec{k}+\vec{q}+\vec{Q}}}-\frac{1}{E+\hbar\omega_{\vec{q}\lambda}+E_{\vec{k}+\vec{q}+\vec{Q}}}\right.$$
$$\left.-\frac{1}{E_{\vec{k}}-\hbar\omega_{\vec{q}\lambda}-E_{\vec{k}+\vec{q}+\vec{Q}}}+\frac{1}{E_{\vec{k}}+\hbar\omega_{\vec{q}\lambda}+E_{\vec{k}+\vec{q}+\vec{Q}}}\right].$$

(3.3.27)

The first term survives into the normal state and evolves into the usual electron–phonon self–energy due to the $c_{\vec{k}\sigma}$ operators. The second term will give us the corrections due to the superconducting state. The two self–energies, $\Sigma^{ret}_{\gamma\gamma^\dagger}(\vec{k},E)$, and $\Sigma^{ret}_{\gamma^\dagger\gamma^\dagger}(\vec{k},E)$, have a similar functional form and we can split off a common function,

$$\Im\left(\hbar\,\Xi(\vec{k},E)\right) = -\pi\sum_{\vec{q}\vec{Q}\lambda}\left|g(\vec{q},\vec{Q},\lambda)\right|^2\frac{\Delta_{\vec{k}+\vec{q}+\vec{Q}}}{2E_{\vec{k}+\vec{q}+\vec{Q}}}$$
$$\times\left[\delta\left(E-\hbar\omega_{\vec{q}\lambda}-E_{\vec{k}+\vec{q}+\vec{Q}}\right)-\delta\left(E+\hbar\omega_{\vec{q}\lambda}+E_{\vec{k}+\vec{q}+\vec{Q}}\right)\right],$$

(3.3.28)

and

$$\Re\left(\hbar\,\Xi(\vec{k},E)\right) = \sum_{\vec{q}\vec{Q}\lambda}\left|g(\vec{q},\vec{Q},\lambda)\right|^2\frac{\Delta_{\vec{k}+\vec{q}+\vec{Q}}}{2E_{\vec{k}+\vec{q}+\vec{Q}}}\left[\frac{1}{E-\hbar\omega_{\vec{q}\lambda}-E_{\vec{k}+\vec{q}+\vec{Q}}}-\frac{1}{E+\hbar\omega_{\vec{q}\lambda}+E_{\vec{k}+\vec{q}+\vec{Q}}}\right.$$
$$\left.-\frac{1}{E_{\vec{k}}-\hbar\omega_{\vec{q}\lambda}-E_{\vec{k}+\vec{q}+\vec{Q}}}+\frac{1}{E_{\vec{k}}+\hbar\omega_{\vec{q}\lambda}+E_{\vec{k}+\vec{q}+\vec{Q}}}\right]. \tag{3.3.29}$$

The real part of this function vanishes at $E = E_{\vec{k}}$ by construction and its magnitude is small compared to the normal piece due to the $\frac{\Delta_{\vec{k}+\vec{q}+\vec{Q}}}{E_{\vec{k}+\vec{q}+\vec{Q}}}$ factor. The imaginary part is zero at $E = 0$. The self–energies become

$$\hbar\Sigma^{ret}_{\gamma\gamma^\dagger}(\vec{k},E) = \frac{1}{2}\sum_{\vec{q}\vec{Q}\lambda}\left|g(\vec{q},\vec{Q},\lambda)\right|^2\left[\frac{1}{E-\hbar\omega_{\vec{q}\lambda}-E_{\vec{k}+\vec{q}+\vec{Q}}+i\delta}+\frac{1}{E+\hbar\omega_{\vec{q}\lambda}+E_{\vec{k}+\vec{q}+\vec{Q}}+i\delta}\right]$$
$$-\frac{\Delta_{\vec{k}}}{E_{\vec{k}}}\,\hbar\,\Xi(\vec{k},E) \tag{3.3.30}$$

and

$$\hbar\Sigma^{ret}_{\gamma^\dagger\gamma^\dagger}(\vec{k},E) = -\frac{\xi_{\vec{k}}}{E_{\vec{k}}}\,\hbar\,\Xi(\vec{k},E). \tag{3.3.31}$$

3.4 Solution of the Gap Equation in Pb

The gap equation was given by

$$\lim_{T\to 0}\Delta_{\vec{k}} = \sum_{\vec{q}\vec{Q}\lambda}\left|g(\vec{q},\vec{Q},\lambda)\right|^2\frac{\Delta_{\vec{k}+\vec{q}+\vec{Q}}}{2E_{\vec{k}+\vec{q}+\vec{Q}}}\mathcal{P}\left[\frac{1}{E_{\vec{k}}+\hbar\omega_{\vec{q}\lambda}+E_{\vec{k}+\vec{q}+\vec{Q}}}-\frac{1}{E_{\vec{k}}-\hbar\omega_{\vec{q}\lambda}-E_{\vec{k}+\vec{q}+\vec{Q}}}\right]. \tag{3.4.1}$$

The gap equation (3.4.1) implicitly defines the gap function in terms of an integral equation. This gap function is further renormalized by the self–energy $\Sigma_{\gamma\gamma^\dagger}(\vec{k},E)$ which will shift the pole in the

single–particle Green's function at the Fermi surface. This is a small effect and we will ignore it here.

A solution can be calculated by iteration for instance. One starts with some approximate values of $\Delta_{\vec{k}}$ and calculates the right hand side of eq. (3.4.1). The left hand side replaces the initially assumed gap function better approximating the "true" gap function. The whole process is repeated until the change between two successive iterative steps is only very small. Since the characteristic energies of the gap function is about a factor of 1000 smaller than the characteristic electron energies, we can expect that only states $\vec{k}+\vec{q}+\vec{Q}$ which are close to the Fermi surface will contribute to the integral in eq. (3.4.1). This suggests that we use $\vec{k}'=\vec{k}+\vec{q}+\vec{Q}$ and write

$$\Delta_{\vec{k}} = \sum_{\vec{k}'\lambda} \left| g(\vec{k}'-\vec{k},\lambda) \right|^2 \frac{\Delta_{\vec{k}'}}{2E_{\vec{k}'}} \mathcal{P}\left[\frac{1}{E_{\vec{k}}+\hbar\omega_{\vec{q}}+E_{\vec{k}'}} - \frac{1}{E_{\vec{k}}-\hbar\omega_{\vec{q}}-E_{\vec{k}'}} \right]. \tag{3.4.2}$$

Our electron model contains two bands. There will be contributions from scattering from one band to the same band and from one band to the other. The gap equation will therefore have to be summed over the two bands and will have to allow for two different gap functions on the two bands. We therefore write

$$\begin{aligned} \Delta^{(2)}_{\vec{k}} &= \sum_{\vec{k}'\lambda}^{(2)} \left| g(\vec{k}'-\vec{k},\lambda) \right|^2_{(22)} \frac{\Delta^{(2)}_{\vec{k}'}}{2E_{\vec{k}'}} \mathcal{P}\left[\frac{1}{E_{\vec{k}}+\hbar\omega_{\vec{q}}+E_{\vec{k}'}} - \frac{1}{E_{\vec{k}}-\hbar\omega_{\vec{q}}-E_{\vec{k}'}} \right] \\ &\quad + \sum_{\vec{k}'\lambda}^{(3)} \left| g(\vec{k}'-\vec{k},\lambda) \right|^2_{(23)} \frac{\Delta^{(3)}_{\vec{k}'}}{2E_{\vec{k}'}} \mathcal{P}\left[\frac{1}{E_{\vec{k}}+\hbar\omega_{\vec{q}}+E_{\vec{k}'}} - \frac{1}{E_{\vec{k}}-\hbar\omega_{\vec{q}}-E_{\vec{k}'}} \right] \end{aligned} \tag{3.4.3}$$

and

$$\begin{aligned} \Delta^{(3)}_{\vec{k}} &= \sum_{\vec{k}'\lambda}^{(2)} \left| g(\vec{k}'-\vec{k},\lambda) \right|^2_{(32)} \frac{\Delta^{(2)}_{\vec{k}'}}{2E_{\vec{k}'}} \mathcal{P}\left[\frac{1}{E_{\vec{k}}+\hbar\omega_{\vec{q}}+E_{\vec{k}'}} - \frac{1}{E_{\vec{k}}-\hbar\omega_{\vec{q}}-E_{\vec{k}'}} \right] \\ &\quad + \sum_{\vec{k}'\lambda}^{(3)} \left| g(\vec{k}'-\vec{k},\lambda) \right|^2_{(33)} \frac{\Delta^{(3)}_{\vec{k}'}}{2E_{\vec{k}'}} \mathcal{P}\left[\frac{1}{E_{\vec{k}}+\hbar\omega_{\vec{q}}+E_{\vec{k}'}} - \frac{1}{E_{\vec{k}}-\hbar\omega_{\vec{q}}-E_{\vec{k}'}} \right]. \end{aligned} \tag{3.4.4}$$

The sums $\sum_{\vec{k}'\lambda}^{(i)}$ are to be summed only over $\vec{k}'$ in the i$^{\text{th}}$ band. We recall the definition of the electron–phonon interaction, eq. (2.1.28).

$$g(\vec{q},\vec{Q},\lambda) = -i\sqrt{\frac{\hbar^2}{2N_0\,M\,\hbar\omega_{\vec{q}\lambda}}}\left(\vec{q}+\vec{Q}\right)\cdot\hat{\eta}_{\vec{q}\lambda}U(\vec{q}+\vec{Q}), \tag{3.4.5}$$

where $U(\vec{q}+\vec{Q})$ is $\langle\kappa_1|\,u(\vec{r})\,|\kappa_2\rangle$, which is taken between two electron states. In the case of different bands we have to allow for different matrix elements indicated by the two subscripts, (ij), in $\left|g(\vec{k}'-\vec{k},\lambda)\right|^2_{(ij)}$. They will be symmetric however with respect to the state scattered from and the state scattered to. In other words we can write

$$\left|g(\vec{k}'-\vec{k},\lambda)\right|^2_{(23)} = \left|g(\vec{k}'-\vec{k},\lambda)\right|^2_{(32)}. \tag{3.4.6}$$

For simplicity we will use only one pseudopotential function and allow for differences in the matrix elements through an additional scaling factor. The gap equation then yields

$$\begin{aligned}\Delta^{(2)}_{\vec{k}} &= \sum_{\vec{k}'\lambda}^{(2)} a^2_{(22)}\left|g(\vec{k}'-\vec{k},\lambda)\right|^2\frac{\Delta^{(2)}_{\vec{k}'}}{2E_{\vec{k}'}}\mathcal{P}\left[\frac{1}{E_{\vec{k}}+\hbar\omega_{\vec{q}}+E_{\vec{k}'}}-\frac{1}{E_{\vec{k}}-\hbar\omega_{\vec{q}}-E_{\vec{k}'}}\right]\\ &\quad+\sum_{\vec{k}'\lambda}^{(3)} a^2_{(23)}\left|g(\vec{k}'-\vec{k},\lambda)\right|^2\frac{\Delta^{(3)}_{\vec{k}'}}{2E_{\vec{k}'}}\mathcal{P}\left[\frac{1}{E_{\vec{k}}+\hbar\omega_{\vec{q}}+E_{\vec{k}'}}-\frac{1}{E_{\vec{k}}-\hbar\omega_{\vec{q}}-E_{\vec{k}'}}\right]\end{aligned} \tag{3.4.7}$$

and

$$\begin{aligned}\Delta^{(3)}_{\vec{k}} &= \sum_{\vec{k}'\lambda}^{(2)} a^2_{(23)}\left|g(\vec{k}'-\vec{k},\lambda)\right|^2\frac{\Delta^{(2)}_{\vec{k}'}}{2E_{\vec{k}'}}\mathcal{P}\left[\frac{1}{E_{\vec{k}}+\hbar\omega_{\vec{q}}+E_{\vec{k}'}}-\frac{1}{E_{\vec{k}}-\hbar\omega_{\vec{q}}-E_{\vec{k}'}}\right]\\ &\quad+\sum_{\vec{k}'\lambda}^{(3)} a^2_{(33)}\left|g(\vec{k}'-\vec{k},\lambda)\right|^2\frac{\Delta^{(3)}_{\vec{k}'}}{2E_{\vec{k}'}}\mathcal{P}\left[\frac{1}{E_{\vec{k}}+\hbar\omega_{\vec{q}}+E_{\vec{k}'}}-\frac{1}{E_{\vec{k}}-\hbar\omega_{\vec{q}}-E_{\vec{k}'}}\right].\end{aligned} \tag{3.4.8}$$

The $a_{(ij)}$ are determined by constraints given by experiment. Although the values of $\Delta_{\vec{k}}^{(2)}$ and $\Delta_{\vec{k}}^{(3)}$ are renormalized by $\Sigma_{\gamma\gamma^\dagger}(\vec{k}, E)$ we will assume that these renormalizations are small and require that the $\Delta_{\vec{k}}^{(i)}$ at $\vec{k} = \vec{k}_F$ are equal to the experimental values. From electronic specific heat measurements we can calculate the effective mass enhancement due to the electron–phonon interaction. The coefficient in front of the linear T term in the electronic specific heat is measured as $\gamma = 3.14$ mJ K^{-2} mol^{-1} (Geschneidner, 1964,Table XIII). The coefficient is related to the density of states at the Fermi surface (Ashcroft and Wilkins, 1965) by

$$\gamma = \frac{1}{3}\pi^2 \, k_B^2 \, N^*(0), \tag{3.4.9}$$

where $N^*(0)$ is the electronic density of states at the Fermi surface. It is given in terms of the band structure density of states, $N_{bs}(0) = 2\left\{\sum_{\vec{k}}^{(2)} \delta(\xi_{\vec{k}}) + \sum_{\vec{k}}^{(3)} \delta(\xi_{\vec{k}})\right\} = N_2(0) + N_3(0)$, as

$$N^*(0) = (1 + \lambda) \, N_{bs}(0), \tag{3.4.10}$$

where the enhancement factor, λ, is given by

$$\lambda = 2 \int d\omega \, \frac{\alpha^2 F(\omega)}{\omega}, \tag{3.4.11}$$

where $(1 + \lambda)$ is the effective mass enhancement due to the electron–phonon interaction. The quantity $\alpha^2 F(\omega)$ is an effective electron–phonon coupling strength, defined as

$$\alpha^2 F(\omega) = \frac{\sum_{\vec{k}} \sum_{\vec{k}'} \sum_{\lambda} \left| g(\vec{k}' - \vec{k}, \lambda) \right|^2 \delta(\omega - \omega_{\vec{k}'-\vec{k}\lambda}) \delta(\xi_{\vec{k}}) \delta(\xi_{\vec{k}'})}{N_{bs}(0)}. \tag{3.4.12}$$

Note that we use $\xi_{\vec{k}}$ since we mean the electron dispersion effected by band structure only. We will use the experimental electron and phonon dispersions to calculate $\alpha^2 F(\omega)$. Fig. 3.6 shows a plot of

Figure 3.6: Calculated Pb phonon density of states per atom and the electron–phonon coupling strength, $\alpha^2F(E)$ compared to values quoted in Scalapino (1969)

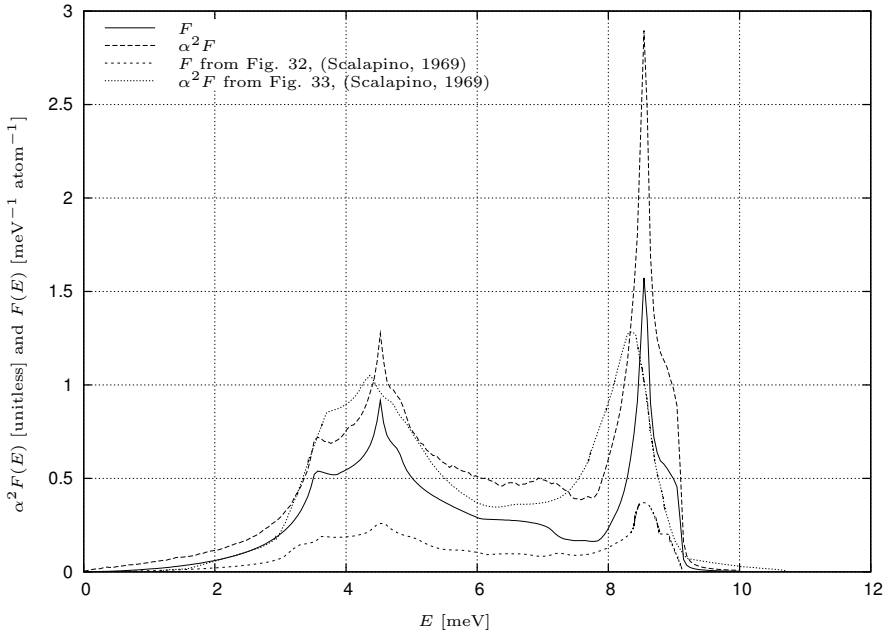

the phonon density of states and the electron–phonon coupling strength $\alpha^2F(\omega)$ as calculated using the phonon dispersion from Cowley (1974b) and the Ashcroft pseudopotential with parameters given in Table 2.1. The specific heat coefficient γ is given by

$$\gamma = \frac{1}{3}\pi^2 \, k_B^2 \, N_{bs}(0) \, (1 + \lambda). \tag{3.4.13}$$

We calculated the density of states using the model by Anderson and Gold and found $N_2(0) = 8.96 \times 10^{-2}$ atom^{-1} spin^{-1} eV^{-1} and $N_3(0) = 2.22 \times 10^{-1}$ atom^{-1} spin^{-1} eV^{-1} for the second and third bands, respectively. With the experimentally determined value for $\gamma = 3.14$ mJ K^{-2} mol^{-1}, the effective mass enhancement factor was found to be $\lambda = 1.138$. Going back to the definition of $\alpha^2F(\omega)$, eq. (3.4.12), the extension to two bands is given by,

$$\alpha^2F_{(ij)}(\omega) = \frac{\sum_{\vec{k}}^{(i)} \sum_{\vec{k}'}^{(j)} \sum_{\lambda} \left| g(\vec{k}' - \vec{k}, \lambda) \right|^2 \delta(\omega - \omega_{\vec{k}' - \vec{k}\lambda}) \delta(\xi_{\vec{k}}) \delta(\xi_{\vec{k}'})}{N_{bs}(0)}, \tag{3.4.14}$$

where the band–labels, $i, j \in \{2, 3\}$, and λ is given by

$$\lambda = a^2_{(22)}\lambda_{(22)} + 2a^2_{(23)}\lambda_{(23)} + a^2_{(33)}\lambda_{(33)}, \tag{3.4.15}$$

where

$$\lambda_{(ij)} = 2\int d\omega \, \frac{\alpha^2 F_{(ij)}(\omega)}{\omega}. \tag{3.4.16}$$

3.5 Gap Calculation Results

Given the coupled equations for $\Delta^{(2)}_{\vec{k}}$ and $\Delta^{(3)}_{\vec{k}}$, and the constraint equation for λ we can determine the scaling parameters $a_{(22)}$, $a_{(23)}$, and $a_{(33)}$. We calculated the $\lambda_{(ij)}$ and found, $\lambda_{(22)} = 1.24 \times 10^{-1}$, $\lambda_{(23)} = 5.50 \times 10^{-1}$, and $\lambda_{(33)} = 2.03$. In Farnworth's Ph.D. thesis (Farnworth, 1976) and in a journal publication with Timusk (Farnworth and Timusk, 1974), measurements the superconducting gap on thin lead films by infrared absorption were published and it was found that lead exhibits two distinct gaps which were attributed to the existence of two bands in the electronic spectrum. The values found are

$$\Delta_0 = \begin{cases} 1.286 \text{ meV} \\ 1.379 \text{ meV}. \end{cases} \tag{3.5.1}$$

This measurement can not determine which of the two bands has the larger value of Δ_0. We therefore carried out the gap calculation for both possibilities later in this chapter.

Table 3.3: Comparison of different runs of the gap equation for constant gaps on the two bands

$\Delta_0^{(2)}$ [meV]	$\Delta_0^{(3)}$ [meV]	$a_{(22)}$	$a_{(23)}$	$a_{(33)}$	λ
1.286	1.379	0.386502	0.5	0.482772	0.76679
		0.653063	0.4	0.518665	0.77516
		0.942515	0.1	0.573517	0.789145
1.379	1.286	0.483813	0.5	0.464433	0.7421
		0.699406	0.4	0.504701	0.75393
		0.956204	0.1	0.565479	0.77377

3.5.1 Constant Gap Calculation

In a first pass, we calculated the superconducting gap in the simplest approximation. We did not allow for any angular or radial dependence of the gap function but allowed the gap to be different on the two bands. We did not consider the λ–condition eq. (3.4.15) yet, but included the effective mass enhancement in our results. This means that we needed to find three independent parameters, such that the gap on the Fermi surface converges toward the values given in eqs. (3.5.1). Our results are given in Table 3.3.

We have included the effective mass enhancement factor, λ, which would be implied through eq. (3.4.15) for comparison. We considered different values of $a_{(23)}$ and our calculated λ turns out to be remarkably insensitive to the different cases. It is interesting to note also that the calculated values for λ are all consistently lower than the value expected from specific heat measurements. We keep in mind however that we have, as stated earlier, assumed simple model in this calculation, which presumably is quite a rough approximation. We therefore might not expect good agreement with the specific heat data.

3.5.2 $\left|\vec{k}\right|$–dependent Gap Calculation

In a second pass we therefore allowed the gaps on the two bands to have a $\left|\vec{k}\right|$–dependence. In Figs. 3.7 and 3.8 we show our results for a calculation using 12 points in k. For the second band gap, we chose the direction to be along the z–axis. We do not expect much of an angular dependence in

Figure 3.7: Converged $\left|\vec{k}\right|$–dependent gap on both bands, assuming $\Delta_0^{(2)} = 1.286$ meV, and $\Delta_0^{(3)} = 1.379$ meV

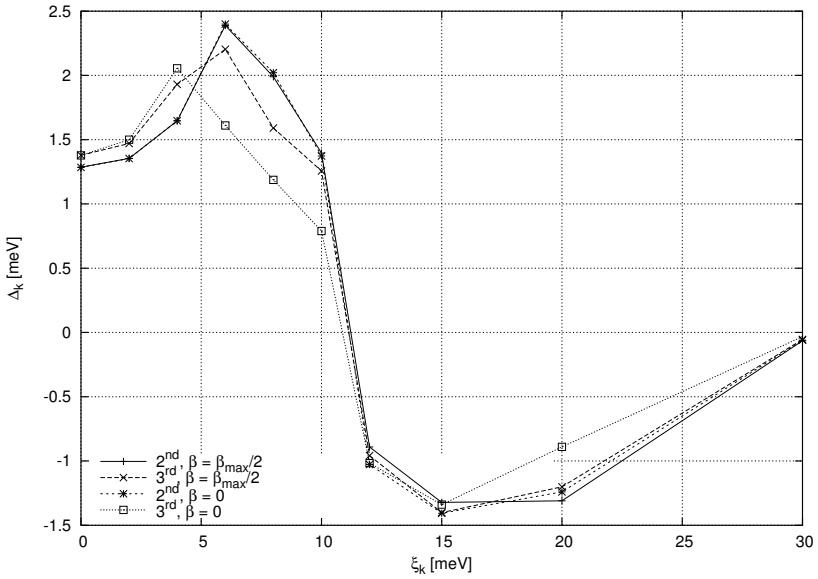

the second band since the Fermi surface is close to spherical. The third band Fermi surface is quite anisotropic and we performed the gap calculation along two different directions.

There are two types of "pipes" making up the third band which we discussed earlier. One type is between two hexagonal faces of the Brillouin zone, and the other type between a hexagonal face and a square face. We parametrized the third band in terms of cylindrical coordinates, with β representing the polar angle and z the height on the cylinder. For the direction in the third band, we chose a vector starting from the center of the first type of pipes. The polar angles are such that $\beta = 0$ means a direction perpendicular to the zone edge pointing along the zone surface. The angle $\hat{\beta}$ represents the angle between the two zone surfaces that intersect at the zone edge. The angle $\hat{\beta}/2$ therefore is a direction half way between the two surfaces which is a direction pointing toward the zone center, Γ.

Again we did not use the λ–condition in this calculation but rather adjusted the three coefficients independently from one another to generate convergence on the Fermi surface to the measured gap values. The values for the coefficients $a_{(ij)}$ we found are shown in Table 3.4.

As expected, the calculated effective mass enhancement factors are now much closer to the exper-

Figure 3.8: Converged $\left|\vec{k}\right|$–dependent gap on both bands, assuming $\Delta_0^{(2)} = 1.379$ meV, and $\Delta_0^{(3)} = 1.286$ meV

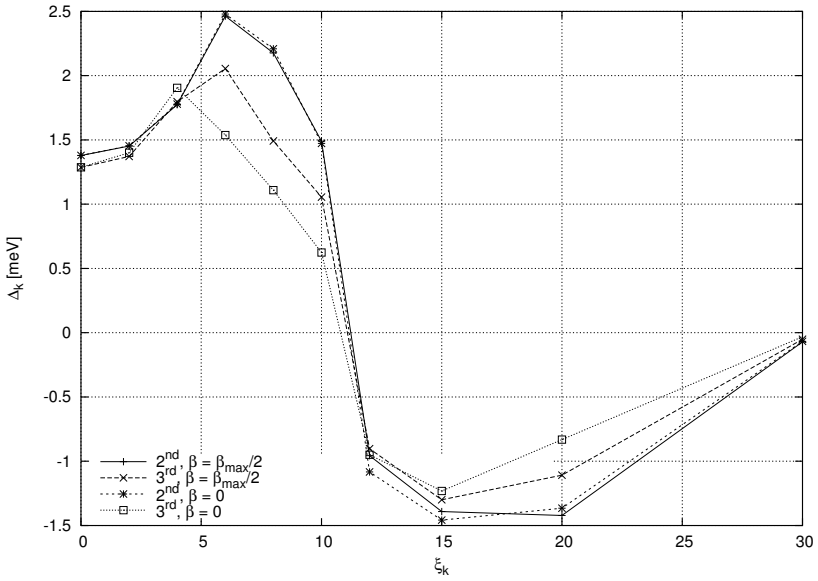

Table 3.4: Comparison of different runs of the gap equation for k–dependent gaps on the two bands using 12 points for k.

$\Delta_0^{(2)}$ [meV]	$\Delta_0^{(3)}$ [meV]	β	$a_{(22)}$	$a_{(23)}$	$a_{(33)}$	λ
1.286	1.379	$\beta = \hat{\beta}/2$	0.612875	0.5	0.557987	0.95381
		$\beta = \hat{\beta}/2$	0.194861	0.6	0.516413	0.94221
		$\beta = 0$	0.636930	0.5	0.552350	0.94483
1.379	1.286	$\beta = \hat{\beta}/2$	0.681441	0.5	0.539507	0.9236
		$\beta = \hat{\beta}/2$	0.378770	0.6	0.493400	0.90809
		$\beta = 0$	0.701047	0.5	0.531859	0.9104

imental value of $\lambda = 1.138$ as found from specific heat data. The largest effective mass enhancement was found for the case in which we put the smaller one of Farnworth's gaps on the second band, and chose the direction in the third band to be toward the Γ point.

One expects that one can further improve on the agreement between the calculated effective mass enhancement and the measured one by either using more points in k or making the gap angle dependent. This angular dependence should be especially important on the third band. Due to the iterative nature of the current 12–point calculation we need to run our program for about a CPU day of calculation time to find a convergent solution[3.3]. A more complete treatment would involve allowing the $\Delta_{\vec{k}}$ on the two types of pipe surfaces making up the Fermi surface of the third band to be different. However a further increase in points will render this calculation computationally intractable[3.4].

3.6 Single–Particle Self–Energies, $\Sigma_{\gamma\gamma^\dagger}$ and $\Sigma_{\gamma^\dagger\gamma^\dagger}$

At zero temperature, we found that the two self–energies, $\Sigma^{ret}_{\gamma\gamma^\dagger}(\vec{k},E)$, and $\Sigma^{ret}_{\gamma^\dagger\gamma^\dagger}(\vec{k},E)$, to leading order in the electron–phonon interaction were given by

$$\begin{aligned}\hbar\Sigma^{ret}_{\gamma\gamma^\dagger}(\vec{k},E) &= \frac{1}{2}\sum_{\vec{q}\vec{Q}\lambda}\left|g(\vec{q},\vec{Q},\lambda)\right|^2\left[\frac{1}{E-\hbar\omega_{\vec{q}\lambda}-E_{\vec{k}+\vec{q}+\vec{Q}}+i\delta}+\frac{1}{E+\hbar\omega_{\vec{q}\lambda}+E_{\vec{k}+\vec{q}+\vec{Q}}+i\delta}\right] \\ &\qquad -\frac{\Delta_{\vec{k}}}{E_{\vec{k}}}\,\hbar\,\Xi(\vec{k},E) \\ &= \hbar\Sigma^{N}_{\gamma\gamma^\dagger}(\vec{k},E)-\frac{\Delta_{\vec{k}}}{E_{\vec{k}}}\,\hbar\,\Xi(\vec{k},E), \qquad (3.6.1)\end{aligned}$$

where the function $\Xi(\vec{k},E)$ was defined as

[3.3] We ran the program with 23 k–points for $\beta = \hat{\beta}/2$ and found that the gap hardly differs from our 12 k–point calculation.

[3.4] This calculation was done on a 4 node computer cluster in the physics department. The main CPU was a Athlon XP 2700+ and the three secondary nodes ran Intel Celeron 1400MHz CPUs. In addition a dual Athlon MP 1200MHz SMP workstation was used.

$$\begin{aligned}\Im\left(\hbar\,\Xi(\vec{k},E)\right) &= -\pi\sum_{\vec{q}\vec{Q}\lambda}\left|g(\vec{q},\vec{Q},\lambda)\right|^2\frac{\Delta_{\vec{k}+\vec{q}+\vec{Q}}}{2E_{\vec{k}+\vec{q}+\vec{Q}}}\\ &\quad\times\left[\delta\left(E-\hbar\omega_{\vec{q}\lambda}-E_{\vec{k}+\vec{q}+\vec{Q}}\right)-\delta\left(E+\hbar\omega_{\vec{q}\lambda}+E_{\vec{k}+\vec{q}+\vec{Q}}\right)\right],\end{aligned}\tag{3.6.2}$$

and

$$\begin{aligned}\Re\left(\hbar\,\Xi(\vec{k},E)\right) &= \sum_{\vec{q}\vec{Q}\lambda}\left|g(\vec{q},\vec{Q},\lambda)\right|^2\frac{\Delta_{\vec{k}+\vec{q}+\vec{Q}}}{2E_{\vec{k}+\vec{q}+\vec{Q}}}\left[\frac{1}{E-\hbar\omega_{\vec{q}\lambda}-E_{\vec{k}+\vec{q}+\vec{Q}}}-\frac{1}{E+\hbar\omega_{\vec{q}\lambda}+E_{\vec{k}+\vec{q}+\vec{Q}}}\right.\\ &\quad\left.-\frac{1}{E_{\vec{k}}-\hbar\omega_{\vec{q}\lambda}-E_{\vec{k}+\vec{q}+\vec{Q}}}+\frac{1}{E_{\vec{k}}+\hbar\omega_{\vec{q}\lambda}+E_{\vec{k}+\vec{q}+\vec{Q}}}\right].\end{aligned}\tag{3.6.3}$$

The off–diagonal part of the quasi–particle self–energy was given by

$$\hbar\Sigma_{\gamma^\dagger\gamma^\dagger}(\vec{k},E)=-\frac{\xi_{\vec{k}}}{E_{\vec{k}}}\;\hbar\,\Xi(\vec{k},E).\tag{3.6.4}$$

We calculated the normal part of the self–energy and the function $\Xi(\vec{k},E)$ for the four possible scattering events $2\rightarrow 2$, $2\rightarrow 3$, $3\rightarrow 2$, and $3\rightarrow 3$. Although we have assumed symmetry in the pseudopotential matrix elements with respect to $2\rightarrow 3$ ad $3\rightarrow 2$, we do not expect this symmetry for $\Sigma^{(23)}(\vec{k},E)$ and $\Sigma^{(32)}(\vec{k},E)$ because of the very different topology of the Fermi surface in the two bands.

As our results show, the self–energy is not sensitive to the incoming electron momentum. Due to our subtracting of the gap condition from the real part of $\Sigma_{\gamma\gamma^\dagger}(\vec{k},E)$, the real part of $\Xi(\vec{k},E)\propto(E-E_{\vec{k}})$ and will vanish on shell at $E=E_{\vec{k}}$. There will be a slight $\vec{k}$–dependence in this contribution. In the following we show plots of $\Sigma^{(ij),N}(\vec{k},E)$ and $\Xi^{(ij)}(\vec{k},E)$ for two incoming momenta $\vec{k}$, $\xi_{\vec{k}}=0$ meV and $\xi_{\vec{k}}=-2$ meV. The direction of $\vec{k}$ on the second band (contributions $2\rightarrow 2$ and $3\rightarrow 2$) was chosen along the z–axis and for the third band (contributions $2\rightarrow 3$ and $3\rightarrow 3$) on a type 1 third band in the center of the "pipe", $z=1/2$, and in a direction toward the zone center, Γ,

Figure 3.9: Fig. 16.6 from Mahan (1990) showing the normal state second order self–energy.

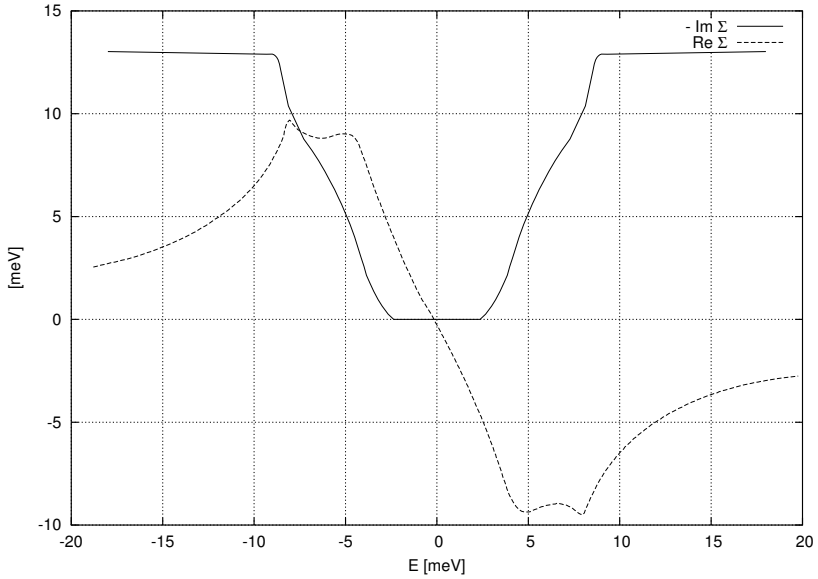

$\beta = \hat{\beta}/2$. Because the self–energies hardly exhibit any momentum dependence, we omitted symbols in the graphs for the $\xi_{\vec{k}} = -2$ meV data. The energies at which we calculated this contribution are identical to the energies used for $\xi_{\vec{k}} = 0$ meV. The four contributions are shown in Figs. 3.10, 3.11, 3.12, and 3.13. It is evident that scattering into the third band is by far the dominant scattering contribution and that scattering into the second band plays only a minor role. This can be seen by comparing the magnitudes of the self–energies. This can not only be explained on the basis of the fact that the surface area of the third band Fermi surface is much larger than the surface area of the second band. As we will discuss in the following chapter, the complicated topology of the third band is important in a qualitatively accurate description of the superconducting properties of lead and it is necessary to include it.

There are several things to note. In the normal state, the self–energy reduces to essentially what is shown in Fig. 3.9. The calculation shown was done by Grimvall (1981) using a simple model phonon dispersion relation and a spherical free electron like electron dispersion relation. The imaginary part is zero until at around 4.5 meV which coincides with the occurrence with the first large peak in the α^2F for lead. At around 9 meV, the phonon spectrum is exhausted and the imaginary part flattens out. The real part which peaks between 4.5 meV, the first peak in α^2F, and 8.5 meV, the second

Figure 3.10: $\Sigma^{(22),N}(\vec{k},E)$ and $\Xi^{(22)}(\vec{k},E)$ contributions to intra–band scattering of the self–energy in the second band.

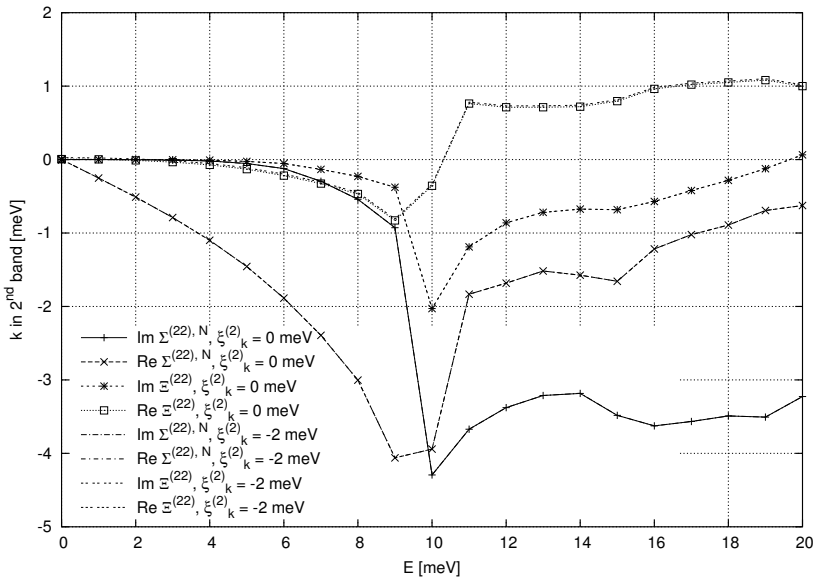

peak in α^2F falls off at higher energies and asymptotically goes to zero because there are no phonon energies that can satisfy the energy difference in the denominators and make it diverge.

The normal piece in our calculation goes over to the normal state result when $\Delta \to 0$ and we see very similar behavior in our results. The two α^2F related features now occur at energies 4.5 meV + Δ_0, and 8.5 meV + Δ_0, which corresponds to energies of 5.8 meV and 9.8 meV if the average gap measured by Farnworth is taken to be 1.3 meV. The phase space accessible for the $2 \to 2$ and $3 \to 2$ contributions causes a feature at the high energy 8.5 meV peak only and no features are evident at the lower 4.5 meV peak. Scattering to the third band, the $2 \to 3$ and $3 \to 3$ contributions, show features at both energies which demonstrates the importance of the third band in our model.

Due to the $\frac{\Delta_{\vec{k}+\vec{q}+\vec{Q}}}{E_{\vec{k}+\vec{q}+\vec{Q}}}$ factor in $\Xi(\vec{k},E)$ the magnitude of the real and imaginary parts of $\Xi(\vec{k},E)$ are smaller than the corresponding parts in $\Sigma^N(\vec{k},E)$. Because the gap changes sign at around 10 meV, the sign of $\Xi(\vec{k},E)$ also changes, but at much higher energies. The high energy behavior beyond $E = 20$ meV is not shown but our calculations show that $\Im\left(\Sigma^N(\vec{k},E>20\text{ meV})\right)$ and $\Re\left(\Xi(\vec{k},E>20\text{ meV})\right)$ asymptotically approach zero. The other two contributions stay flat to at least 70 meV.

Figure 3.11: $\Sigma^{(23),N}(\vec{k},E)$ and $\Xi^{(23)}(\vec{k},E)$ contributions to the self–energy for $\vec{k}$ in the second band due to scattering into third band states.

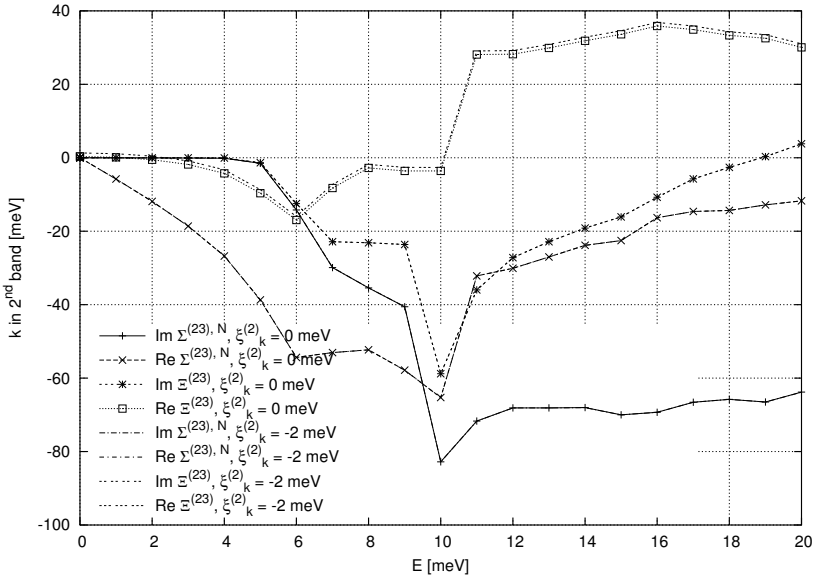

Figure 3.12: $\Sigma^{(32),N}(\vec{k},E)$ and $\Xi^{(32)}(\vec{k},E)$ contributions to the self–energy for $\vec{k}$ in the third band due to scattering into second band states.

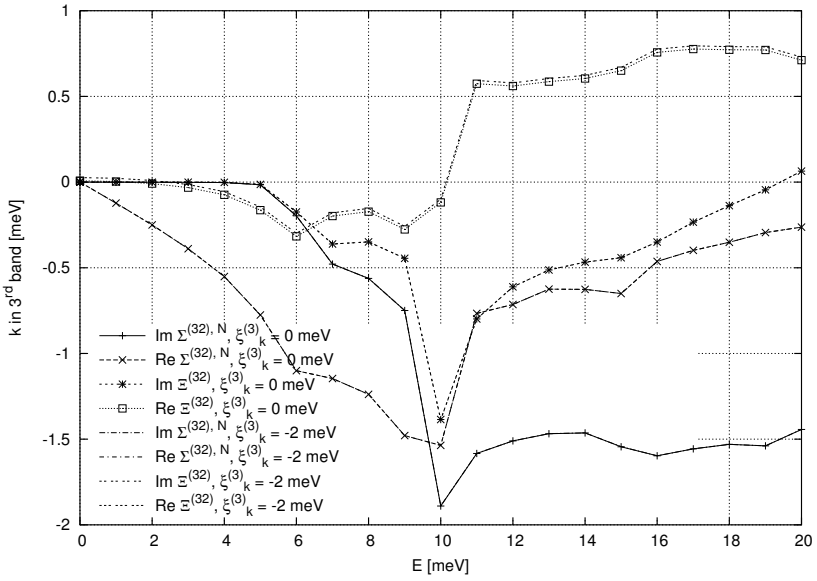

Figure 3.13: $\Sigma^{(33),N}(\vec{k},E)$ and $\Xi^{(33)}(\vec{k},E)$ contributions to intra–band scattering of the self–energy in the third band.

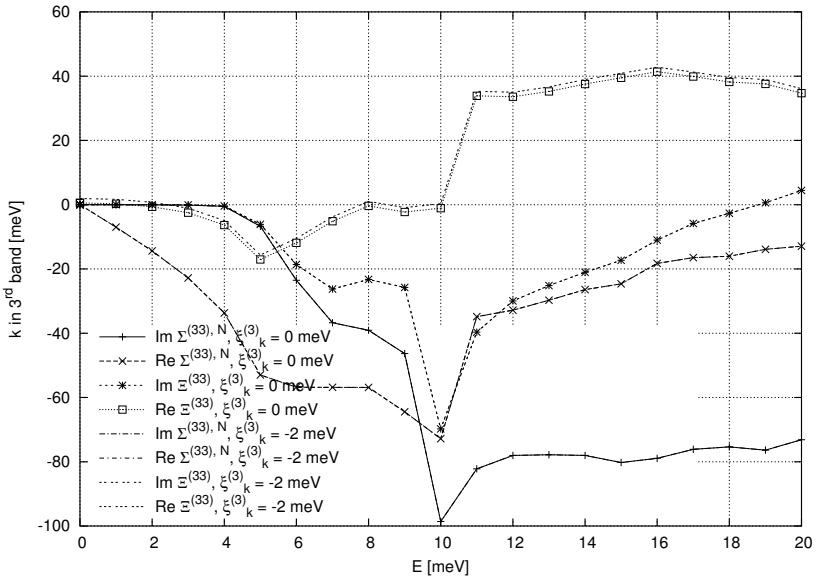

Figure 3.14: $\Sigma_{\gamma\gamma^\dagger}(\vec{k},E)$ and $\Sigma_{\gamma^\dagger\gamma^\dagger}(\vec{k},E)$ for $\vec{k}$ in the second band.

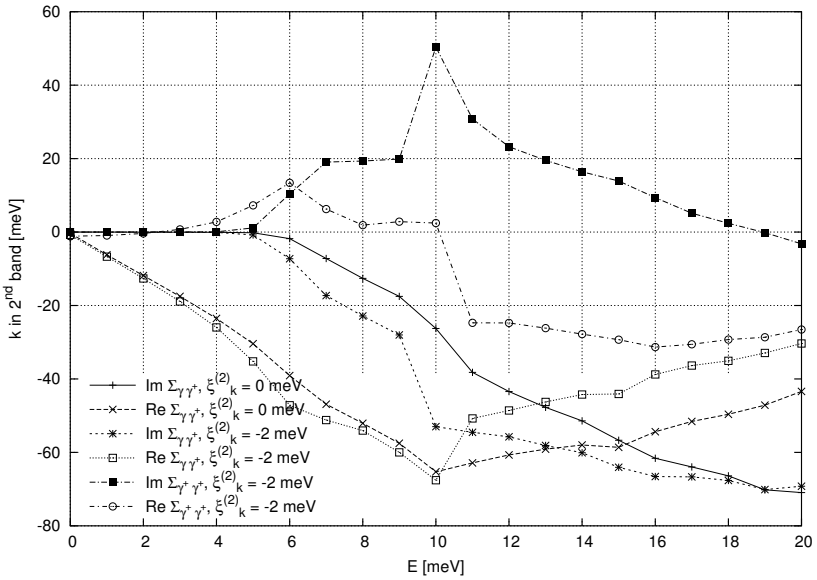

Figure 3.15: $\Sigma_{\gamma\gamma^\dagger}(\vec{k}, E)$ and $\Sigma_{\gamma^\dagger\gamma^\dagger}(\vec{k}, E)$ for $\vec{k}$ in the third band.

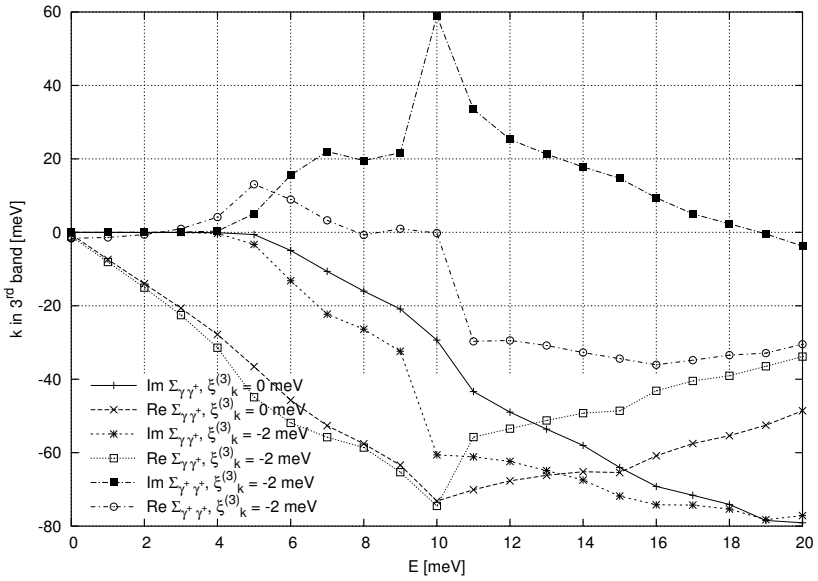

3.7 Spectral Density and ARPES

The spectral density is given by the imaginary part of the retarded Greens function.

$$A(\vec{k}\sigma, E) = -2\,\Im\left(\mathcal{G}^{ret}(\vec{k}\sigma, E)\right), \tag{3.7.1}$$

and satisfies the sum–rule,

$$1 = \int_{-\infty}^{\infty} \frac{dE}{2\pi\,\hbar}\; A(\vec{k}, E). \tag{3.7.2}$$

It is usually interpreted as a probability distribution and therefore has to be ≥ 0. Using Dyson's equation, the expression for the spectral density can be rewritten in terms of the self–energies,

$$A(\vec{k}\sigma, E) = -2 \frac{\Im\left(\Sigma^{ret}(\vec{k}\sigma, E)\right)}{\left[\hbar^{-1}E - \hbar^{-1}\xi_{\vec{k}} - \Re\left(\Sigma^{ret}(\vec{k}\sigma, E)\right)\right]^2 + \left[\Im\left(\Sigma^{ret}(\vec{k}\sigma, E)\right)\right]^2}. \tag{3.7.3}$$

We calculated the self–energy to second order in the interaction strength, $\left|g(\vec{q}, \vec{Q}, \lambda)\right|^2$. In order to be self–consistent with the spectral density, we will not use the above definition, but approximate the self–energy by

$$A(\vec{k}\sigma, E) \approx -2 \frac{\Im\left(\Sigma^{ret}(\vec{k}\sigma, E)\right)}{\left[\hbar^{-1}E - \hbar^{-1}E_{\vec{k}}\right]^2 + \Gamma^2}, \tag{3.7.4}$$

where $\Gamma = 0.2$ meV is a small parameter which will mimic lifetime broadening effects in the superconductor.

Angular resolved photo emission spectroscopy (ARPES) is a probe for occupied electron states below the Fermi surface. It is directly related to the spectral density, being given by the single–electron spectral density multiplied by the thermal Fermi–Dirac distribution (Damascelli *et al.*, 2003). We will therefore calculate the spectral density in the superconducting state from the self–energies calculated earlier. The single–particle Greens function splits into four terms within the BCS ground state formalism as shown in eq. (3.3.15). In the superconducting state, the single–particle spectral density is given by

$$\begin{aligned} A(\vec{k}\sigma, E) \quad = \quad & -2\left\{\left|u_{\vec{k}}\right|^2 \Im\left(\mathcal{G}^{ret}_{\gamma}(\vec{k}\sigma, E)\right) - \left|v_{\vec{k}}\right|^2 \Im\left(\mathcal{G}^{ret}_{\gamma}(\vec{k}\sigma, -E)\right)\right. \\ & \left. + u^*_{\vec{k}} v^*_{\vec{k}} \Im\left(\mathcal{F}^{\dagger}_{\gamma}(\vec{k}\sigma, E)\right) + u_{\vec{k}} v_{\vec{k}} \Im\left(\mathcal{F}^{\dagger}_{\gamma}(\vec{k}\sigma, -E)\right)\right\}. \end{aligned} \tag{3.7.5}$$

where we have used the relation stated previously, $\mathcal{F}_{\gamma}(\vec{k}, ik_n) = \mathcal{F}^{\dagger}_{\gamma}(\vec{k}, -ik_n)$. In terms of self–energies

Figure 3.16: The spectral density for $\vec{k}$ in the second band.

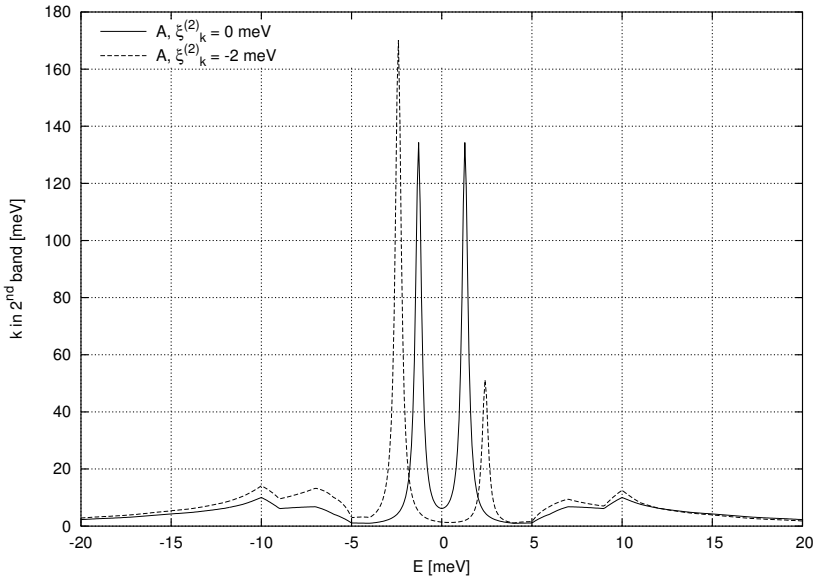

$$
\begin{aligned}
A(\vec{k}\sigma, E) \quad = \quad & -2 \Bigg\{ \left|u_{\vec{k}}\right|^2 \frac{\Im\left(\Sigma^{ret}_{\gamma\gamma^\dagger}(\vec{k}\sigma, E)\right)}{\left[\hbar^{-1}E - \hbar^{-1}E_{\vec{k}}\right]^2 + \Gamma^2} - \left|v_{\vec{k}}\right|^2 \frac{\Im\left(\Sigma^{ret}_{\gamma\gamma^\dagger}(\vec{k}\sigma, -E)\right)}{\left[\hbar^{-1}E + \hbar^{-1}E_{\vec{k}}\right]^2 + \Gamma^2} \\
& + u_{\vec{k}} v_{\vec{k}} \frac{\Im\left(\Sigma^{ret}_{\gamma^\dagger\gamma^\dagger}(\vec{k}\sigma, -E)\right)}{\left[\hbar^{-1}E + \hbar^{-1}E_{\vec{k}}\right]^2 + \Gamma^2} + u^*_{\vec{k}} v^*_{\vec{k}} \frac{\Im\left(\Sigma^{ret}_{\gamma^\dagger\gamma^\dagger}(\vec{k}\sigma, E)\right)}{\left[\hbar^{-1}E - \hbar^{-1}E_{\vec{k}}\right]^2 + \Gamma^2} \Bigg\}.
\end{aligned}
\tag{3.7.6}
$$

In passing we would like to point out that we got the self–energies at negative energies using $\Im\left(\Sigma^N_{\gamma\gamma^\dagger}(\vec{k}\sigma, -E)\right) = \Im\left(\Sigma^N_{\gamma\gamma^\dagger}(\vec{k}\sigma, E)\right)$, $\Re\left(\Sigma^N_{\gamma\gamma^\dagger}(\vec{k}\sigma, -E)\right) = -\Re\left(\Sigma^N_{\gamma\gamma^\dagger}(\vec{k}\sigma, E)\right)$, $\Im\left(\Xi(\vec{k}\sigma, -E)\right) = -\Im\left(\Xi(\vec{k}\sigma, E)\right)$, and $\Re\left(\Xi(\vec{k}\sigma, -E)\right) = \Re\left(\Xi(\vec{k}\sigma, E)\right)$.

Since we approximated the spectral density with eq. (3.7.6), the features in Figs. 3.16 and 3.17 are due to the imaginary parts of the self–energies. As we already discussed in the previous section, the main contribution to the self–energy and therefore spectral density comes from scattering into the third band. Both spectral densities for $\vec{k}$ on the second and third bands are dominated by this scattering contribution. The higher energy features in the spectral density at around 6 meV and 10 meV are due to corresponding features in th self–energies and ultimately due to large phonon density of states due to transverse and longitudinal phonon modes at 4.5 meV and 8.5 meV, respectively.

Figure 3.17: The spectral density for $\vec{k}$ in the third band.

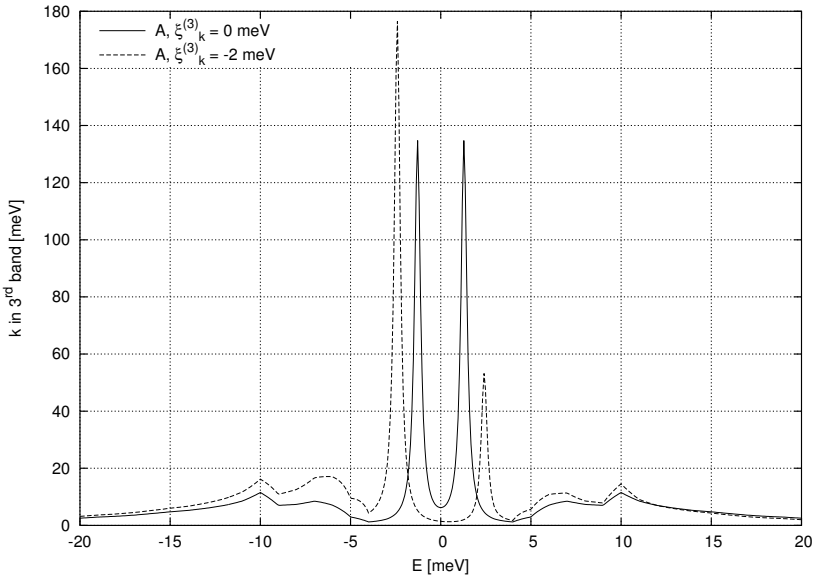

Figure 3.18: From (Chainani *et al.*, 2000,Fig. 1, left panel): Angle–integrated photoemission data on lead at $T = 5.3$ K (superconducting state) and $T = 12.0$ K (normal state).

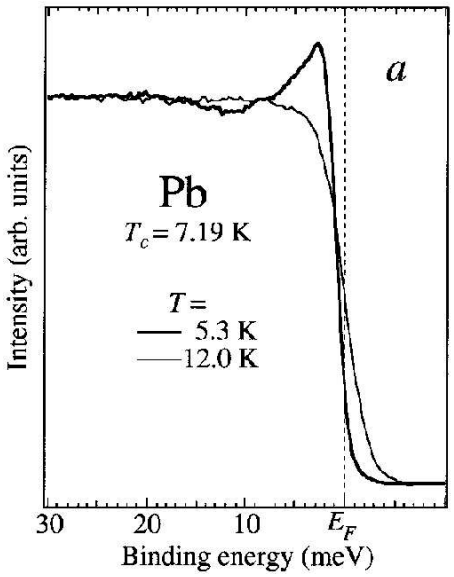

3.8 Comparison with Photoemission Data on Lead

We will compare our results with angle–integrated photoemission measurements by Chainani *et al.* (2000) on lead. Fig. 3.18 shows their angle–integrated photoemission data on lead in the superconducting and the normal states. In the superconducting state, the density of states below the Fermi surface exhibits piling up as expected due to the opening up of the gap. In order to compare our results with their data, we would need to integrate our spectral density function over momenta $\vec{k}$, i.e.

$$N(E) = \sum_{\vec{k}} A(\vec{k}, E). \tag{3.8.1}$$

Although we calculated the self–energy for two values of $\xi_{\vec{k}}$ only, we can predict its behavior at higher energies for the following reasons. Because the gap vanishes at energies $\xi_{\vec{k}} > 30$ meV, we expect the normal piece of the self–energy to go over into the normal state self–energy. The superconducting piece will not affect $\Sigma_{\gamma\gamma^\dagger}(\xi_{\vec{k}} > 30 \text{ meV}, E)$ for that same reason because of the $\frac{\Delta_{\vec{k}}}{E_{\vec{k}}}$ factor. Features in $\Xi(\vec{k}, E)$ will be pushed to higher energies in E because the $\frac{\Delta_{\vec{k}+\vec{q}+\vec{Q}}}{E_{\vec{k}+\vec{q}+\vec{Q}}}$ factor ensures that the scattered state, $\vec{k}+\vec{q}+\vec{Q}$, will be close to $\vec{k}_F$, and the phonon spectrum provides phonons only up to $\hbar\omega_{max} \approx 10$ meV. Its contribution will be small compared to the normal piece. Away from the Fermi surface the normal state behavior will therefore be recovered.

In the data, Fig. 3.18, a quasiparticle peak at around 3 meV, a dip features centered at around 11 meV and a broad hump centered at around 21 meV are visible in the superconducting spectrum. The normal spectrum essentially shows a Fermi–Dirac distribution. Chainani et al. interpret the dip and hump features as due to transverse and longitudinal phonon modes at 4.5 meV and 8.5 meV, respectively. We would like to comment on the possibility that this is the case.

There are a number of difficulties with a direct comparison of the calculation and the data. We calculated the self–energies and spectral densities at zero temperature, whereas the measurements were done at $T = 5.3$ K and $T = 12.0$ K for the superconducting and normal states, respectively. 5.3 K is about 50% of Δ_0 so that there could be some temperature dependence in the data missing from our calculation. Further the data is averaged over momenta which raises the question of whether the self–energy effects survive or are absorbed into the quasiparticle resonance for $E_{\vec{k}} \approx 4\Delta_0 \to 7\Delta_0$.

Having said this it is hard to imagine how a dip feature at 11 meV and a hump at 21 meV which is at least 10 meV higher in energy than the calculated features in $A(\vec{k}, E)$ can be accounted for by the electron–phonon interaction. Further the magnitude of the strong–coupling features — magnitude of the self–energy — is the same in the normal and superconducting states and so it is not clear why the features seen in the superconducting state would not also be seen in the normal state at the same temperature if they arise from the electron–phonon interaction. This could be done by driving the sample normal with a magnetic field. This seems to bring into question the procedure of normalizing data at 5.3 K with data measured at 12.0 K.

3.9 Higher Order Corrections

Higher order corrections in the electron–phonon interaction to our results for $\Sigma_{\gamma\gamma^\dagger}(\vec{k}, E)$ and $\Sigma_{\gamma\gamma}(\vec{k}, E)$ can be straight–forwardly calculated using perturbation theory. The next order corrections are represented in the diagrams

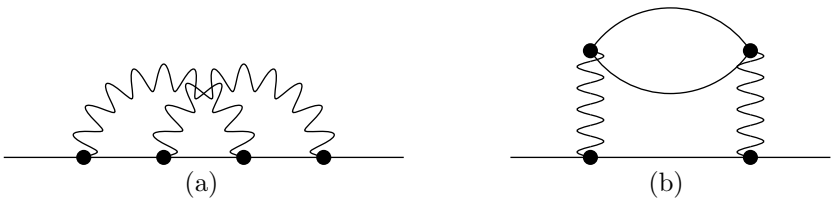

The corrections of type (a) can be neglected following Migdal's approximation (Migdal, 1958). This approximation has been recently investigated as the strength of the interaction increases by Doğan and Marsiglio (2003) who found that the approximation works quite well even as the strength of the interaction approaches the polaron limit. We therefore can safely ignore this type. The correction of type (b) can be considered to be a phonon self–energy correction and since we are using the experimental phonons in our calculations, this correction has already been incorporated in the lowest order calculated and we can safely ignore it. However the fit to the phonon spectrum which we use is determined from room temperature phonons. Below T_c the nature of the fermion excitations change which in principle causes changes in the location of the poles in the phonon propagator and in the phonon lifetimes. In particular as $T \to 0$ this contribution to the phonon self–energy is real for $\omega < 2\Delta_0$ and suddenly develops a finite lifetime at $\omega = 2\Delta_0$ due to the superconducting density of

states. This in turn leads to a sudden increase in lifetimes for superconducting quasiparticles for $E > 3\Delta_0$. This threshold is also seen in $\Sigma_{\gamma\gamma^\dagger}$ and $\Sigma_{\gamma\gamma}$ in the case of the electron gas below T_c (Coffey, 1997, 1998) since the effective interaction among the superconducting quasiparticles also contains quasiparticle pairs. At $T = 0$ this contribution is given by

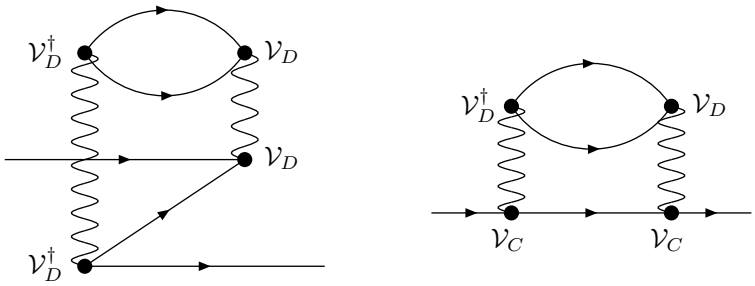

The diagrams represent the following expression

$$\begin{aligned}\Sigma^{(4)}_{\gamma\gamma^\dagger}(\vec{k}, ik_n) \quad \propto \quad & \sum_{\vec{q}\vec{Q}\lambda} \sum_{iq_n} \left[\frac{2\omega_{\vec{q}\lambda}}{(iq_n)^2 - \omega^2_{\vec{q}\lambda}}\right]^2 \Pi(\vec{q}\lambda, iq_n) \\ & \times \left\{ \left| u_{\vec{k}} u^*_{\vec{k}+\vec{q}+\vec{Q}} - v_{\vec{k}} v^*_{\vec{k}+\vec{q}+\vec{Q}} \right|^2 \mathcal{G}^0_\gamma(\vec{k}+\vec{q}+\vec{Q}\sigma, ik_n + iq_n) \right. \\ & \left. + \left| u_{\vec{k}} v_{\vec{k}+\vec{q}+\vec{Q}} + v_{\vec{k}} u_{\vec{k}+\vec{q}+\vec{Q}} \right|^2 \mathcal{G}^0_\gamma(-\vec{k}-\vec{q}-\vec{Q}-\sigma, -ik_n - iq_n) \right\},\end{aligned} \tag{3.9.1}$$

where the polarization $\Pi(\vec{q}\lambda, iq_n)$ is given by

$$\Pi(\vec{q}\lambda, iq_n) \propto \sum_{\vec{Q}'\vec{k}'\sigma'} \left| u_{\vec{k}'} v_{\vec{k}'+\vec{q}+\vec{Q}'} + v_{\vec{k}'} u_{\vec{k}'+\vec{q}+\vec{Q}'} \right|^2 \frac{1 - f_{\vec{k}'} - f_{\vec{k}'+\vec{q}+\vec{Q}'}}{iq_n - \hbar^{-1}E_{\vec{k}'} - \hbar^{-1}E_{\vec{k}'+\vec{q}+\vec{Q}'}}. \tag{3.9.2}$$

In calculating this contribution care must be taken not to double count the phonon self–energy. The normal state self–energy evaluated at $T = 0$ must be subtracted and as a result $\Pi(\vec{q}, \omega) \approx 0$ for $\omega \gg \Delta_0$. This correction to $\Sigma_{\gamma\gamma^\dagger}(\vec{k}, E)$ and $\Sigma_{\gamma\gamma}(\vec{k}, E)$ leads to features in the density of states and, in principle, can be observed in tunneling characteristics of superconductor–insulator–superconductor junctions at bias equal to $4\Delta_0 = 5.2$ meV (Coffey, 1997, 1998), where we used $\Delta_0 = 1.3$ meV as the average gap value.

We argue in the next chapter that this feature is in fact present in high resolution optical conductivity data on lead. This happens because the energy, $4\Delta_0 = 5.2$ meV, lies below the first peak at $2\Delta_0 + 4.5$ meV $= 7.1$ meV in the strong–coupling $\alpha^2 F$. From the data, this contribution the effect is $\approx 20\%$ of the magnitude of the $\alpha^2 F$ features in lead. Although we have not evaluated this contribution because of the complexity of the computation involved due to our model for the lead electron bands, which makes this calculation intractable, we expect that it comes predominantly from intra third band scattering as is the case with the leading order contribution to $\Sigma_{\gamma\gamma\gamma}(\vec{k}, E)$.

3.10 Conclusions

In the first part of this chapter we showed how a description of the superconducting state can be derived that includes experimental details of the electronic excitation spectrum and the quanta of the lattice vibrations, the phonons. We applied this description to superconducting lead, investigating the nature of the superconducting gap.

Measurements by Farnworth et al. indicated that lead exhibits two distinct gaps and our results support this observation. We find this to be due to the topology of the Fermi surface in lead and its two–band nature. The topology makes detailed calculations of the gap function computationally difficult however and it was necessary to approximate the gap function by a function that is $\left|\vec{k}\right|$–dependent only. We compared our results for the gap equation with data of specific heat measurements on lead and found an effective mass enhancement of the electrons due to the electron–phonon interaction that is about 16% smaller than the measured one. As we argue in the text, this is due to our crude approximation of the functional form of the gap and we expect much better agreement between experiment and our calculation when a more complicated functional form is taken into consideration.

In the second half of the chapter we calculate the self–energy for states in the second and third bands and their spectral densities. The features away from the the quasiparticle poles can be identified with the features in the imaginary parts of the self–energies at energies equal to $\Delta_0 +$ 4.5 meV $= 5.8$ meV and $\Delta_0 + 8.5$ meV $= 9.8$ meV ans so are seen to arise from the large phonon density of states due to the longitudinal phonons at 4.5meV and the transverse phonons at 8.5 meV. These features had previously been identified by Chainani *et al.* (2000) in their photoemission data. Finally we discussed corrections to the self–energies beyond the leading order we believe lead to

features in optical conductivity as we discuss in the next chapter.

Chapter 4

Strong-Coupling Features in Optical Conductivity

In this chapter we will calculate the phonon assisted contribution to optical conductivity. This is done in both the superconducting and normal states. We will use the strong–coupling features as a probe of the model we use for the electron–phonon interaction and the bandstructure and phonon dispersion. The optical conductivity can be found by measuring the surface impedance, which can be split into two contributions. The first one is associated with the anomalous skin effect whereas the second is due to "bulk" properties of the metal. These two contributions have different physical origins. The anomalous skin effect depends on whether the scattering of electrons from the surface is diffuse or specular[4.1] and arises from the breakdown of momentum conservation at the surface. The second contribution, the "bulk" part, comes from scattering of the incident photons on phonons, impurities, or other forms of scattering centers, within a distance comparable to the skin depth from the surface. We will focus on this bulk piece using a memory function approach.

[4.1]The difference between the two scattering types is the following. Specular scattering describes the process in which an electron is scattered from the surface of the sample under the condition of momentum conservation in the plane of the surface. Diffuse scattering describes a process in which the scattering completely destroys the drift velocity of the electrons, i.e. the scattering is to a random momentum state. An average over all the final momenta is zero (Reuter and Sondheimer, 1948,p. 342).

4.1 Previous Work

From Reuter and Sondheimer (1948) we get an expression for the surface impedance in the case of specular and diffuse scattering.

$$\begin{aligned} Z_s(\omega) &= -\frac{8i\omega}{c^2}\int_0^\infty \frac{dq}{q^2 - \left(\frac{\omega}{c}\right)^2 \epsilon(q,\omega)} \\ Z_d(\omega) &= -\frac{4\pi^2 i\omega}{c^2}\int_0^\infty dq\ \ln\left(1 - \left(\frac{\omega}{c\,q}\right)^2 \epsilon(q,\omega)\right), \end{aligned} \tag{4.1.1}$$

where

$$\epsilon(q,\omega) = 1 + \frac{4\pi i}{\omega}\sigma(q,\omega). \tag{4.1.2}$$

Once the conductivity, $\sigma(q,\omega)$, is known, $Z_s(\omega)$ or $Z_d(\omega)$ can be calculated.

The anomalous skin effect, or the surface contribution, comes about through exponential decay of the incident electromagnetic fields. It is described by large values of q. In this regime, given by the condition $qv_F > \omega$, the mean free path, l, is comparable to the classical skin depth. This is also called the collisionless regime. In the superconducting state, energies of order Δ, the superconducting energy gap, are of importance, and this limit can be written as $q \gg \xi_0^{-1}$, where

$$\xi_0 = \frac{\hbar v_F}{\pi \Delta_0} \tag{4.1.3}$$

is the coherence length. The motion of the electrons in this so–called Pippard limit, is determined by the electric field everywhere and not only at the position of the electron. Essentially the electron does not suffer inelastic collisions with phonons or impurities so that its momentum is determined non-locally by the electric field only.

The opposite limit, the "bulk" limit, can be described by the condition that $q\ l = q\ v_F\ \tau \ll 1$ or $\omega\ \tau \ll 1$, where τ describes the relaxation time. In this limit many scattering events take place

within the skin depth. This regime is therefore also described as the local limit, since the electric field away from the position of the electron does not play a strong role anymore due to the inelastic collisions and we only need to consider the electric field at the position of the electron. We can write, $\sigma(q,\omega) = \sigma(\omega)$ and the impedance reduces to

$$Z(\omega) = \frac{4\pi}{c}\frac{1}{\sqrt{\epsilon(\omega)}} = \frac{4\pi}{c}\frac{1}{\sqrt{1+\frac{4\pi i}{\omega}\sigma(\omega)}}. \tag{4.1.4}$$

In the case of very low temperatures and very pure samples, the relaxation time τ increases so that the region of q values in which the "bulk" contribution dominates decreases. Strictly speaking, the two regimes overlap, but it is reasonable to assume that the two types of contributions act additively when we compare absorptivity measurements from experiments with theory. We will first take a look at the anomalous skin effect contribution.

The anomalous skin effect was investigated theoretically by a number of authors in the normal state (Reuter and Sondheimer, 1948; Chambers, 1952; Pippard, 1954). In superconductors it was studied by Pippard using the phenomenological London model (Pippard, 1954) and by Mattis and Bardeen on the basis of the BCS theory (Mattis and Bardeen, 1958).

In the normal or the superconducting state, the current induced by an external vector potential, $\vec{A}(\vec{r})$, is given by

$$\vec{J}(\vec{r},\omega) = -\frac{e^2 N(0) v_F}{2\pi^2 \hbar c}\int d^3r' \frac{\vec{R}\left[\vec{R}\cdot\vec{A}(\vec{r}')\right]}{R^4} I(\omega,R,T)e^{-R/l}, \tag{4.1.5}$$

where $R = |\vec{r}-\vec{r}'|$. Chamber's result for the normal state is

$$I(\omega,R,T) = i\pi\hbar\omega e^{iR\omega/v_F}. \tag{4.1.6}$$

Pippard's result for the superconducting state based on the London theory is

$$I(\omega, R, T) = \left[\frac{\rho_s(T)}{\rho_s(0)}\right] \frac{\pi\hbar v_F}{\xi_0} e^{-R/\xi}, \tag{4.1.7}$$

where $\rho_S(T)$ is the density of superconducting electrons. Mattis and Bardeen (Mattis and Bardeen, 1958) found that

$$I(\omega, R, T) = \int_{-\infty}^{\infty}\int_{-\infty}^{\infty} d\epsilon\; d\epsilon' \left(L(\omega, \epsilon, \epsilon') - \frac{[f(\epsilon) - f(\epsilon')]}{\epsilon - \epsilon'}\right) \cos\left[\frac{R(\epsilon - \epsilon')}{\hbar v_F}\right], \tag{4.1.8}$$

where

$$\begin{aligned} L(\omega, \epsilon, \epsilon') &= \frac{1}{2}p^2(\epsilon, \epsilon')\left[\frac{1}{E + E' + \hbar\omega - i\delta} + \frac{1}{E + E' - \hbar\omega - i\delta}\right](1 - f(E) - f(E')) \\ &\quad + \frac{1}{2}l^2(\epsilon, \epsilon')\left[\frac{1}{E - E' + \hbar\omega - i\delta} + \frac{1}{E - E' - \hbar\omega - i\delta}\right](f(E) - f(E')). \end{aligned} \tag{4.1.9}$$

The $p^2(\epsilon, \epsilon')$ and $l^2(\epsilon, \epsilon')$ are coherence factors which are given by

$$\begin{aligned} p^2(\epsilon, \epsilon') &= \frac{1}{2}\left(1 - \frac{\epsilon\epsilon' + \Delta\Delta'}{EE'}\right) \\ l^2(\epsilon, \epsilon') &= \frac{1}{2}\left(1 + \frac{\epsilon\epsilon' + \Delta\Delta'}{EE'}\right), \end{aligned} \tag{4.1.10}$$

where $E = \sqrt{\epsilon^2 + \Delta^2}$ and $f(E)$ is the Fermi-Dirac distribution function. As the temperature is lowered to zero, only the first term survives. The contribution to the optical conductivity is zero for frequencies less than 2Δ and rapidly reaches the frequency independent value found in the normal state, $\omega = 4\,\Delta$. The anomalous skin effect contribution to the absorptivity, $A(\omega)$, in the normal and superconducting states are essentially the same for $\omega \gtrsim 4\,\Delta$ and by considering the difference between derivatives of $A(\omega)$ in the normal and superconducting states it is possible to isolate and to extract information on the "bulk" contributions directly from experiment. This enables us to

separate out the strong–coupling features associated with the electron–phonon interaction in the bulk contribution. The frequency independent contribution to the conductivity from the anomalous skin effect leads to the following expression for the absorptivity,

$$A(\omega) = 4\ \Re\ (Z(\omega)) = \sqrt{3}\left[\frac{4}{3\pi}\frac{v_F}{c}\left(\frac{\omega}{\omega_{pl}}\right)^2\right]^{1/3}, \tag{4.1.11}$$

which is valid for the case where $\omega\,\tau \gg 1$ (Allen, 1971).

As we already mentioned earlier, the "bulk" contribution arises from scattering events within the skin depth from the surface and its frequency dependence can provide information on the mechanisms involved. Evidence of the so–called Holstein process, the simultaneous absorption and emission of phonons by an electron, were first reported on by Joyce and Richards from data on superconducting lead (Joyce and Richards, 1970). This finding triggered a series of experimental and theoretical studies. To name a few, there are the works of Timusk and coworkers (Gavini and Timusk, 1971; Farnworth and Timusk, 1974, 1976), Brändli and Sievers (Brändli and Sievers, 1972), and theoretical investigations by Sher (Scher, 1970), Allen (Allen, 1971), and Brändli (Brändli, 1972). Brändli and Sievers measured the far infrared surface impedance in the normal and the superconducting state by measuring the attenuation of a TEM mode in a parallel plate waveguide. They found the resistivity of lead to exhibit a Drude like dependence on frequency at room temperature,

$$R_N(\omega) = \frac{1}{2}\sqrt{\frac{\omega\rho_0}{2\pi}}\ Z_0, \tag{4.1.12}$$

where Z_0 is the impedance of free space and the d.c. resistivity is given by

$$\frac{\rho_0}{2\pi\,\hbar} = 5.92 \times 10^{-3}\ \mathrm{eV}^{-1}. \tag{4.1.13}$$

The conductivity is given by

(4.1.14) $$\sigma(\omega) \simeq \sigma_0 \, (1 + i\omega \, \tau)$$

reflecting the fact that lead is a poor conductor at room temperature at frequencies less than 15 meV, or $\omega \, \tau \ll 1$. Brändli and Sievers found that structure in their data in the superconducting state below the superconducting transition temperature extends into surprisingly high frequency, $\sim 20 \, \Delta_0$. They furthermore found this frequency dependence to satisfy a sum rule,

(4.1.15) $$\int_0^\infty [R_S(\omega) - Z_0] \, d\omega = \int_0^\infty [R_N(\omega) - Z_0] \, d\omega.$$

Farnworth and Timusk studied the strong–coupling effects associated with the electron–phonon interaction by taking the derivative with respect to frequency of their data in the normal and the superconducting state, $\frac{dS(\omega)}{d\omega}$. This treatment of the data has the effect of reducing the effects of frequency independent anomalous contributions, as mentioned above, and to enhance the difference between the normal and the superconducting states. The measured absorptivity spectra in the normal and the superconducting states were analyzed by taking their ratio,

(4.1.16) $$S(\omega) = \frac{1 - n \, A_S(\omega)}{1 - n \, A_N(\omega)} \simeq 1 - n \, [A_S(\omega) - A_N(\omega)] \, ,$$

where n represents the average number of reflections (about 100) from the sample surface. The derivative of $S(\omega)$ is taken then, which brings out the strong–coupling features associated with the electron–phonon interaction. In Fig. 4.1 from Farnworth and Timusk (1976), Farnworth and Timusk compare the results of their measurements of $S(\omega)$ after taking the derivative with the same strong–coupling features measured in tunneling data.

Shown in this graph are data on a bulk sample which was shifted by $2 \, \Delta_0$ to be able to compare this data with the phonon density of states measured in neutron scattering. The data show features associated with the phonon density of states, which are labeled B, C, D, E, F, and G. In addition

Figure 4.1: (Farnworth and Timusk, 1976,Fig. 2) Comparison of $\alpha^2 F$ numerically inverted from infrared absorption (solid line) and tunneling (dashed line)

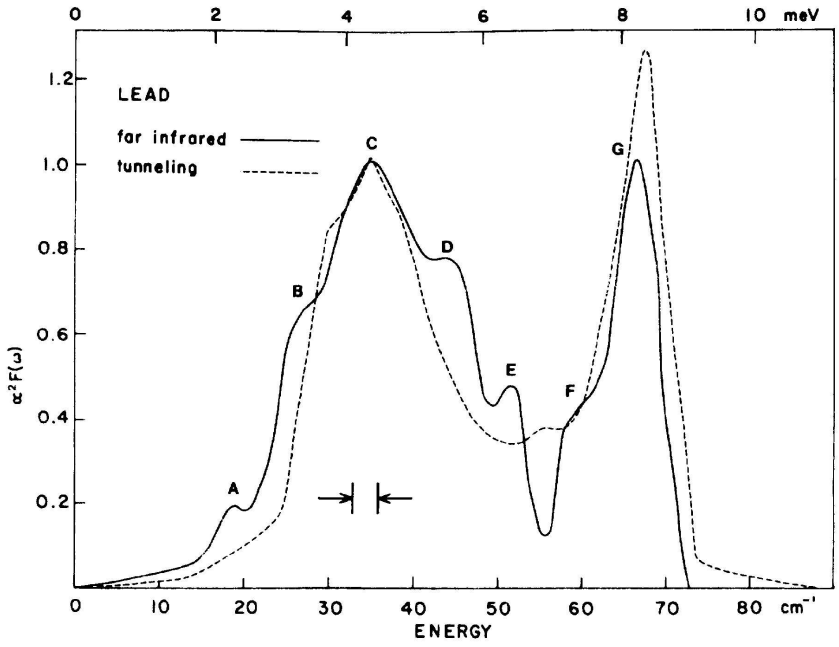

they exhibit a feature labeled A at $\omega = 2\,\Delta_0$. This feature could be thought of arising either from phonon–mediated interaction between the superconducting quasi–particles or as an effect due to the change in the phonon density of states in the superconducting state. In the unshifted curve, it appears at an energy of $\omega = 4\,\Delta_0$ and has the same origin as the feature at $\omega = 3\,\Delta_0$ in the self–energy $\Sigma_{\gamma\gamma\dagger}$ which we discussed earlier in chapter 3. The data of Farnworth and Timusk on thin films reveals a splitting of this feature into two slightly different but distinct energies which is associated with the fact that we are dealing with two conduction bands in lead. These two energies we used as the values of the two superconducting gaps on the two bands in determining the parameters of the microscopic models of the electron–phonon interaction that we use. This analysis of data was suggested by the theoretical work on the phonon–assisted contribution to the conductivity, $\sigma(\omega)$, which we will discuss now.

Holstein was the first to identify the two contributions to the absorptivity we mentioned above (Holstein, 1952). He calculated the bulk contribution associated with the electron–phonon interaction in lead for energies above 8.3 meV and was able to identify a frequency independent effective relaxation time. This relaxation time determines the so called Holstein volume absorption,

$$\frac{2}{\omega_{pl}\,\tau_{eff}}, \tag{4.1.17}$$

where the effective relaxation time $\tau_{eff} = 4.7 \times 10^{-14}$ s. This relaxation time is analogous to the quasiparticle lifetime, given by $\Im\left(\Sigma_{\gamma\gamma^\dagger}\right)$, which is also independent of E above ≈ 10 meV. The frequency dependence of the data of Joyce and Richards appears at energies less than this and Scher evaluated the expression derived by Holstein to be able to directly compare with their data (Scher, 1970). As Holstein showed, $\sigma(\omega)$, is determined by a Holstein process and a vertex renormalization given by single phonon exchanges between electron–hole pairs, or in other words ladder diagrams[4.2]. These contributions lead to a transport equation for the square of the effective electron–phonon interaction matrix elements, the Holstein–Boltzmann equation, which Scher solved using tunneling data on lead as input. He was able to identify the region where the local limit is valid by using the appropriate parameters as $\hbar\omega > 30$ cm^{-1}. Below, at energies $\omega < 30$ cm^{-1}, the "bulk" and the anomalous skin effect contributions are approximately additive and they can be separated.

Subsequently, Allen derived expressions for the phonon–assisted conductivity in the superconducting state and approximated the absorptivity by a sum of the anomalous skin effect contribution, as derived by Mattis and Bardeen, and the absorption due to the electron–phonon mediated scattering, the bulk effect. His results for the absorptivity in the normal and the superconducting states are

$$\begin{aligned} A_N(\omega) &= \frac{\phi_N(\omega)}{\omega\ \omega_{pl}} \int_0^{\omega} d\Omega\ (\omega - \Omega)\,\alpha^2_{tr}F(\Omega) \\ A_S(\omega) &= \frac{\phi_S(\omega)}{\omega\ \omega_{pl}} \int_0^{\omega-2\Delta_0} d\Omega\ (\omega - \Omega)\,\alpha^2_{tr}F(\Omega)\ E(k). \end{aligned} \tag{4.1.18}$$

The function $E(k)$ is the complete elliptic integral of the second kind, where its argument is given by

[4.2]This vertex renormalization can also be seen as an electron–photon vertex renormalization, where the electron–photon vertex is renormalized with the electron–phonon interaction (Holstein, 1964,Fig. 6).

(4.1.19) $$k^2 = 1 - \left(\frac{2\Delta_0}{\omega - \Omega}\right)^2.$$

$\phi_S(\omega)$ and $\phi_N(\omega)$ are weak functions of ω which Farnworth and Timusk took to be equal to unity in their analysis. The function $\alpha^2_{tr}F(\omega)$ represents the transport version of the usual electron–phonon coupling function from Eliashberg theory. Just as in Eliashberg theory or the normal state analysis of the electron–phonon interaction, the shape of the Fermi surface is ignored in calculating $\alpha^2F(\omega)$ and the dirty limit is taken by an averaging process over scattering events from different points on the Fermi surface. This approach therefore is not able to pick out effects due to the character of the two bands in lead and the differences between the superconducting gap on the two Fermi surfaces. We will consequently use a different approach in calculating the strong–coupling effects based on the memory function formalism which makes it possible to distinguish between the contributions from intra– *and* inter–band scattering events.

4.2 Memory Function Formalism

It is well known that the time evolution of correlation functions, $A(t)$, are determined by (Zwanzig, 1961; Forster, 1983)

(4.2.1) $$\frac{dA(t)}{dt} = -\int_0^t ds\ K(s)\ A(t-s),$$

where $K(s)$ is that part of the time evolution operator necessary to determine the time evolution of the correlation function. Here we have used Zwanzig's notation and normalization. These correlation functions are directly related to transport parameters such as the conductivity, $\bar{\sigma}(0)$, by (Montroll, 1961)

(4.2.2) $$\bar{\sigma}(0) = \lim_{\epsilon \to 0} \int_0^\infty dt\ e^{-\epsilon t}\ A(t).$$

At finite frequency $\bar{\sigma}(\omega)$ becomes

$$\bar{\sigma}(\omega) = \frac{1}{\left[\omega + \int_0^\infty dt\ e^{-\omega t}\ K(t)\right]} = \frac{1}{\left[\omega + \bar{M}(\omega)\right]}, \tag{4.2.3}$$

where $\bar{M}(\omega)$ is the memory function. Without much difficulty one can extract $\bar{\sigma}(0)$ from this expression once the memory function, $\bar{M}(\omega)$, is known.

This approach was used by Götze and Wölfle (Götze and Wölfle, 1972) to calculate the contributions to $\sigma(\omega)$ due to scattering events from phonons, impurities, and spin fluctuations under the assumption that the memory function, $M(\omega)$, can be expressed as a power series in the electron–phonon interaction strength, which makes this approach in principle a weak coupling approach. The validity of this formalism breaks down however, when the scattering mechanism is too strong as Cox et al. pointed out in the presence of resonant scattering (Cox *et al.*, 1986).

Here we review the application of this memory function formalism in the calculation of $\sigma(\omega)$ before we present our results for lead. The optical conductivity is given by

$$\sigma(\omega) = -i\left(\frac{e^2}{\omega}\right)\chi(\omega) + i\,\frac{\omega_{pl}^2}{4\pi\omega}, \tag{4.2.4}$$

where $\chi(\omega)$ denotes the current–current correlation function. Let us take a closer look at the above expression. In the normal state, the d.c. conductivity, $\sigma(0)$, is finite which means that the poles in the two terms have to exactly cancel. Consequently, the current–current correlation function, $\chi(0) = \frac{\omega_{pl}^2}{4\pi e^2} = \frac{n\ e^2}{m^*_{opt}}$, where n is the carrier density and involves the ladder diagram summation mentioned earlier. A simple Golden rule approximation ignoring the ladder diagrams gives erroneous results. For instance, a simple Golden rule calculation applied to the case of impurity scattering, leads to the nonsensical result that the conductivity $\sigma(\omega)$ increases as the concentration of impurities increases. However using the memory function calculated to lowest order in the impurity concentration n_i, leads to $\sigma(\omega) \propto \frac{1}{n_i}$.

Götze and Wölfle define the memory function $M(\omega)$ as

$$M(\omega) = \frac{\omega\ \chi(\omega)}{\chi(0) - \chi(\omega)}. \tag{4.2.5}$$

This leads to

$$\sigma(\omega) = \frac{i}{4\pi} \frac{\omega_{pl}^2}{\omega + M(\omega)}. \tag{4.2.6}$$

The poles of eq. (4.2.4) have disappeared and the problem is changed into the problem of finding the memory function. The analytic properties of the correlation functions require that the real part of the memory function, $\Re\,(M(\omega))$, is odd in the energy ω and that the imaginary part, $\Im\,(M(\omega))$, is even.

The functional form of $M(\omega)$ is then found from $\chi(\omega)$ by assuming that the memory function can be expanded in a power series in the strength of the electron–phonon interaction, g. Expanding the right hand side of eq. (4.2.6) one finds

$$\omega\ \chi(\omega) = \chi(0)\ M(\omega) + O(g^4). \tag{4.2.7}$$

Here the electron–phonon interaction contains only terms linear in the ion displacement. Clearly higher order contributions can be calculated. The current–current correlation function, $\chi(\omega)$, which is given by

$$\chi(\omega) = \langle\langle j; j \rangle\rangle = -i \int_0^\infty dt\ \langle [j(t), j(0)] \rangle\ e^{i\omega t}. \tag{4.2.8}$$

The i$^{\text{th}}$ component of the current operator is given by

$$j_i = \sum_{\vec{k}\sigma\nu} \frac{\partial \xi_{\vec{k}\sigma\nu}}{\partial k_i}\ c^\dagger_{\vec{k}\sigma\nu} c_{\vec{k}\sigma\nu}. \tag{4.2.9}$$

As usual, ν is the band index and σ represents the electron spin. $\vec{k}$ is the electron's wavenumber. The correlation function satisfies the following equation of motion,

$$\omega \langle\langle j; j\rangle\rangle = \langle [j(t), j(0)]\rangle + \langle\langle [j, H]; j\rangle\rangle \,. \tag{4.2.10}$$

We used Zubarev's notation, $\langle\langle \cdots \rangle\rangle$, for correlation functions (Zubarev, 1960) in the above expression[4.3]. The brackets, $\langle \cdots \rangle$ denote a thermodynamic average where the operators $j(t)$ denote the Heisenberg representation of the operators j. It follows that

$$\begin{aligned} \omega \ \langle\langle [j; j]\rangle\rangle &= \langle [j(t), j(0)]\rangle + \langle\langle [j, H]\,; j\rangle\rangle \\ \langle [[j, H]\,, j]\rangle &= \langle\langle [j, H]\,; [j, H]\rangle\rangle_{\omega=0} \,. \end{aligned} \tag{4.2.12}$$

Putting these results together, the memory function $M(\omega)$ is given by

$$M(\omega) = \frac{\left[\langle\langle [j, H]\,; [j, H]\rangle\rangle_{\omega} - \langle\langle [j, H]\,; [j, H]\rangle\rangle_{\omega=0}\right]}{\omega\chi(0)} + O(g^4), \tag{4.2.13}$$

and

$$[j_i, H] = \sum_{\vec{k}\nu, \vec{k}'\nu', \sigma} \left[\frac{\partial \xi_{\vec{k}\sigma\nu}}{\partial k_i} - \frac{\partial \xi_{\vec{k}'\sigma\nu'}}{\partial k_i'}\right] c^{\dagger}_{\vec{k}\sigma\nu} c_{\vec{k}'\sigma\nu'} \left(b^{\dagger}_{\vec{k}-\vec{k}',\lambda} + b_{-\vec{k}+\vec{k}',\lambda}\right), \tag{4.2.14}$$

[4.3] The causal Green's function in this notation is written as

$$\mathcal{G}(t, t') = \langle\langle A(t); B(t')\rangle\rangle = -i \langle T\left[A(t)B(t')\right]\rangle \,. \tag{4.2.11}$$

where λ is the phonon branch index. These correlation functions are calculated in the normal or in the superconducting state. In the normal state it is straight forward to make contact with the Drude model for conductivity. At low frequencies

$$\omega + \Re\left(M(\omega)\right) \simeq \omega \left(1 + \left.\frac{d\Re\left(M(\omega)\right)}{d\omega}\right|_{\omega=0}\right) = \frac{\omega}{a}, \tag{4.2.15}$$

and $\Im\left(M(\omega)\right) \simeq \Im\left(M(0)\right)$. The d.c. conductivity is given by

$$\sigma_0 = \frac{n\,e^2}{m} a^2\, \Im\left(M(0)\right), \tag{4.2.16}$$

and $\tau = \frac{1}{a\,\Im(M(0))}$. Consequently the usual Drude expression for $\sigma(\omega)$ is recovered,

$$\sigma(\omega) = \frac{\omega_{pl}^2}{4\pi} \frac{1}{1 - i\omega\tau}. \tag{4.2.17}$$

There is an important qualitative difference between the superconducting and the normal state. The response of the supercurrent to the external field leads to a delta–function in the conductivity, $\sigma(\omega)$, at $\omega = 0$ in the real part and a pole in the imaginary part. The additional term in $\sigma(\omega)$ is given by

$$A\ \delta(\omega) + i\frac{2A}{\pi\omega}. \tag{4.2.18}$$

The delta function accounts for the missing weight in the f–sum rule. We will follow Tinkham (Tinkham, 1980) and write the magnitude of A as

$$|A| = \frac{c^2}{4\pi\lambda^2}, \tag{4.2.19}$$

where λ represents the penetration depth. In the superconducting state, $\sigma(\omega)$ becomes

$$\begin{aligned}\sigma_S(\omega) &= \frac{i}{4\pi}\frac{\omega_{pl}^2}{\omega+M_S(\omega)}+i\frac{M_S(\omega)}{\omega+M_S(\omega)}\left(\frac{\omega_{pl}^2}{4\pi}-e^2\chi_S(0)\right)\frac{1}{\omega}\\ &= \frac{\omega_{pl}^2}{4\pi}(1-\alpha)\frac{\Im\left(M_S(\omega)\right)+i\left[\omega+\Re\left(M_S(\omega)\right)\right]}{\left|\omega+M_S(\omega)\right|^2}+i\frac{\omega_{pl}^2}{4\pi}\frac{\alpha}{\omega}.\end{aligned} \tag{4.2.20}$$

The real part of $\sigma_s(\omega)$ is then given by

$$\Re\left(\sigma_S\right)=\frac{\omega_{pl}^2}{4\pi}(1-\alpha)\frac{\Im\left(M_S(\omega)\right)}{\left|\omega+M_S(\omega)\right|^2}+\frac{\omega_{pl}^2}{4\pi}\;\alpha\;\delta(\omega). \tag{4.2.21}$$

The fractional change from $\chi_N(0)$ is

$$\alpha=\left[\frac{2}{\pi}\,A\right]/\left[\frac{\omega_{pl}^2}{4\pi}\right]. \tag{4.2.22}$$

Using experimental values for lead, $\alpha \simeq 0.026$. Since the quantitative effect of this change for energies $\omega > 2\,\Delta_0$ is negligible and we will therefore ignore it in the following.

The correlation function is given by

$$\begin{aligned}\langle\langle[j,H]\,;[j,H]\rangle\rangle_\omega = -i\int_0^\infty dt\; e^{i\omega\,t}\sum_{\vec{k}_1,\vec{q}_1,\vec{k}_2,\vec{q}_2,\lambda}\tilde{g}^*(\vec{k}_1,\vec{q}_1,\lambda)\;\tilde{g}(\vec{k}_2,\vec{q}_2,\lambda)\\ \times\Big\langle\Big\langle T\; e^{i\int dt' H_{ep}}\left[b_{\vec{q}_1}(t)+b^\dagger_{-\vec{q}_1}(t)\right]\left[b_{\vec{q}_2}(0)+b^\dagger_{-\vec{q}_2}(0)\right]c^\dagger_{\vec{k}_1+\vec{q}_1}(t)\,c_{\vec{k}_1}(t)\,c^\dagger_{\vec{k}_2+\vec{q}_2}(0)\,c_{\vec{k}_2}(0)\\ -\left[b_{\vec{q}_2}(0)+b^\dagger_{-\vec{q}_2}(0)\right]\left[b_{\vec{q}_1}(t)+b^\dagger_{-\vec{q}_1}(t)\right]c^\dagger_{\vec{k}_2+\vec{q}_2}(0)\,c_{\vec{k}_2}(0)\,c^\dagger_{\vec{k}_1+\vec{q}_1}(t)\,c_{\vec{k}_1}(t)\Big\rangle\Big\rangle.\end{aligned} \tag{4.2.23}$$

$\tilde{g}(\vec{k},\vec{q},\lambda)$ is the electron-phonon interaction defined in eq. (2.1.28), $g(\vec{k},\vec{q},\lambda)$, times the derivatives of the quasiparticle spectrum in the current operator,

$$\tilde{g}(\vec{k},\vec{q},\lambda) = i\sqrt{\frac{\hbar^2}{2N_0\, M_\nu\, \hbar\omega_{\vec{k}'-\vec{k}\lambda}}}\;\hat{\eta}_{\nu,\vec{k}-\vec{k}'\lambda}\cdot\left(\vec{k}'-\vec{k}\right)U(\vec{k}'-\vec{k})\left[\frac{\partial\xi_{\vec{k}\sigma\nu}}{\partial k_i}-\frac{\partial\xi_{\vec{k}'\sigma\nu'}}{\partial k_i'}\right]. \tag{4.2.24}$$

In the superconducting state and to lowest order in the electron–phonon interaction strength, $O(g^2)$, this becomes

$$\langle\langle[j,H]\,;[j,H]\rangle\rangle_\omega = \langle\langle[j,H]\,;[j,H]\rangle\rangle_\omega^{(N)} + \langle\langle[j,H]\,;[j,H]\rangle\rangle_\omega^{(S)}\,, \tag{4.2.25}$$

where

$$\begin{aligned}\langle\langle[j,H]\,;[j,H]\rangle\rangle_\omega^{(N)} &= \sum_{\vec{k},\vec{q},\lambda}\left[u_{\vec{k}}^2u_{\vec{k}+\vec{q}}^2+v_{\vec{k}}^2v_{\vec{k}+\vec{q}}^2+2u_{\vec{k}}v_{\vec{k}}u_{\vec{k}+\vec{q}}u_{\vec{k}+\vec{q}}\right]\left|\tilde{g}(\vec{k},\vec{q},\lambda)\right|^2\\ &\quad\times\left[\frac{f_{\vec{k}+\vec{q}}\left(1-f_{\vec{k}}\right)\left(1+n_{\vec{q}}\right)-f_{\vec{k}}\left(1-f_{\vec{k}+\vec{q}}\right)n_{\vec{q}}}{E_{\vec{k}+\vec{q}}-E_{\vec{k}}-\omega_{\vec{q}}}\right]\\ &\quad\times\left(\frac{1}{E_{\vec{k}+\vec{q}}-E_{\vec{k}}-\omega_{\vec{q}}-\omega}+\frac{1}{E_{\vec{k}+\vec{q}}-E_{\vec{k}}-\omega_{\vec{q}}+\omega}\right),\end{aligned} \tag{4.2.26}$$

and

$$\begin{aligned}\langle\langle[j,H]\,;[j,H]\rangle\rangle_\omega^{(S)} &= \omega\sum_{\vec{k},\vec{q},\lambda}\left[u_{\vec{k}}^2v_{\vec{k}+\vec{q}}^2+v_{\vec{k}}^2u_{\vec{k}+\vec{q}}^2+2u_{\vec{k}}v_{\vec{k}}u_{\vec{k}+\vec{q}}u_{\vec{k}+\vec{q}}\right]\left|\tilde{g}(\vec{k},\vec{q},\lambda)\right|^2\\ &\quad\times\left[\left(1-f_{\vec{k}+\vec{q}}\right)\left(1-f_{\vec{k}}\right)\left(\frac{1+n_{\vec{q}}}{\omega^2-\left(\omega_{\vec{q}}+E_{\vec{k}+\vec{q}}+E_{\vec{k}}\right)^2}+\frac{n_{\vec{q}}}{\omega^2-\left(\omega_{\vec{q}}-E_{\vec{k}+\vec{q}}-E_{\vec{k}}\right)^2}\right)\right.\\ &\quad\left.-f_{\vec{k}}f_{\vec{k}+\vec{q}}\left(\frac{1+n_{\vec{q}}}{\omega^2-\left(\omega_{\vec{q}}-E_{\vec{k}+\vec{q}}-E_{\vec{k}}\right)^2}+\frac{n_{\vec{q}}}{\omega^2-\left(\omega_{\vec{q}}+E_{\vec{k}+\vec{q}}+E_{\vec{k}}\right)^2}\right)\right].\end{aligned} \tag{4.2.27}$$

The correlation function $\langle\langle [j,H]\,;[j,H]\rangle\rangle_{\omega}^{(N)}$ exhibits the same characteristic as a particle–hole contribution and it smoothly evolves into the normal state result as derived by Allen and by Götze and Wölfle. It is furthermore exponentially small for temperatures much smaller than the gap and it is negligible at the temperature at which Farnworth and Timusk took their data on lead in the superconducting phase, 0.35 K. The combinations of coherence factors and the particle–particle and hole–hole distribution functions ensure that $\langle\langle [j,H]\,;[j,H]\rangle\rangle_{\omega}^{(S)}$ vanishes as the gap vanishes. This term produces the conductivity at finite frequencies and low temperatures below T_c. Taking the limit as $T \to 0$, the real and the imaginary parts of $M_S(\omega)$ become

$$\begin{aligned}
\Re\left(M(\omega)_S\right) &= \sum_{\vec{k},\vec{q}} \left[u_{\vec{k}}^2 v_{\vec{k}+\vec{q}}^2 + u_{\vec{k}}^2 v_{\vec{k}+\vec{q}}^2 + 2u_{\vec{k}} v_{\vec{k}} u_{\vec{k}+\vec{q}} u_{\vec{k}+\vec{q}}\right] \frac{\left|\tilde{g}(\vec{k},\vec{q},\lambda)\right|^2}{\chi(0)} \\
&\quad \times \frac{\omega}{\left[\omega^2 - \left(\omega_{\vec{q}} + E_{\vec{k}+\vec{q}} + E_{\vec{k}}\right)^2\right]} \\
\Im\left(M(\omega)_S\right) &= \sum_{\vec{k},\vec{q}} \left[u_{\vec{k}}^2 v_{\vec{k}+\vec{q}}^2 + u_{\vec{k}}^2 v_{\vec{k}+\vec{q}}^2 + 2u_{\vec{k}} v_{\vec{k}} u_{\vec{k}+\vec{q}} u_{\vec{k}+\vec{q}}\right] \frac{\left|\tilde{g}(\vec{k},\vec{q},\lambda)\right|^2}{\chi(0)} \\
&\quad \times \left(\delta\left[\omega - \left(\omega_{\vec{q}} + E_{\vec{k}+\vec{q}} + E_{\vec{k}}\right)\right] + \delta\left[\omega + \left(\omega_{\vec{q}} + E_{\vec{k}+\vec{q}} + E_{\vec{k}}\right)\right]\right).
\end{aligned} \tag{4.2.28}$$

$\Re\left(M_S(\omega)\right)$ is dominated by quasiparticle energies $\gg \Delta$ and is equal to $\Re\left(M_N(\omega)\right)$ to a very good approximation. Furthermore $\Re\left(M_S(\omega)\right)$ is approximately proportional to ω in the range of ω's of interest here so that $\Re\left(\frac{M_S(\omega)}{\omega}\right)$ is a weak function of ω. This simplifies the expression for $\frac{dS(\omega)}{d\omega}$ discussed above. These results can be extended to include the effect of higher order powers in the electron–phonon interaction as is discussed in Appendix D. However a quantitatively accurate evaluation of higher orders which includes the band structure of lead is computationally prohibitive.

4.3 Results for Lead

The Fermi surface of lead consists of two bands. Here we are going to concentrate on the effect of bandstructure and Δ_0. As a minimal model we will ignore the difference between the values of the gaps on the Fermi surfaces associated with the second and third bands and take $\Delta_0 = 1.37$ meV.

We will therefore get three contributions to the memory function, $M(\omega)$ and to the absorptivity. These three are from intra–band scattering within the second band, $M_{(22)}(\omega)$, intra–band scattering within the third band, $M_{(33)}(\omega)$, and inter–band scattering between the second and the third band, $M_{(23)}(\omega)$. Since the frequencies of interest are much smaller than the plasma frequency, ω_{pl}, and since furthermore the magnitude of the memory function, $|M(\omega)| \ll 1$, the expression for the spectral density $A(\omega)$ can be greatly simplified.

$$\begin{aligned} A(\omega) &= 4\,\Re\left(\frac{1}{\sqrt{1+\frac{4\pi i}{\omega}\sigma(\omega)}}\right) \\ &= 4\frac{\omega}{\omega_{pl}}\Im\left(\sqrt{\frac{1+\frac{M(\omega)}{\omega}}{1-\left(\frac{\omega}{\omega_{pl}}\right)^2\left(1+\frac{M(\omega)}{\omega}\right)}}\right) \\ &\simeq \frac{2}{\omega_{pl}}\frac{\Im\left(M(\omega)\right)}{1+\frac{\Re(M(\omega))}{\omega}} \\ &\simeq \frac{2}{\omega_{pl}}\frac{\Im\left(M_{(22)}(\omega)\right)+\Im\left(M_{(33)}(\omega)\right)+\Im\left(M_{(23)}(\omega)\right)}{1+\frac{\Re(M(\omega))}{\omega}}, \end{aligned} \tag{4.3.1}$$

and it can be considered to have three distinct contributions from the different types of scattering.

The $\Im\left(M_{(22)}\right)$ and $\Im\left(M_{(33)}\right)$ contributions in the normal and superconducting states to order g^2 are compared in figures 4.2, 4.3. $\Im\left(M_{(23)}(\omega)\right)$ in the normal and superconducting states are similar to those and have magnitudes intermediate between them. The different magnitudes of the memory functions $M_{(ij)}(\omega)$, reflects their dependence on the surface area of the different parts of the Fermi surface involved in the scattering processes and on the phonons which connect different parts of the Fermi surface. It appears as if this dominates any effects the density of states on the different Fermi surfaces might have on the $M_{(ij)}(\omega)$. This comes about due to the cancellation of the Fermi velocity factors in the density of states with those from the current operator matrix elements. The dominant contribution comes from $\Im\left(M_{(33)}(\omega)\right)$ which involves the scattering between the 36 "pipes" which make up the third band. The geometry of the third band suggests that "nesting", scattering between parallel pipes with a single phonon momentum, could be important. There are $36^2 = 1296$ different combinations of pipes and of those, pipes whose mid–points can be connected by momentum vectors $\vec{Q}_1 = \frac{2\pi}{a}(1, 1/2, 1/2)$ and $\vec{Q}_2 = \frac{2\pi}{a}(3/2, 0, 0)$ lead to contributions much larger than other combinations by about a factor of ~ 10. However, there are only about 100

Figure 4.2: $\Im\left(M_{(22)}(\omega)\right)$ vs. ω. The full line is $\Im\left(M_{(22)}(\omega)\right)$ in the normal state while the dashed line is $\Im\left(M_{(22)}(\omega)\right)$ in the superconducting state.

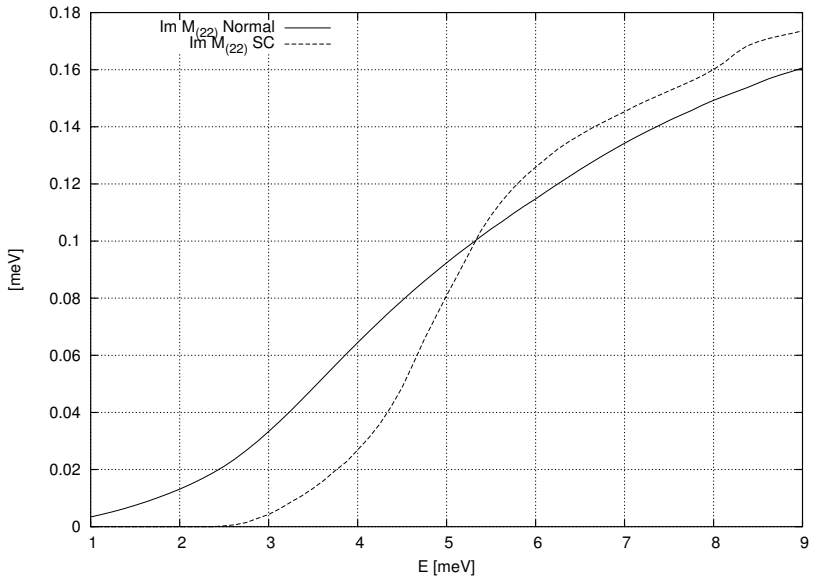

Figure 4.3: $\Im\left(M_{(33)}(\omega)\right)$ vs. ω. The full line is $\Im\left(M_{(33)}(\omega)\right)$ in the normal state while the dashed line is $\Im\left(M_{(33)}(\omega)\right)$ in the superconducting state.

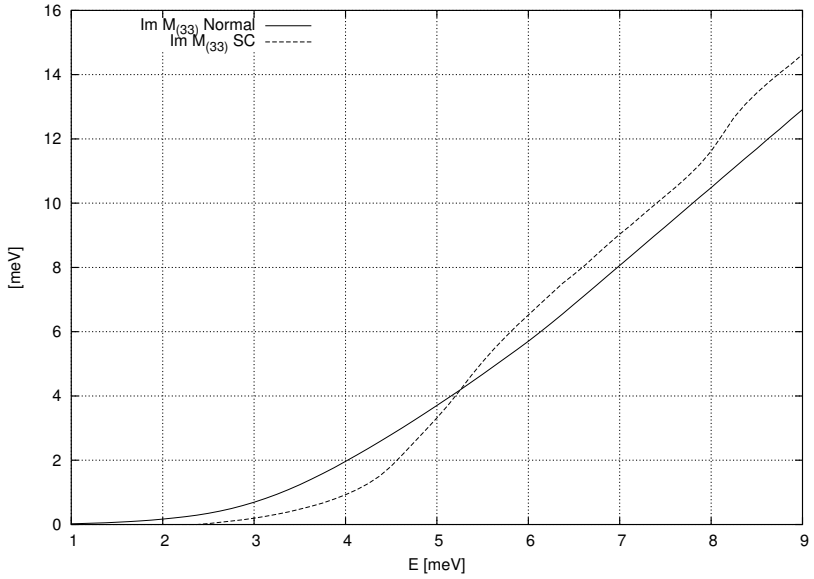

of these combinations and their contribution does not dominate $\Im\left(M_{(33)}(\omega)\right)$. In contrast to the intra–band scattering events on the second band, there are many more phonons that connect the more complicated surface of the third band. This and the larger surface area of the third zone Fermi surface is responsible for the big difference in magnitude of the two contributions.

The real parts of the $M_{(ij)}$ are related to the imaginary parts through a spectral relation

$$M_{(ij)}(\omega) = \int_{-\infty}^{\infty} dz \; \frac{\Im\left(M_{(ij)}(z)\right)}{\omega - z}, \tag{4.3.2}$$

so that the magnitudes of the real parts of the $M_{(ij)}$ have a similar relation to one another as the imaginary parts. Therefore

$$\frac{\Re\left(M(\omega)\right)}{\omega} \simeq \frac{\Re\left(M_{(33)}(\omega)\right)}{\omega}, \tag{4.3.3}$$

where $\frac{\Re\left(M_{(33)}(\omega)\right)}{\omega}$ corresponds to the effective mass enhancement due to the electron–phonon interaction as seen in $\sigma(\omega)$. Returning to the discussion of the connection with the Drude form eq. (4.1.14)

$$a = \left[1 + \frac{\partial M(\omega)}{\partial \omega}\right]^{-1} \simeq \left(1 + \left.\frac{\Re\left(M_{(33)}(\omega)\right)}{\omega}\right|_{\omega=0}\right)^{-1} > 1. \tag{4.3.4}$$

$\Re\left(M_{(33)}(\omega)\right)/\omega$ fluctuates in value by $\lesssim 5\%$ between $\omega = 0$ and $\omega = 10\Delta$. In order to analyze the results further, we will take the derivative of $A(\omega)$ with respect to energy. This reveals the strong–coupling electron–phonon features.

$$\begin{aligned} \frac{dA_S(\omega)}{d\omega} - \frac{dA_N(\omega)}{d\omega} &= \frac{2}{\omega_{pl}}\left(\frac{d\Im\left(M_S(\omega)\right)/d\omega}{1+\Re\left(M_S(\omega)\right)/\omega} - \frac{d\Im\left(M_N(\omega)\right)/d\omega}{1+\Re\left(M_N(\omega)\right)/\omega}\right) \\ &\quad + \frac{2}{\omega_{pl}}\left(\frac{\Im\left(M_S(\omega)\right)}{\left(1+\Re\left(M_S(\omega)\right)/\omega\right)^2}\frac{d\left(\Re\left(M_S(\omega)\right)/d\omega\right)}{d\omega}\right. \\ &\quad \left. - \frac{\Im\left(M_N(\omega)\right)}{\left(1+\Re\left(M_N(\omega)\right)/\omega\right)^2}\frac{d\left(\Re\left(M_N(\omega)\right)/d\omega\right)}{d\omega}\right). \end{aligned} \tag{4.3.5}$$

Figure 4.4: The difference between $\frac{dM_{(22)}(\omega)}{d\omega}$ in the superconducting and normal states. The smooth increase in both the normal and the superconducting values is removed revealing strong–coupling features.

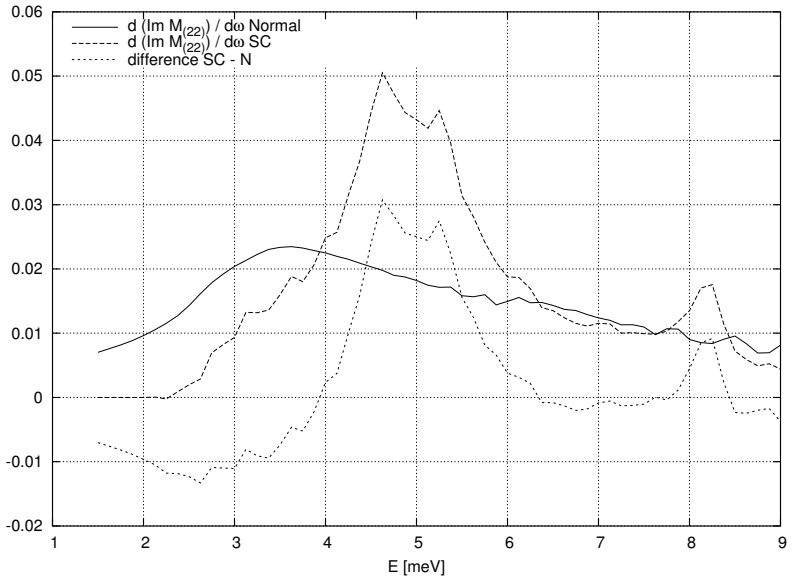

As mentioned above, $\Re\left(M_N(\omega)\right)/\omega$ and $\Re\left(M_S(\omega)\right)/\omega$ are weak functions of ω in the frequency range of interest here as well as being almost equal and therefore the second term can therefore be dropped. Since to a good approximation

$$\frac{dA_S(\omega)}{d\omega} - \frac{dA_N(\omega)}{d\omega} \simeq \frac{2}{\omega_{pl}} \frac{1}{1+\Re\left(M_S(\omega)\right)/\omega} \left(\frac{d\Im\left(M_S(\omega)\right)}{d\omega} - \frac{d\Im\left(M_N(\omega)\right)}{d\omega} \right). \tag{4.3.6}$$

In Figs. 4.4 and 4.5, $dA_S(\omega)/d\omega - dA_N(\omega)/d\omega$ is compared for the inter–band contributions to scattering. The sharp peaks correspond in the graph correspond to the peaks found in neutron scattering.

The derivatives of the memory function contributions, $M_{(ij)}(\omega)$ are shown in Figs. 4.4 and 4.5[4.4]. In both $\Im\left(M_{(22)}(\omega)\right)$ and $\Im\left(M_{(33)}(\omega)\right)$ for the superconducting state the peaks at ≈ 35 cm^{-1} and

[4.4]The derivative of A((ω) was evaluated using the difference formula for a function f evaluated at equally spaced points Δx apart,

Figure 4.5: Derivative of $M_{(33)}(\omega)$

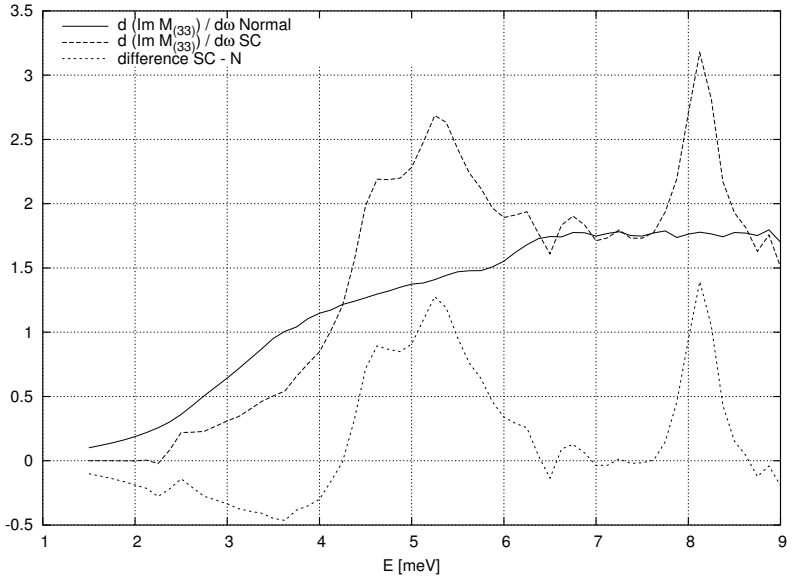

$\approx 70\ \mathrm{cm}^{-1}$ seen in the data of Farnworth and Timusk, Fig. 4.1, can be seen. These peaks come from peaks in the phonon density of states. However the magnitude of the higher energy peak in $\Im\left(M_{(22)}(\omega)\right)$ is much smaller than that of the low energy peak.

The $\Im\left(M_{(ij)}(\omega)\right)$ in the normal state is fairly featureless above $4\,\Delta$ and subtracting from the superconducting $\Im\left(M_{(ij)}(\omega)\right)$ does not introduce features not already present. $\Im\left(M_{(33)}(\omega)\right)$ is the dominant contribution to $\Im\left(M(\omega)\right)$ and strongly resembles the data shown in Fig. 4.1. The two prominent peaks closely resemble the peaks in data from the point of view of both height and width. In Allen's calculated $\alpha^2_{tr}F(\omega)$ (Allen, 1971,Fig. 4) the failure of the simple approximation for the Fermi surface to capture the magnitude of 8 meV peak is seen.

The difference between $\Im\left(M_{(22)}(\omega)\right)$ and $\Im\left(M_{(33)}(\omega)\right)$ arise from the shape of the two pieces of the Fermi surface involved in the two contributions. Scattering between difference parts of the third

$$f'_i = \left(0.8(f_{i+1} - f_{i-1}) - 0.2(f_{i+2} - f_{i-2}) + \frac{4}{105}(f_{i+3} - f_{i-3}) - \frac{1}{280}(f_{i+4} - f_{i-4})\right)\frac{1}{\Delta x} \tag{4.3.7}$$

This gives the derivative of a ninth order polynomial exactly.

band Fermi surface introduces all the phonon modes and as a result it is the dominant contribution and closely resembles the phonon density of states. By contrast scattering within the second band constrains the phase space for phonons which conserve energy and momentum. The phonon associated with the high energy peak contribute less in this case. To good approximation the phonon assisted contribution to $\sigma(\omega)$ is given solely by the scattering within the third band.

4.4 Conclusion

The results of this calculation demonstrate the importance of an accurate model for the Fermi surface in order to get agreement with the strong–coupling features in $\sigma(\omega)$. Our model is derived from experiment and was described in Chapter 3. Conventional approaches which ignore the nature of the Fermi surface, either conventional Eliashberg theory or assuming a circular Fermi surface, would assume that the phonon density of state alone determines the form of the strong–coupling corrections. Consequently since aluminum has a very similar phonon density of states to lead, the $\alpha^2F(\omega)$ terms in $\sigma(\omega)$ should be very similar to those in lead with this assumption. However the third band is reduced in magnitude compared to lead (Ashcroft and Wilkins, 1965) and so the strong–coupling features can be expected to be quite different.

The present calculation to order g^2 involved a considerable numerical calculation especially since great accuracy was needed to accurately evaluate the derivatives with respect to ω. As we mentioned above there is a feature in the data at $\omega = 4\,\Delta$ associated with the decay of quasiparticles at $3\,\Delta$. The calculation of this feature employing the model we have used for the Fermi surface in $\sigma(\omega)$ is not practical. An investigation of this feature would have to use model Fermi surfaces and address the issue of the "vertex corrections" in the memory function formalism raised in the appendix.

Chapter 5

Thermodynamics at Intermediate Temperatures

5.1 Introduction

In this chapter we consider the contribution of the interaction between electrons and the lattice to the thermodynamics of metals for temperatures from 100 K up to the melting temperature. As it turns out, at these temperatures these contributions are insensitive to the details of the phonon spectrum and the electron–phonon interaction, but rather show a generic temperature dependence. We will discuss two different approaches to this temperate regime. One starts out from the low temperature limit which we already discussed previously in the discussion of the electron–phonon interaction, Chapter 2, the discussion of superconductivity, Chapter 3, and the discussion of strong–coupling features in optical conductivity, Chapter 4. The interactions between the electrons and the lattice are described as interactions between electrons and phonons. The other approach starts from high temperatures above the degeneracy temperature of the ions, which is roughly estimated of the order of 100K. This approach is based on an electron–ion model rather than an electron–phonon model. In this case, the ion motion is considered "classical". We will show how the strongest temperature dependence calculated with the electron–phonon approach can be recovered starting from this high–temperature region.

At intermediate temperatures there are several different contributions to the free energy of a

metal. For a metal crystal the free energy consists of three contributions (Wallace, 1998): Φ_o(V), the static lattice potential, which is the total energy when the ions are located at lattice sites and the electrons are in their ground state; F_I(V,T), the free energy from ion vibrations, and F_E(V,T), the free energy associated with thermal excitation of electrons from their ground state. F_I(V,T) is the dominant temperature contribution and consists of the quasi-harmonic phonon contribution, F_{ph}(V,T) plus the small anharmonic term F_{anh}(V,T) which expresses phonon-phonon interactions. F_E(V,T) consists of F_{el}(V,T) representing the thermal excitation of independent electrons, plus F_{ep}(V,T), the contribution from interaction between electronic excitations and phonons. Here we are interested in the latter contribution at all temperatures, from T=0 to melt, and especially at intermediate temperatures, several times the largest phonon frequency and many times smaller than the Fermi energy. In this temperature regime the ion motion is classical so that F_{ep} could be calculated from the low-temperature electron-phonon approach or from the electron-ion picture mentioned above.

The quasi-harmonic approximation is a universal highly-accurate description of the nature of crystals. In this description the phonon frequencies depend only on the crystal volume, more specifically on the lattice parameters, and the temperature dependence of the phonons arises only through thermal expansion, a very small effect. When electron-phonon and phonon-phonon interactions are both treated as perturbations, the two processes do not interact in low order, so that electron-phonon interactions are properly studied in the quasi-harmonic approximation. Of course, special cases do exist, such as the temperature-dependent phonon softening in Ti and Zr near the hcp-bcc phase transition.

To compare the relative magnitudes of the various contributions it is appropriate to consider the entropy S_{el}(V,T)+ S_{ep}(V,T), since the sum of these contributions to the entropy is positive and has a simple (increasing) T dependence at constant V. At the very low temperatures much smaller than the average phonon frequency, the electronic contribution, S_{el}+S_{ep}, dominates the entropy of the metal. At all higher temperatures, the quasi-harmonic contribution, S_{ph}, is estimated to be 85-99% of the total experimental entropy, while S_{anh} is estimated to be around 0-6% for elemental metals. S_{el} is around 1-2% of the total entropy at the melting temperature for nearly free electron metals and around 10% for transition metals (Wallace, 1997). For comparison, experimental entropy data are generally known to an accuracy of 0.1-0.2 %.

It is possible also to calculate the contribution to the free energy from electron-ion interactions

starting from uncorrelated ion motion. This is a good approximation at high temperatures where the ion motion is classical(Wallace, 1997). Classical molecular and lattice dynamics simulations have been used to calculate the contribution of the ion motion to the free energy at high temperatures. The motion is described by a classical Hamiltonian in which the ions interact through a potential consisting of the Coulomb repulsion between the ions and an effective potential due to the presence of the electrons. These simulations do not take into account corrections to the classical treatment of ions or the change in the contribution from the electron-phonon interaction with temperature. Kirkwood was the first to estimate the leading corrections to the classical approximation for the ions by expanding in powers of the Planck constant in the kinetic energy term for the ions(Kirkwood, 1933). Zwanzig subsequently included electrons in the Hamiltonian but did not go beyond verifying the leading contribution which Kirkwood had found for the quantum mechanical nature of the ion motion(Zwanzig, 1957). In the Zwanzig's formalism it is assumed that the Schrödinger equation for the electrons is solved as a function of ion configuration. So in contrast to the electron-phonon Hamiltonian treatment there are no transitions between electronic states and the interaction between ions and electrons leads to a purely adiabatic contribution.

First we will derive expressions for the electron–phonon contributions in the electron–phonon interaction formalism. We will discuss the temperature dependences found for the different components of this contributions. Then we will derive expressions starting from the electron–ion approach making a connection to the contributions calculated in the first part. We will show that the leading temperature dependence in two approaches are equivalent.

5.2 The Thermodynamic Potential

We are in the grand canonical ensemble and adjust the mean particle number via the chemical potential. The ground state energy is calculated using a linked cluster expansion and will give us the free energy of the system, i.e. either the Helmholtz or Gibbs free energy, $F(T, V, N)$, and $G(T, P, N)$, respectively. These two are given by the usual thermodynamic relations

$$F = E - TS \qquad G = E - TS + PV, \tag{5.2.1}$$

where E is the internal energy of the system, T specifies its temperature, P the pressure the system is under, and V the volume of the system. The quantity S denotes the entropy. We are working with infinite crystals and are not concerned with pressure or volume changes. The free energy can be transformed into the thermodynamic potential, $\Omega(T, V, \mu) = F - \mu N$, which is related to observable thermodynamic quantities.

$$S = -\left.\frac{\partial \Omega}{\partial T}\right|_{V\mu} \qquad P = -\left.\frac{\partial \Omega}{\partial V}\right|_{T\mu} \qquad N = -\left.\frac{\partial \Omega}{\partial \mu}\right|_{TV}. \tag{5.2.2}$$

We will calculate the low–order corrections to the thermodynamic potential due to the electron–phonon interaction using a linked cluster expansion method. Within this expansion, the thermodynamic potential is given by

$$\Omega - \Omega_0 = \frac{1}{2\beta}\int_0^1 \frac{d\eta}{\eta} \sum_{\vec{k}\sigma} \sum_{ik_n} \Sigma^\eta(\vec{k}\sigma, ik_n)\mathcal{G}^\eta(\vec{k}\sigma, ik_n), \tag{5.2.3}$$

where the self–energy and the one particle Greens function implicitly depend on the coupling constant, η (Fetter and Walecka, 1971,Section 23). We will consider terms of up to second order in the interaction. Our Hamiltonian is given by

$$\mathcal{H} = \mathcal{H}_0 + \mathcal{H}_{ep}^{(0)} + \mathcal{H}_{ep}^{(1)} + \mathcal{H}_{ep}^{(2)}, \tag{5.2.4}$$

as derived in eqs. (2.1.15), (2.1.26), and (2.1.29). The unperturbed Hamiltonian, $\mathcal{H}_0$, is given by

$$\mathcal{H}_0 = \sum_{\vec{k}\sigma} \frac{\hbar^2 k^2}{2m} c^\dagger_{\vec{k}\sigma} c_{\vec{k}\sigma}. \tag{5.2.5}$$

We will use free electron states in this calculation. This is very different in spirit than the calculations done in chapter 3 where we used a realistic band structure from experiments and include $\mathcal{H}_{ep}^{(0)}$ in

$\mathcal{H}_0$. The exact expression for the expansion of the thermodynamic potential involves the exact self–energy and the exact single–particle Greens function. We will approximate the expansion by taking the Greens function to be the unperturbed $\mathcal{G}^0(\vec{k}\sigma, \tau_2 - \tau_1)$, and will calculate the self–energy up to second order. The S–Matrix expansion of the one–particle Greens function is given by eqs. (C.67) and (C.74),

$$\Sigma^{(1)}(\vec{k}\sigma, ik_n) = \frac{U(0)}{\hbar}, \tag{5.2.6}$$

where the pseudopotential, $U(\vec{q})$, was defined by eq. (2.1.16) as the Fourier transform of the real space single ion potential. The second order contribution is given by

$$\begin{aligned}\Sigma^{(2)}(\vec{k}\sigma, ik_n) = \left(\frac{1}{\hbar}\right)^2 \sum_{\vec{q}\vec{Q}\lambda} \Bigg[& 2\, U(\vec{Q}) h(\vec{q}, -\vec{q}, \vec{Q}, \lambda, \lambda) \mathcal{G}^0(\vec{k} + \vec{Q}\sigma, ik_n) \left[\frac{1}{2} + n_{\vec{q}\lambda}\right] \\ & + \left| g(\vec{q}, \vec{Q}, \lambda) \right|^2 \left\{ \frac{n_{\vec{q}\lambda} + f_{\vec{k}+\vec{q}+\vec{Q}}}{ik_n + \omega_{\vec{q}\lambda} - \hbar^{-1}\xi_{\vec{k}\vec{q}\vec{Q}}} + \frac{1 + n_{\vec{q}\lambda} - f_{\vec{k}+\vec{q}+\vec{Q}}}{ik_n - \omega_{\vec{q}\lambda} - \hbar^{-1}\xi_{\vec{k}\vec{q}\vec{Q}}} \right\} \Bigg],\end{aligned} \tag{5.2.7}$$

where we have introduced a short–hand notation for the Fermi–Dirac distribution, $f_{\vec{k}} = f(\xi_{\vec{k}})$. The electron–phonon interaction matrix elements, $g(\vec{q}, \vec{Q}, \lambda)$, and $h(\vec{q}, -\vec{q}, \vec{Q}, \lambda, \lambda)$ were defined in eqs. (2.1.28) and (2.1.31). As usual, the Fermi–Dirac and the Bose–Einstein distribution functions are represented by $f_{\vec{k}}$, and $n_{\vec{q}\lambda}$, respectively. The first order contribution will shift the chemical potential in the single–particle excitation spectrum. We are interested in electron–phonon interaction contributions only, and will not consider $\Sigma^{(1)}(\vec{k}\sigma, ik_n)$ from this point onward[5.1]. We find for the correction to the thermodynamic potential

$$\Omega - \Omega_0 = \frac{1}{2\beta} \int_0^1 \frac{d\eta}{\eta} \sum_{\vec{k}\sigma} \sum_{ik_n} \eta^2 \Sigma^{(2)}(\vec{k}\sigma, ik_n) \mathcal{G}^0(\vec{k}\sigma, ik_n). \tag{5.2.8}$$

[5.1] One might ask whether we should consider the combination $\Sigma^{(1)}\mathcal{G}^{(1)}$ in our expansion to second order in g. Since any term involving the electron–phonon interaction g needs to be of even order, $\mathcal{G}^{(1)}$ will not involve the electron–phonon interaction and we neglect $\Sigma^{(1)}\mathcal{G}^{(1)}$ for the same reason we neglected $\Sigma^{(1)}$ itself: It does not contain the electron–phonon interaction.

After the coupling constant integration, this expression becomes

$$\Omega - \Omega_0 = \frac{1}{2\beta} \sum_{\vec{k}\sigma} \sum_{ik_n} \frac{1}{2} \Sigma^{(2)}(\vec{k}\sigma, ik_n) \mathcal{G}^0(\vec{k}\sigma, ik_n). \tag{5.2.9}$$

which written out is given by

$$\begin{aligned} &\frac{1}{2\beta} \sum_{\vec{k}\sigma} \sum_{ik_n} \frac{1}{2\hbar^2} \sum_{\vec{q}\vec{Q}\lambda} \left[2\, U(\vec{Q}) h(\vec{q}, -\vec{q}, \vec{Q}, \lambda, \lambda) \mathcal{G}^0(\vec{k} + \vec{Q}\sigma, ik_n) \mathcal{G}^0(\vec{k}\sigma, ik_n) \left[\frac{1}{2} + n_{\vec{q}\lambda} \right] \right. \\ &\left. + \left| g(\vec{q}, \vec{Q}, \lambda) \right|^2 \mathcal{G}^0(\vec{k}\sigma, ik_n) \left\{ \frac{n_{\vec{q}\lambda} + f_{\vec{k}+\vec{q}+\vec{Q}}}{ik_n + \omega_{\vec{q}\lambda} - \hbar^{-1}\xi_{\vec{k}\vec{q}\vec{Q}}} + \frac{1 + n_{\vec{q}\lambda} - f_{\vec{k}+\vec{q}+\vec{Q}}}{ik_n - \omega_{\vec{q}\lambda} - \hbar^{-1}\xi_{\vec{k}\vec{q}\vec{Q}}} \right\} \right]. \end{aligned} \tag{5.2.10}$$

We are still left with a sum over the Matsubara frequencies ik_n. To this end we have to calculate the sums,

$$\sum_{ik_n} \mathcal{G}^0(\vec{k} + \vec{Q}\sigma, ik_n) \mathcal{G}^0(\vec{k}\sigma, ik_n), \tag{5.2.11}$$

and

$$\sum_{ik_n} \mathcal{G}^0(\vec{k}\sigma, ik_n) \left\{ \frac{n_{\vec{q}\lambda} + f_{\vec{k}+\vec{q}+\vec{Q}}}{ik_n + \omega_{\vec{q}\lambda} - \hbar^{-1}\xi_{\vec{k}\vec{q}\vec{Q}}} + \frac{1 + n_{\vec{q}\lambda} - f_{\vec{k}+\vec{q}+\vec{Q}}}{ik_n - \omega_{\vec{q}\lambda} - \hbar^{-1}\xi_{\vec{k}\vec{q}\vec{Q}}} \right\}. \tag{5.2.12}$$

The first one is summed by considering the following contour integral.

$$\oint \frac{dz}{2\pi i} \frac{1}{z - \hbar^{-1}\xi_{\vec{k}+\vec{Q}}} \frac{1}{z - \hbar^{-1}\xi_{\vec{k}}} f(z), \tag{5.2.13}$$

which will vanish as we take the contour to infinity around the complex plane. The residues of the Fermi distribution function are $(-1/\hbar\beta)$, and with the remaining two residues we find,

$$\frac{1}{\hbar\beta}\sum_{ik_n}\mathcal{G}^0(\vec{k}+\vec{Q}\sigma,ik_n)\mathcal{G}^0(\vec{k}\sigma,ik_n)=\frac{f_{\vec{k}}-f_{\vec{k}+\vec{Q}}}{\hbar^{-1}\xi_{\vec{k}}-\hbar^{-1}\xi_{\vec{k}+\vec{Q}}}, \tag{5.2.14}$$

The second sum is best split into two terms, which can then be summed separately. One finds,

$$\begin{aligned}&\frac{1}{\hbar\beta}\sum_{ik_n}\mathcal{G}^0(\vec{k}\sigma,ik_n)\left\{\frac{n_{\vec{q}\lambda}+f_{\vec{k}+\vec{q}+\vec{Q}}}{ik_n+\omega_{\vec{q}\lambda}-\hbar^{-1}\xi_{\vec{k}\vec{q}\vec{Q}}}+\frac{1+n_{\vec{q}\lambda}-f_{\vec{k}+\vec{q}+\vec{Q}}}{ik_n-\omega_{\vec{q}\lambda}-\hbar^{-1}\xi_{\vec{k}\vec{q}\vec{Q}}}\right\}=\\&\frac{f_{\vec{k}}n_{\vec{q}\lambda}+f_{\vec{k}}f_{\vec{k}+\vec{q}+\vec{Q}}-f_{\vec{k}+\vec{q}+\vec{Q}}-f_{\vec{k}+\vec{q}+\vec{Q}}n_{\vec{q}\lambda}}{\hbar^{-1}\xi_{\hbar^{-1}\vec{k}}-\hbar^{-1}\xi_{\vec{k}+\vec{q}+\vec{Q}}-\omega_{\vec{q}\lambda}}+\frac{f_{\vec{k}}+f_{\vec{k}}n_{\vec{q}\lambda}-f_{\vec{k}}f_{\vec{k}+\vec{q}+\vec{Q}}-f_{\vec{k}+\vec{q}+\vec{Q}}n_{\vec{q}\lambda}}{\hbar^{-1}\xi_{\hbar^{-1}\vec{k}}-\hbar^{-1}\xi_{\vec{k}+\vec{q}+\vec{Q}}+\omega_{\vec{q}\lambda}}.\end{aligned} \tag{5.2.15}$$

The thermodynamic potential up to second order is now given by

$$\begin{aligned}\Omega-\Omega_0=\frac{1}{2}\sum_{\vec{k}\vec{q}\vec{Q}\lambda}\Bigg[&2\,U(\vec{Q})h(\vec{q},-\vec{q},\vec{Q},\lambda,\lambda)\left(\frac{1}{2}+n_{\vec{q}\lambda}\right)\frac{f_{\vec{k}}-f_{\vec{k}+\vec{Q}}}{\xi_{\vec{k}}-\xi_{\vec{k}+\vec{Q}}}\\&+\left|g(\vec{q},\vec{Q},\lambda)\right|^2\left\{\frac{f_{\vec{k}}n_{\vec{q}\lambda}+f_{\vec{k}}f_{\vec{k}+\vec{q}+\vec{Q}}-f_{\vec{k}+\vec{q}+\vec{Q}}-f_{\vec{k}+\vec{q}+\vec{Q}}n_{\vec{q}\lambda}}{\xi_{\vec{k}}-\xi_{\vec{k}+\vec{q}+\vec{Q}}+\hbar\omega_{\vec{q}\lambda}}\right.\\&\left.+\frac{f_{\vec{k}}+f_{\vec{k}}n_{\vec{q}\lambda}-f_{\vec{k}}f_{\vec{k}+\vec{q}+\vec{Q}}-f_{\vec{k}+\vec{q}+\vec{Q}}n_{\vec{q}\lambda}}{\xi_{\vec{k}}-\xi_{\vec{k}+\vec{q}+\vec{Q}}-\hbar\omega_{\vec{q}\lambda}}\right\}\Bigg].\end{aligned} \tag{5.2.16}$$

We will combine the last two terms by bringing them onto a common denominator. This procedure yields,

$$\begin{aligned}\Omega-\Omega_0 &= \frac{1}{2}\sum_{\vec{k}\vec{q}\vec{Q}\lambda}\Bigg[2\,U(\vec{Q})h(\vec{q},-\vec{q},\vec{Q},\lambda,\lambda)\left(\frac{1}{2}+n_{\vec{q}\lambda}\right)\frac{f_{\vec{k}}-f_{\vec{k}+\vec{Q}}}{\xi_{\vec{k}}-\xi_{\vec{k}+\vec{Q}}} \\ &\quad+\left|g(\vec{q},\vec{Q},\lambda)\right|^2\frac{2\left(\xi_{\vec{k}}-\xi_{\vec{k}+\vec{q}+\vec{Q}}\right)\left(f_{\vec{k}}-f_{\vec{k}+\vec{q}+\vec{Q}}\right)\left(\frac{1}{2}+n_{\vec{q}\lambda}\right)}{\left(\xi_{\vec{k}}-\xi_{\vec{k}+\vec{q}+\vec{Q}}\right)^2-\left(\hbar\omega_{\vec{q}\lambda}\right)^2} \\ &\quad+\left|g(\vec{q},\vec{Q},\lambda)\right|^2\frac{\omega_{\vec{q}\lambda}\left(f_{\vec{k}}-2f_{\vec{k}}f_{\vec{k}+\vec{q}+\vec{Q}}+f_{\vec{k}+\vec{q}+\vec{Q}}\right)}{\left(\xi_{\vec{k}}-\xi_{\vec{k}+\vec{q}+\vec{Q}}\right)^2-\left(\hbar\omega_{\vec{q}\lambda}\right)^2}.\Bigg]. \end{aligned} \tag{5.2.17}$$

We can separate the middle term into a part that depends on the lattice vibrations only through the electron–phonon interaction matrix elements, $\left|g(\vec{q},\vec{Q},\lambda)\right|^2$, and a part that explicitly depends on the phonon frequencies. We will call the former term the "adiabatic" contribution and the latter, the "non–adiabatic" contribution. Using this terminology, we find that the last term can not be separated in this fashion and is purely non–adiabatic. The very first term is therefore purely adiabatic. The middle term is given by

$$\begin{aligned}&\frac{1}{2}\sum_{\vec{k}\vec{q}\vec{Q}\lambda}\left|g(\vec{q},\vec{Q},\lambda)\right|^2\left(f_{\vec{k}}-f_{\vec{k}+\vec{q}+\vec{Q}}\right)\left(\frac{1}{2}+n_{\vec{q}\lambda}\right)\Bigg\{\frac{1}{\xi_{\vec{k}}-\xi_{\vec{k}+\vec{q}+\vec{Q}}-\hbar\omega_{\vec{q}\lambda}}-\frac{1}{\xi_{\vec{k}}-\xi_{\vec{k}+\vec{q}+\vec{Q}}} \\ &\qquad+\frac{1}{\xi_{\vec{k}}-\xi_{\vec{k}+\vec{q}+\vec{Q}}+\hbar\omega_{\vec{q}\lambda}}-\frac{1}{\xi_{\vec{k}}-\xi_{\vec{k}+\vec{q}+\vec{Q}}}+\frac{2}{\xi_{\vec{k}}-\xi_{\vec{k}+\vec{q}+\vec{Q}}}\Bigg\}\end{aligned} \tag{5.2.18}$$

We will then write the thermodynamic potential as

$$\Omega-\Omega_0=\Omega_1^{ad}+\Omega_1^{na}+\Omega_2^{na}, \tag{5.2.19}$$

where the adiabatic contribution is given by

$$\begin{aligned}\Omega_1^{ad} &= \sum_{\vec{k}\vec{q}\vec{Q}\lambda}\Bigg\{U(\vec{Q})h(\vec{q},-\vec{q},\vec{Q},\lambda,\lambda)\left(\frac{1}{2}+n_{\vec{q}\lambda}\right)\frac{f_{\vec{k}}-f_{\vec{k}+\vec{Q}}}{\xi_{\vec{k}}-\xi_{\vec{k}+\vec{Q}}} \\ &\quad+\left|g(\vec{q},\vec{Q},\lambda)\right|^2\left(\frac{1}{2}+n_{\vec{q}\lambda}\right)\frac{f_{\vec{k}}-f_{\vec{k}+\vec{q}+\vec{Q}}}{\xi_{\vec{k}}-\xi_{\vec{k}+\vec{q}+\vec{Q}}}\Bigg\}.\end{aligned} \tag{5.2.20}$$

The non–adiabatic contributions are given by

$$\begin{aligned}\Omega_1^{na} &= \frac{1}{2}\sum_{\vec{k}\vec{q}\vec{Q}\lambda}\left|g(\vec{q},\vec{Q},\lambda)\right|^2\left(f_{\vec{k}}-f_{\vec{k}+\vec{q}+\vec{Q}}\right)\left(\frac{1}{2}+n_{\vec{q}\lambda}\right)\\ &\times\left\{\frac{1}{\xi_{\vec{k}}-\xi_{\vec{k}+\vec{q}+\vec{Q}}-\hbar\omega_{\vec{q}\lambda}}-\frac{1}{\xi_{\vec{k}}-\xi_{\vec{k}+\vec{q}+\vec{Q}}}+\frac{1}{\xi_{\vec{k}}-\xi_{\vec{k}+\vec{q}+\vec{Q}}+\hbar\omega_{\vec{q}\lambda}}-\frac{1}{\xi_{\vec{k}}-\xi_{\vec{k}+\vec{q}+\vec{Q}}}\right\}\end{aligned} \tag{5.2.21}$$

and

$$\Omega_2^{na}=\frac{1}{2}\sum_{\vec{k}\vec{q}\vec{Q}\lambda}\left|g(\vec{q},\vec{Q},\lambda)\right|^2\frac{\omega_{\vec{q}\lambda}\left(f_{\vec{k}}-2f_{\vec{k}}f_{\vec{k}+\vec{q}+\vec{Q}}+f_{\vec{k}+\vec{q}+\vec{Q}}\right)}{\left(\xi_{\vec{k}}-\xi_{\vec{k}+\vec{q}+\vec{Q}}\right)^2-\left(\hbar\omega_{\vec{q}\lambda}\right)^2}. \tag{5.2.22}$$

In a plane wave basis, the electron–phonon interaction matrix elements are given by eqs. (2.1.28) and (2.1.31). The corrections to the thermodynamic potential are given by,

$$\begin{aligned}\Omega_1^{ad} &= \sum_{\vec{k}\vec{q}\vec{Q}\lambda}\frac{\hbar^2}{2\,N_0M\hbar\omega_{\vec{q}\lambda}}\left(\frac{1}{2}+n_{\vec{q}\lambda})\right)\left\{\frac{\left[\left(\vec{q}+\vec{Q}\right)\cdot\hat{\eta}_{\vec{q}\lambda}\right]^2\left[U(\vec{q}+\vec{Q})\right]^2\left(f_{\vec{k}}-f_{\vec{k}+\vec{q}+\vec{Q}}\right)}{\xi_{\vec{k}}-\xi_{\vec{k}+\vec{q}+\vec{Q}}}\right.\\ &\left.-\frac{\left[\vec{Q}\cdot\hat{\eta}_{\vec{q}\lambda}\right]^2\left[U(\vec{Q})\right]^2\left(f_{\vec{k}}-f_{\vec{k}+\vec{Q}}\right)}{\xi_{\vec{k}}-\xi_{\vec{k}+\vec{Q}}}\right\},\end{aligned} \tag{5.2.23}$$

$$\Omega_1^{na}=\sum_{\vec{k}\vec{q}\vec{Q}\lambda}\frac{\hbar^2}{2\,N_0M}\left[\left(\vec{q}+\vec{Q}\right)\cdot\hat{\eta}_{\vec{q}\lambda}\right]^2\left[U(\vec{q}+\vec{Q})\right]^2\frac{f_{\vec{k}}-f_{\vec{k}+\vec{q}+\vec{Q}}}{\xi_{\vec{k}}-\xi_{\vec{k}+\vec{q}+\vec{Q}}}\frac{\hbar\omega_{\vec{q}\lambda}\left(\frac{1}{2}+n_{\vec{q}\lambda}\right)}{\left(\xi_{\vec{k}}-\xi_{\vec{k}+\vec{q}+\vec{Q}}\right)^2-\left(\hbar\omega_{\vec{q}\lambda}\right)^2}, \tag{5.2.24}$$

and

$$\Omega_2^{na} = \frac{1}{2}\sum_{\vec{k}\vec{q}\vec{Q}\lambda} \frac{\hbar^2}{2\,N_0 M}\left[\left(\vec{q}+\vec{Q}\right)\cdot\hat{\eta}_{\vec{q}\lambda}\right]^2\left[U(\vec{q}+\vec{Q})\right]^2 \frac{f_{\vec{k}}\left(1-f_{\vec{k}+\vec{q}+\vec{Q}}\right)+f_{\vec{k}+\vec{q}+\vec{Q}}\left(1-f_{\vec{k}}\right)}{\left(\xi_{\vec{k}}-\xi_{\vec{k}+\vec{q}+\vec{Q}}\right)^2-\left(\hbar\omega_{\vec{q}\lambda}\right)^2}. \tag{5.2.25}$$

Taking a closer look at the integrands in the two terms Ω_1^{na} and Ω_2^{na}, one notices that they share a number of coefficients. The largest contribution presumably stems from the diverging denominator,

$$\left(\xi_{\vec{k}}-\xi_{\vec{k}+\vec{q}+\vec{Q}}\right)^2-\left(\hbar\omega_{\vec{q}\lambda}\right)^2=0. \tag{5.2.26}$$

Using a free electron dispersion and a Debye model, this equation can be rewritten as

$$q^2+2kq\mu=\pm\frac{c_L q}{\hbar^2/(2m)}, \tag{5.2.27}$$

where μ denotes the angle between the momenta $\vec{k}$ and $\vec{q}$. Solving for q,

$$q=-\frac{2p}{\mu}\pm\frac{c_L}{\hbar^2/2m}, \tag{5.2.28}$$

shows that mainly q values will contribute to the integrals that satisfy the above relation. Taking the ratio of the integrands,

$$\frac{\Omega_2^{na}}{\Omega_1^{na}}=\frac{f_{\vec{k}}\left(1-f_{\vec{k}+\vec{q}+\vec{Q}}\right)}{\left(f_{\vec{k}}-f_{\vec{k}+\vec{q}+\vec{Q}}\right)\hbar\omega_{\vec{q}\lambda}\left(\frac{1}{2}+n_{\vec{q}\lambda}\right)/\left(\xi_{\vec{k}}-\xi_{\vec{k}+\vec{q}+\vec{Q}}\right)}, \tag{5.2.29}$$

and expanding about $q=-\frac{2p}{\mu}$, one finds in leading order,

$$\frac{4\left(\hbar^2/2m\right)\exp(\frac{4\left(\hbar^2/2m\right)k^2}{\mu^2})\left(\exp(\frac{2\,c_L\,k}{\mu})-1\right)\,k\,\left(\mu^2-1\right)}{c_L\,\left(\exp(\frac{4\left(\hbar^2/2m\right)k^2}{\mu^2})-\exp(4\left(\hbar^2/2m\right)k^2)\right)\left(1+\exp(\frac{2\,c_L\,k}{\mu})\right)\,\mu}, \tag{5.2.30}$$

which diverges strongly for $\mu \to 0^-$. Higher orders do not show this kind of behavior and do not contribute significantly to eq. (5.2.29) for $q \to$ eq. (5.2.28). This means that the term Ω_2^{na} will be emphasized over Ω_1^{na} and we expect it to be much larger than aforementioned Ω_1^{na}.

5.3 Discussion of Results

5.3.1 Low Temperatures – Non–Adiabatic Contribution

At low temperatures, long wavelength phonons dominate the thermodynamic properties. We will use a simple model for the electron–phonon interaction, $|g(\vec{q},\lambda)|^2 = \frac{\hbar^2}{2N_0 M c_L} |\vec{q}| \, \Theta(q_c - |\vec{q}|)$, to determine the leading temperature dependences. In this model, we used longitudinal phonons in a Debye model with speed c_L, and replaced the pseudopotential with a square well potential of width q_c. One finds

$$\begin{aligned} \Omega_1^{na} &= b_1^{(0)} + b_1^{(2)} T^2 + b_1^{(4)} T^4 + \cdots \\ \Omega_2^{na} &= b_2^{(0)} + b_2^{(2)} T^2 + b_2^{(4)} T^4 \ln\left(\frac{T}{T_0}\right) + \cdots \end{aligned} \tag{5.3.1}$$

The low temperature dependences are dominated by Ω_2^{na}. The non–adiabatic contributions lead to a temperature independent part to the electronic groundstate potential, which are extremely small compared to Φ_0, and are generally considered negligible. $b_1^{(2)}$ is smaller than $b_2^{(2)}$ by a factor $\sim \frac{<\hbar\omega>}{\epsilon_F}$. These T^2 terms correspond to contributions to the electronic effective mass and lead to an enhancement of the entropy, $S_{ep} = S_{el}(1+\lambda)$. λ can be obtained from analysis of experimental data and also from theoretical estimates for nearly–free–electron metals. From experiment λ is roughly between $0 - 0.4$ for nearly–free–electron metals while it is between $0.4 - 1.0$ for transition metals. With theoretical estimates one finds that λ is determined by the strength of the square of the electron–phonon coupling and the average of the inverse of the phonon frequency averaged over the phonon density of states. Theoretical calculations for nearly–free–electron metals agree with experimental values to within 25%.

The leading corrections to the T^2 term in Ω_2^{na} was originally derived by Eliashberg (Eliashberg, 1960a,b). $b^{(4)}$ is proportional to $\frac{1}{c_L^2}$ and arises from the effective interaction between electrons

mediated by phonons. This term is generic to Fermi Liquids. There is an analogous term in almost ferromagnetic Fermi Liquids which leads to a strong temperature dependence in the specific heat due to the soft paramagnon energies associated with the incipient transition to ferromagnetism (Doniach and Engelsberg, 1966).

5.3.2 High Temperatures

This regime is defined by $(\hbar\omega_{\vec{q}\lambda})_{max} \ll k_B T \ll \epsilon_F$. Ω_2^{na} is found to be two orders of magnitude larger than $\Omega_1^{(na)}$. We approximate the electron-ion pseudopotential by the Harrison potential which is a screened bare potential (Harrison, 1966) since unlike in the low temperature regime an accurate model for large q values are important in comparing the relative magnitudes of adiabatic and non–adiabatic contributions.

The temperature dependence of the non–adiabatic contributions $\Omega_1^{(na)}$ and Ω_2^{na} do not depend even quantitatively on whether we use a Debye or Einstein phonon spectrum in this temperature range. However there is a weak dependence on the cutoff parameter, q_D. This lack of sensitivity comes from the fact that the energy scale of $\hbar\omega_{\vec{q}\lambda}$ is so much smaller than the temperatures and ϵ_F so that $\hbar\omega_{\vec{q}\lambda}\left(\frac{1}{2} + n_{\vec{q}\lambda}\right) = T + \frac{\left(\hbar\omega_{\vec{q}\lambda}\right)^2}{12T}$ and the denominator is dominated by the electronic energies. Once $\hbar\omega_{\vec{q}\lambda}$ is dropped from the denominator and since $\sum_\lambda \left[(\vec{q}+\vec{Q})\cdot\eta(\vec{q},\lambda)\right]^2 = \left(\vec{q}+\vec{Q}\right)^2$ for any set of modes, all details of the phonon spectrum and wavefunctions drop out. The temperature dependences are given by

$$\Omega_1^{na} = A_1 T + B_1 + C_1 T^{-1} \tag{5.3.2}$$

$$\Omega_2^{na} = A_2 + B_2 \ln T. \tag{5.3.3}$$

In figures 5.1 and 5.2 we plot Ω_1^{na} and Ω_2^{na} for a Debye model assuming a spherical Fermi surface with $q_D = 2.5p_F$ and $5.0p_F$. The value of the pseudopotential is $U(0) = \frac{1}{3}\epsilon_F$ and has the same value as the Harrison pseudopotential at $\vec{q} = 0$ with parameters appropriate to Na (Wallace, 1998)[Table 19, p. 406]. We have checked that the same temperature dependences are found in Ω_2^{na} and Ω_1^{na} when more accurate models for the phonon spectra for different metals are used. The only difference between the Debye model results and those for phonon spectra and eigenvectors of Na and Pb is that

the weak cutoff effect translates into a dependence on the lattice parameter, $a_{Lattice}$, which goes as $a_{Lattice}^{-2}$. We discuss these models in the next section on the adiabatic contributions. We note in passing that since the Fermi-Dirac distributions are smooth functions of $\frac{\xi_{\vec{k}}}{T}$ at high temperatures it is tempting to expand $f_{\vec{k}+\vec{q}+\vec{Q}}$ in powers of $\frac{\xi_{\vec{k}+\vec{q}+\vec{Q}}-\xi_{\vec{k}}}{T}$ which results in expressions of the form $AT + B + CT^{-1} + \cdots$ for both Ω_1^{na} and Ω_2^{na} in disagreement with expression for Ω_2^{na} above. The discrepancy between the power series expansions and direct evaluation arises because these series turn out to be only asymptotically convergent.

This temperature dependence for Ω_2^{na}, eq. (5.3.3), is consistent with the results found by previous authors for the non–adiabatic contribution from an Einstein mode (Grimvall, 1981,p. 126), (Grimvall, 1976). The starting point of previous authors is the same as ours, eq. (5.2.3), except for the absence of the contribution from second order electron–ion displacements. Prange and Kadanoff (Prange and Kadanoff, 1964) originally derived an expression for the specific heat contribution which has subsequently been used by others. This expression does not contain Ω_1^{na} or Ω_1^{ad} due to an approximation in its derivation. Dropping Ω_1^{na} is a good approximation at low temperatures and continues to be so in the temperature regime of interest here. However in the high temperature regime the adiabatic contribution dominates the non-adiabatic contributions as we now discuss.

5.3.3 Adiabatic Contributions

At low temperatures the adiabatic contribution contribution is negligible but for temperatures greater than the maximum phonon energy this term eventually dominates. In order to calculate this term a more realistic model for the lattice is required because of the second term in the brackets in eq. (5.2.23) arising from our pseudopotential treatment, cf. eq. (2.1.31) in Chapter 2. Whereas the non-adiabatic terms are not sensitive to the phonon spectra the adiabatic term is roughly proportional to average of $1/\left(\hbar\omega_{\vec{q}\lambda}\right)^2$ over the spectrum.

The phonon spectrum and polarization vectors for Na was calculated for a pseudopotential model, see Fig. 36 in (Wallace, 1997). Following the notation of the same reference the dynamical matrix is given by

$$D_{ij}(\vec{k}) = \frac{1}{M}\sum_{\vec{R}_\alpha} \Phi_{ij}(\vec{R}_\alpha) e^{i\vec{k}\cdot\vec{R}_\alpha}, \tag{5.3.4}$$

Figure 5.1: Ω_1^{na} for Einstein and Debye models. Note that the sign of the slope depends on the average phonon energy used in the Einstein model.

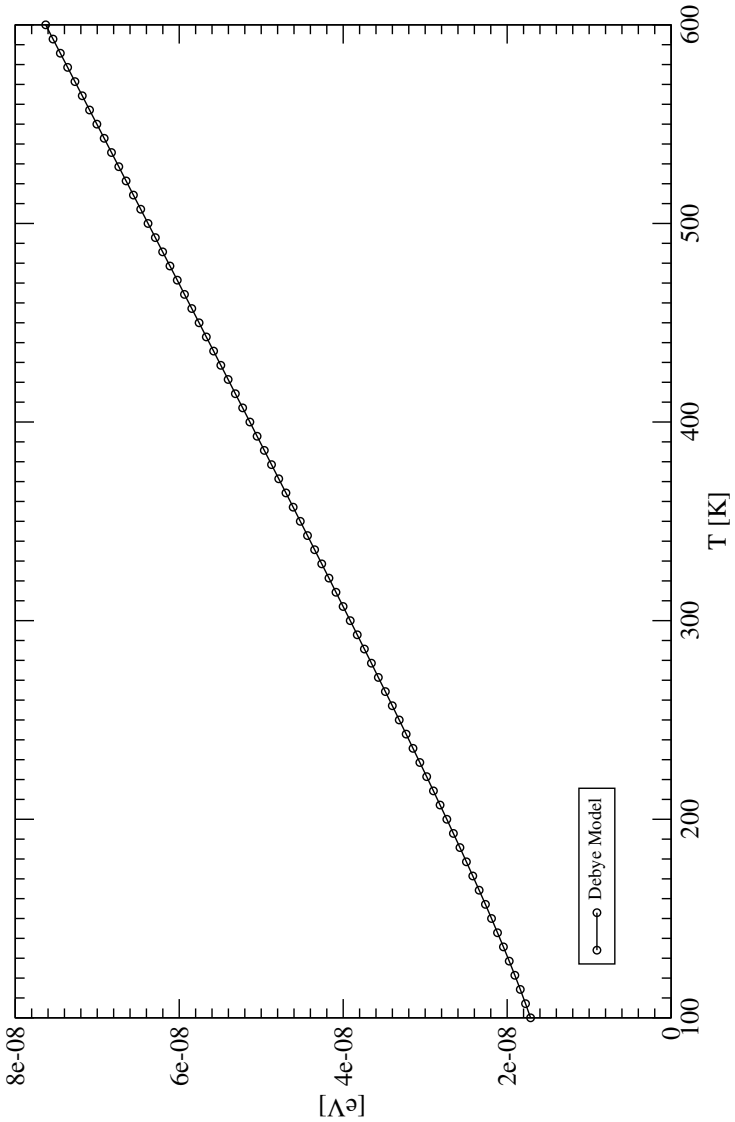

Figure 5.2: Ω_2^{na} for Einstein and Debye models.

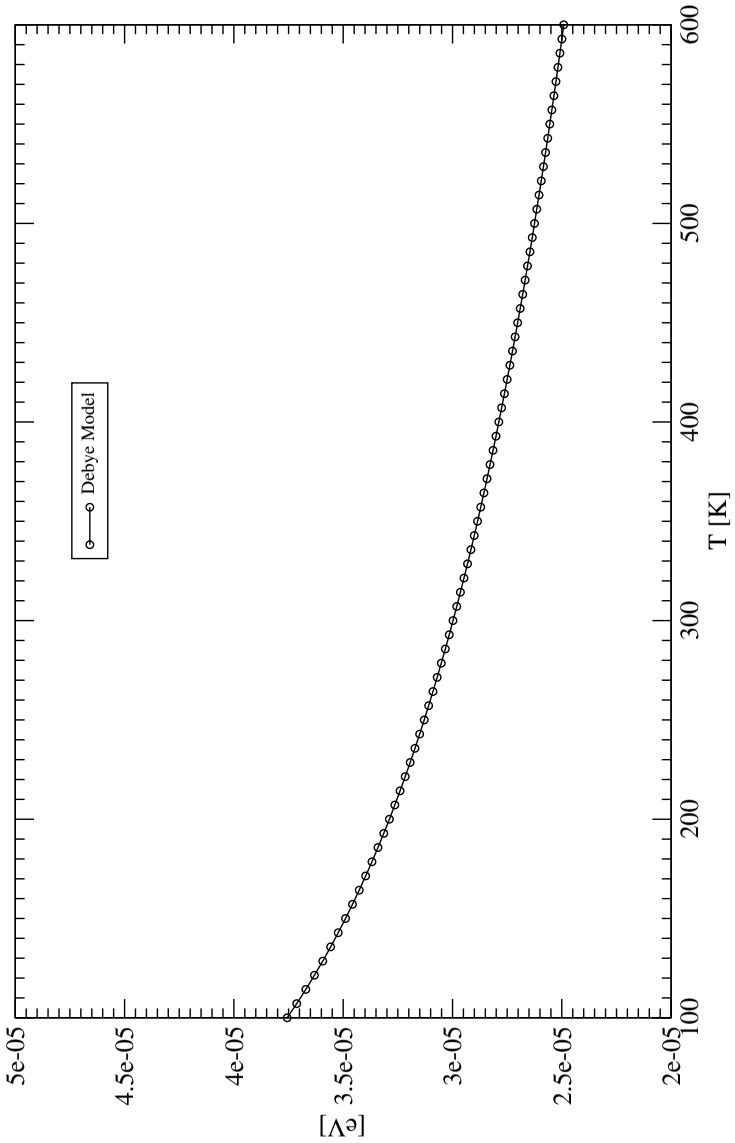

Figure 5.3: Ω_1^{ad} for a Debye model.

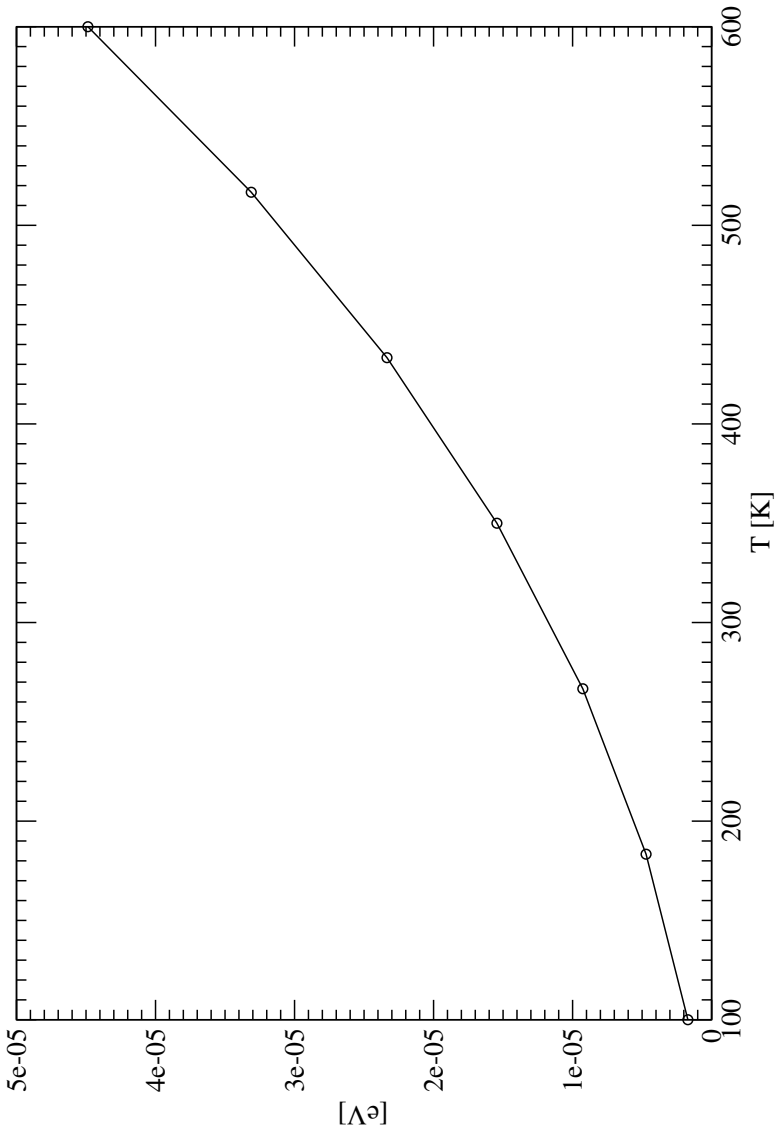

where the sum is over the positions of ions with respect to one whose position is taken to be at the origin and M is the mass of an ion. $\Phi_{ij}(\vec{R}_\alpha)$ are given by equation (W6.3) in (Wallace, 1997) and denote the matrix elements of the second order derivative of the ion potential in the positions of the ions relative to their equilibrium positions. The phonon spectra of Pb and Al have been measured by neutron scattering and we use a Born–von Karman Force constant parameterizations of data which determine the $\Phi_{ij}(\vec{R}_\alpha)$ (Cowley, 1974a,b). The Harrison pseudopotential is also used to model the electron-phonon interaction with the parameters given in Chapter 2 in Table 2.1.

5.4 Electron–Ion Model

The high–temperature limit can also be investigated by considering quantum corrections to the "classical" ion motion. In this approach, the ion part of the Schrödinger equation for the crystal is expanded in a power series in $\hbar$ and only low order terms are retained. In the $\hbar \to 0$ limit, the "classical" electron–ion approach is recovered. The expression for the effective partition function was originally derived by Kirkwood (Kirkwood, 1933) for a system of Bosons or Fermions. Zwanzig (Zwanzig, 1957) expanded the formalism to include a system of ions and electrons. Following his convention, we will use Greek indices to indicate nuclei and Latin indices to refer to electrons. The Hamiltonian Zwanzig considered is given by

$$\mathcal{H} = \mathrm{KE}_\nu + \mathrm{KE}_n + \Omega_{eI}([\vec{r}^{\,\alpha}], [\vec{r}^{\,i}]), \tag{5.4.1}$$

with

$$\begin{aligned} \mathrm{KE}_\nu &= -\sum_{\alpha=1}^{\nu} \frac{\hbar^2 \nabla_\alpha^2}{2M} \\ \mathrm{KE}_n &= -\sum_{i=1}^{n} \frac{\hbar^2 \nabla_i^2}{2m}, \end{aligned} \tag{5.4.2}$$

where the derivatives are taken with respect to ion or electron coordinates, respectively. The ion and electron masses are written as M and m. The potential $\Omega_{eI}([\vec{r}^{\alpha}],[\vec{r}^{i}])$ stands for the total potential due to interactions between the electrons and the ions. $[\vec{r}^{i}]$ or $[\vec{r}^{\alpha}]$ indicate the complete set of electron or ion positions. We will assume that the electron wave functions are given by some complete set of functions and that the ion wave functions are given by plane waves. The partition function of the canonical ensemble is given by

$$Z = \sum_n \int d^3[\vec{r}^{i}] d^3[\vec{r}^{\alpha}] \varphi_n^*([\vec{r}^{i}],[\vec{r}^{\alpha}]) e^{-\beta\mathcal{H}} \varphi_n([\vec{r}^{i}],[\vec{r}^{\alpha}]), \tag{5.4.3}$$

where $\varphi_n([\vec{r}^{i}],[\vec{r}^{\alpha}])$ is a complete set of states. It is understood that $\varphi_n([\vec{r}^{i}],[\vec{r}^{\alpha}])$ is an eigenfunction to the full Hamiltonian, $\mathcal{H}$, with eigenvalue, E_n. The full wavefunction $\varphi_n([\vec{r}^{i}],[\vec{r}^{\alpha}])$ will be replaced by

$$\frac{1}{(2\pi\hbar)^{3\nu/2}} e^{i/\hbar \sum_\alpha \vec{p}_\alpha \cdot \vec{r}} \psi_k([\vec{r}^{i}],[\vec{r}^{\alpha}]), \tag{5.4.4}$$

with

$$\underbrace{\left[\mathrm{KE}_n + \Omega_{eI}([\vec{r}^{\alpha}],[\vec{r}^{i}])\right]}_{\mathcal{H}_e} \psi_k([\vec{r}^{i}],[\vec{r}^{\alpha}]) = \Phi_k([\vec{r}^{\alpha}]) \psi_k([\vec{r}^{i}],[\vec{r}^{\alpha}]). \tag{5.4.5}$$

The partition function can then be written as

$$Z = \frac{1}{(2\pi\hbar)^{3\nu}} \sum_k \int d^3[\vec{r}^{\nu}] d^3[\vec{p}^{\nu}] e^{-\beta\mathcal{H}_k} b_k([\vec{r}^{nu}]), \tag{5.4.6}$$

where

$$b_k([\vec{r}^{\nu}]) = \int d^3[\vec{r}^{n}] \psi_k^*([\vec{r}^{i}],[\vec{r}^{\alpha}]) w_k \psi_k([\vec{r}^{i}],[\vec{r}^{\alpha}]). \tag{5.4.7}$$

The functions w_k are defined by the condition

$$e^{-\beta\mathcal{H}}e^{i/\hbar\sum_\alpha \vec{p}_\alpha\cdot\vec{r}_\alpha}\psi_k([\vec{r}^{\,i}],[\vec{r}^{\,\alpha}]) = e^{i/\hbar\sum_\alpha \vec{p}_\alpha\cdot\vec{r}_\alpha}\psi_k([\vec{r}^{\,i}],[\vec{r}^{\,\alpha}])e^{-\beta\mathcal{H}_k}w_k, \tag{5.4.8}$$

and the Hamiltonian, $\mathcal{H}_k$, is given by

$$\mathcal{H}_k = \sum_{\alpha=1}^{\nu}\frac{p_\alpha^2}{2M} + \Phi_k([\vec{r}^{\,\nu}]). \tag{5.4.9}$$

This procedure isolates all the quantum corrections associated with the electron wavefunction of the k^{th} eigenstate into the function w_k. In $b_k([\vec{r}^{\,\nu}])$, these corrections are averaged over an electronic state k. In order to evaluate these corrections, w_k will be expanded in powers of $\hbar$. We are only interested in factors of $\hbar$ associated with the ion motion, and will write factors of $\hbar$ associated with the electronic part as $\hbar_e$ for clarity. The expansion of w_k can be written as

$$w_k = w_k^{(0)} + \hbar w_k^{(1)} + \hbar^2 w_k^{(2)} + \cdots \tag{5.4.10}$$

Zwanzig found the first two terms in the above series by solving differential equations of the $w_k^{(i)}$. We will here only quote his results.

$$\begin{aligned} w_k^{(0)} &= 1 \\ w_k^{(1)} &= -\frac{i\beta^2}{2}\sum_\alpha \frac{\vec{p}_\alpha\cdot\vec{\nabla}_\alpha}{M} + i\frac{\vec{p}_\alpha}{M}\frac{e^{\beta\Omega_k}-1}{\Omega_k}\cdot\vec{\nabla}_\alpha \ln\Psi_k, \end{aligned} \tag{5.4.11}$$

where

$$\Omega_k = \frac{\hbar_e^2}{2m}\sum_j \left[\nabla_j^2 + 2(\vec{\nabla}_j \ln\psi_k)\cdot\vec{\nabla}_j\right]. \tag{5.4.12}$$

The first term $w_k^{(0)}$ leads to a contribution

$$Z_0 = \int \prod_{\nu=1,\cdots,N} \frac{d\vec{r}^{\nu} d\vec{p}^{\nu}}{(2\pi\hbar)^{3\nu}} e^{-\beta H_g} \sum_k e^{-\beta\epsilon_k([\vec{r}^{\nu}])}, \tag{5.4.13}$$

where $\epsilon_k([\vec{r}^{\alpha}]) = \Phi_k([\vec{r}^{\alpha}]) - \Phi_g([\vec{r}^{\nu}])$ is the electronic excitation spectrum, while the contribution from $w_k^{(1)}$ vanishes when averaged over the ion motion.

The second order corrections to the classical motion are given by $w_k^{(2)} = w_k^{(2a)} + w_k^{(2b)}$. Evaluating $w_k^{(2a)}$ one finds

$$\begin{aligned} w_k^{(2a)} &= \sum_\alpha \frac{1}{2M}\left[\frac{\beta^3}{3}(\vec{\nabla}_\alpha\Phi_k)^2 - \frac{\beta^2}{2}\vec{\nabla}^2\Phi_k\right] + \frac{\beta^3}{6}\sum_{\alpha,\alpha',i,j}\frac{p_\alpha^i p_{\alpha'}^j}{M^2}\nabla_\alpha^i\nabla_{\alpha'}^j\Phi_k \\ &\quad - \frac{\beta^4}{8}\sum_{\alpha,\alpha',i,j}\frac{p_\alpha^i p_{\alpha'}^j}{M^2}\nabla_\alpha^i\Phi_k\nabla_{\alpha'}^j\Phi_k \end{aligned} \tag{5.4.14}$$

This is the dependence given by both Kirkwood and Zwanzig when the average over the kinetic energy of the ions is taken. After averaging over the ion motion

$$\begin{aligned} \left\langle w_k^{(2a)}\right\rangle &= \frac{\int\prod_{\nu=1,\cdots,N} d\vec{p}^{\nu} w_k^{(2a)} e^{-\beta\sum_\alpha \frac{|\vec{p}_\alpha|^2}{2M}}}{\int\prod_{\nu=1,\cdots,N} d\vec{p}^{\nu} e^{-\beta\sum_\alpha \frac{|\vec{p}_\alpha|^2}{2M}}} \\ &= \sum_\nu \frac{\hbar^2}{2M}\left[\frac{\beta^3}{12}(\vec{\nabla}_\nu\Phi_k)^2 - \frac{\beta^2}{3}\vec{\nabla}_\nu^2\Phi_k\right] \end{aligned} \tag{5.4.15}$$

Part of the term involving Φ_k contributes to a surface term when multiplied by $e^{-\beta\Phi_k}$ and integrated over the ion configurations and so that the contribution to the partition function is

$$Z_1 = -\frac{\beta^2\hbar^2}{24M}\int\int\prod_{\nu=1,\cdot,N}\frac{d\vec{r}^{\nu}d\vec{p}^{\nu}}{(2\pi h)^{3\nu}}\sum_k e^{-\beta H_k}\sum_\nu \vec{\nabla}_\nu^2\Phi_k \tag{5.4.16}$$

$w_k^{(2b)}$ is a complicated expression involving all powers of β.

$$\begin{aligned}
w_k^{(2b)} &= \frac{e^{\beta\Omega_k}-1}{\Omega_k}\sum_\alpha\frac{\nabla_\alpha^2\psi_k}{M\psi_k} - \beta^2\left[\frac{e^{\beta\Omega_k}-1-\beta\Omega_k}{(\beta\Omega_k)^2}\right]\sum_\alpha\frac{\vec{\nabla}_\alpha\Phi_k\cdot\vec{\nabla}_\alpha\psi_k}{M\psi_k} \\
&+ \beta^2\sum_{\alpha,\alpha',i,j}\frac{\beta p_\alpha^i p_{\alpha'}^j}{2M^2}\left[\frac{e^{\beta\Omega_k}-1}{\beta\Omega_k}\right]\nabla_\alpha^i\Phi_k\frac{\nabla_\alpha^j\psi_k}{\psi_k} \\
&- \sum_{\alpha,\alpha',i,j}\frac{p_\alpha^i p_{\alpha'}^j}{2M^2}\left(\beta\left[\frac{e^{\beta\Omega_k}-1}{\Omega_k}\right]-\left[\frac{e^{\beta\Omega_k}-1-\beta\Omega_k}{(\Omega_k)^2}\right]\right)\left[\frac{\nabla_\alpha^i\psi_k}{\psi_k}\frac{\nabla_{\alpha'}^j\psi_k}{\psi_k}\right] \\
&- \sum_{\alpha,\alpha',i,j}\frac{p_\alpha^i p_{\alpha'}^j}{M^2}\nabla_\alpha^i\left(\beta\left[\frac{e^{\beta\Omega_k}-1}{\Omega_k}\right]-\left[\frac{e^{\beta\Omega_k}-1-\beta\Omega_k}{(\Omega_k)^2}\right]\right)\frac{\nabla_{\alpha'}^j\psi_k}{\psi_k}
\end{aligned} \tag{5.4.17}$$

$\Omega_k = \frac{\hbar_e^2}{2m}\sum_j\left[\nabla_j^2 + 2\vec{\nabla}_j\ln\psi_k\cdot\vec{\nabla}_j\right]$ is a differential operator which depends on both electron and ion coordinates. Keeping the leading powers of β and averaging over the ion momenta one finds,

$$\begin{aligned}
\left\langle w_k^{(2b)}\right\rangle &= \frac{\int\prod_{\nu=1,\cdots,N}d\vec{p}^{\nu}w_k^{(2b)}e^{-\beta\sum_\alpha\frac{|\vec{p}_\alpha|^2}{2M}}}{\int\prod_{\nu=1,\cdots,N}d\vec{p}^{\nu}e^{-\beta\sum_\alpha\frac{|\vec{p}_\alpha|^2}{2M}}} \\
&\simeq \left(\beta+\frac{\beta^2\Omega_k}{2}+\cdots\right)\sum_\alpha\frac{\nabla_\alpha^2\psi_k}{2M\psi_k} + \sum_\alpha\frac{1}{M}\frac{\beta^3\Omega_k}{12}\vec{\nabla}_\alpha\Phi_k\cdot\frac{\vec{\nabla}_\alpha\psi_k}{M\psi_k} \\
&\quad - \sum_\alpha\frac{\beta\vec{\nabla}_\alpha}{M}\cdot\left[\frac{1}{2}+\frac{\beta\Omega_k}{3}\right]\frac{\vec{\nabla}_\alpha\psi_k}{\psi_k} - \sum_\alpha\frac{\beta}{M}\left[\frac{1}{2}+\frac{\beta\Omega_k}{3}\right]\frac{\vec{\nabla}_\alpha\psi_k}{\psi_k}\cdot\frac{\vec{\nabla}_\alpha\psi_k}{\psi_k} \\
&\simeq \sum_\alpha\frac{1}{M}\frac{\beta^3\Omega_k}{12}\vec{\nabla}_\alpha\Phi_k\cdot\frac{\vec{\nabla}_\alpha\psi_k}{M\psi_k} - \beta^2\sum_\alpha\frac{1}{M}\left(\frac{\Omega_k}{12}\frac{\nabla_\alpha^2\psi_k}{\psi_k}+\frac{\vec{\nabla}_\alpha\Omega_k}{3}\cdot\frac{\vec{\nabla}_\alpha\psi_k}{\psi_k}\right)
\end{aligned} \tag{5.4.18}$$

As with $w_k^{(2a)}$ part of the term involving Φ_k contributes to a surface term when multiplied by $e^{-\beta\Phi_k}$ and integrated over the ion configurations

$$\int d\vec{r}_n\psi_k^*\psi_k\left\langle w_k^{(2b)}\right\rangle = -\frac{\beta^2}{4M}\sum_\nu\int d\vec{r}_n\psi_k^*\vec{\nabla}_\nu\Omega_k\cdot\vec{\nabla}_\nu\psi_k \tag{5.4.19}$$

resulting in a contribution to the partition function

$$Z_2 = -\frac{\beta^2\hbar^2}{4M}\int \prod_{\nu=1,\cdots,N} \frac{d\vec{r}^{\nu}d\vec{p}^{\nu}}{(2\pi\hbar)^{3\nu}} e^{-\beta H_g}\sum_k e^{-\beta\epsilon_k([\vec{r}^{\nu}])}\int d\vec{r}_n \psi_k^*\vec{\nabla}_\nu\Omega_k\cdot\vec{\nabla}_\nu\psi_k \tag{5.4.20}$$

5.4.1 Partition Function

The partition function is given by

$$Z = \frac{1}{(2\pi\hbar)^{3\nu}}\int \prod_{\nu=1,\cdots,N} d\vec{r}^{\nu}d\vec{p}^{\nu}\sum_k e^{-\beta H_k} b_k([\vec{r}^{\nu}],[\vec{p}^{\nu}]) = Z_0 + Z_1 + Z_2. \tag{5.4.21}$$

When the ions are at the crystal lattice sites, $\epsilon_k([\vec{r}^{\alpha}])$ is the bandstructure of the lattice, however all possible ion configurations are averaged over in the partition function so that, in principle disordered lattices as well different lattice symmetries are included. This makes *ab initio* evaluation of this expression intractable. In order to proceed further we expand around a specific ion configuration, $[\vec{R}^{\alpha}]$,

$$\Phi_k([\vec{r}^{\nu}]) = \Phi_k([\vec{R}^{\nu}]) + \sum_\nu \vec{u}_\nu\cdot\vec{\nabla}_\nu\Phi_k([\vec{r}^{\nu}]) + \frac{1}{2}\sum_{\nu,\nu',i,j} u_i^{\nu}u_j^{\nu'}\frac{\partial^2\Phi_k([\vec{r}^{\nu}])}{\partial r_i^{\nu}\partial r_j^{\nu'}} + \cdots \tag{5.4.22}$$

where u_i^{ν} is the i^{th} component of $\vec{r}^{\nu} - \vec{R}^{\nu}$ for the ion labeled by ν. Assuming that the electronic ground state is stable for this ion configuration $\nabla_\nu\Phi_g([\vec{r}^{\nu}]) = 0$ for all ν, and the spectrum can be broken up into a part associated with the fixed ion configuration $\epsilon_k([\vec{R}_c^{\alpha}])$ and a part due to the ion motion $\delta\epsilon_k = \sum_\nu \vec{u}_\nu\cdot\vec{\nabla}_\nu\epsilon_k([\vec{R}^{\nu}]) + \cdots$. Making the assumption that $\delta\epsilon_k$ is a small correction to the electronic spectrum, and keeping leading temperature dependence in each term, the partition function can be written as

$$
\begin{aligned}
Z_0 &= Z_{Ions} Z_E e^{-\beta\Phi_g([\vec{R}^\nu])} \int \prod_{\nu=1,\cdots,N} \frac{d\vec{r}^{\,\nu} d\vec{p}^{\,\nu}}{(2\pi\hbar)^{3\nu}} \frac{e^{-\beta H^C_{Ions}}}{Z_{Ions}} \sum_k \frac{e^{-\beta\epsilon_k([\vec{R}^\alpha])}}{Z_E} \\
&\quad \times \left(1 - \beta \sum_\nu \vec{u}_\nu \cdot \vec{\nabla}_\nu \epsilon_k([\vec{R}^\nu]) - \beta \frac{1}{2} \sum_{\nu,\nu',i,j} u_i^\nu u_j^{\nu'} \frac{\partial^2 \epsilon_k([\vec{R}^\nu])}{\partial r_i^\nu \partial r_j^{\nu'}} \right) \\
Z_1 &= -\frac{\beta^2\hbar^2}{24M} Z_{Ions} Z_E e^{-\beta\Phi_g([\vec{R}^\nu])} \int \prod_{\nu=1,\cdots,N} \frac{d\vec{r}^{\,\nu} d\vec{p}^{\,\nu}}{(2\pi\hbar)^{3\nu}} \frac{e^{-\beta H^C_{Ions}}}{Z_{Ions}} \sum_k \frac{e^{-\beta\epsilon_k([\vec{R}^\nu])}}{Z_E} \vec{\nabla}^2_\nu \Phi_k([\vec{R}^\nu]) \\
Z_2 &= -\frac{\beta^2\hbar^2}{4M} Z_{Ions} Z_E e^{-\beta\Phi_g([\vec{R}^\nu])} \int \prod_{\nu=1,\cdots,N} \frac{d\vec{r}^{\,\nu} d\vec{p}^{\,\nu}}{(2\pi\hbar)^{3\nu}} \frac{e^{-\beta H^C_{Ions}}}{Z_{Ions}} \\
&\quad \times \sum_k \frac{e^{-\beta\epsilon_k([\vec{R}^\nu])}}{Z_E} \int d\vec{r}_n \psi_k^* \vec{\nabla}_\nu \Omega_k \cdot \vec{\nabla}_\nu \psi_k
\end{aligned}
\tag{5.4.23}
$$

where

$$
\begin{aligned}
H^C_{Ions} &= \sum_\nu \frac{|\vec{p}^{\,\nu}|^2}{2M} + \frac{1}{2} \sum_{\nu,\nu',i,j} u_i^\nu u_j^{\nu'} \frac{\partial^2 \Phi_g([\vec{r}^{\,\nu}])}{\partial r_i^\nu \partial r_j^{\nu'}} \\
Z_E &= \sum_k e^{-\beta\epsilon_k([\vec{R}^\alpha])} \\
Z_{Ions} &= \int \prod_{\nu=1,\cdots,N} \frac{d\vec{r}^{\,\nu} d\vec{p}^{\,\nu}}{(2\pi\hbar)^{3\nu}} e^{-\beta H^c_{Ions}}
\end{aligned}
\tag{5.4.24}
$$

H^c_{Ions} is the classical Hamiltonian for the ions expanded about the reference ion positions $[R^\nu]$ whose eigenfunctions are the vibrational modes in the harmonic approximation but the anharmonic corrections can be included by going to higher orders in the ion displacements. Z_E and Z_{Ions} are the partition functions for the electrons and ions. At high temperatures the free energy is

$$
\begin{aligned}
F &= \Phi_g([\vec{R}^\nu]) - \frac{\ln Z_{Ions}}{\beta} - \frac{\ln Z_E}{\beta} \\
&\quad + \int \prod_{\nu=1,\cdots,N} d\vec{r}^{\,\nu}\, d\vec{p}^{\,\nu}\, \frac{e^{-\beta H^C_{Ions}}}{Z_{Ions}} \sum_k \frac{e^{-\beta\epsilon_k([\vec{R}^\alpha])}}{Z_E} \\
&\qquad \times \left(\sum_\nu \vec{u}_\nu \cdot \vec{\nabla}_\nu \epsilon_k([\vec{r}^{\,\nu}]) + \frac{1}{2} \sum_{\nu,\nu',i,j} u^i_\nu u^j_{\nu'} \frac{\partial^2 \epsilon_k([\vec{r}^{\,\nu}])}{\partial r^\nu_i \partial r^{\nu'}_j} \right) \\
&\quad + \frac{\beta\hbar^2}{24M} \sum_\nu \sum_k \vec{\nabla}^2_\nu \Phi_k([\vec{R}^\nu]) \frac{e^{-\beta\epsilon_k([\vec{R}^\alpha])}}{Z_E} \\
&\quad + \frac{\beta\hbar^2}{4M} \int \prod_{\nu=1,\cdots,N} \frac{d\vec{r}^{\,\nu}\, d\vec{p}^{\,\nu}}{(2\pi\hbar)^{3\nu}} \frac{e^{-\beta H^C_{Ions}}}{Z_{Ions}} \sum_k \frac{e^{-\beta\epsilon_k([\vec{R}^\nu])}}{Z_E} \int d\vec{r}_n \psi^*_k \vec{\nabla}_\nu \Omega_k \cdot \vec{\nabla}_\nu \psi_k
\end{aligned}
\tag{5.4.25}
$$

The first three terms are the ground state energy, the free energy of the vibrations and the free energy of the non-interacting electronic states calculated with ions fixed in positions $\left[\vec{R}^\nu\right]$.

Considering the fourth term, $\sum_\nu \vec{u}_\nu \cdot \vec{\nabla}_\nu \epsilon_k([\vec{R}^\nu])$ and $\frac{1}{2}\sum_{\nu,\nu',i,j} u^i_\nu u^j_{\nu'} \frac{\partial^2 \epsilon_k([\vec{R}^\nu])}{\partial r^\nu_i \partial r^{\nu'}_j}$ can be rearranged into the forms which lead directly to the electron–phonon interaction as derived in Chapter 25 of ref. (Wallace, 1998). Taking the electron–ion interaction to be a sum of single–ion potentials for the electrons, $\sum_{\nu'} u(\vec{r} - \vec{R}_{\nu'})$,

$$
\begin{aligned}
\sum_\nu \vec{u}_\nu \cdot \vec{\nabla}_\nu \epsilon_k([\vec{R}^\nu]) &= \sum_\nu \vec{u}_\nu \cdot \vec{\nabla}_\nu \int d\vec{r} \psi^*_k(\vec{r}) \mathcal{H} \psi_k(\vec{r}) \\
&= \sum_\nu \vec{u}_\nu \cdot \vec{\nabla}_\nu \int d\vec{r} \psi^*_k(\vec{r}) \sum_{\nu'} u(\vec{r} - \vec{R}_{\nu'}) \psi_k(\vec{r}) \\
&= \sum_\nu \vec{u}_\nu \cdot \int d\vec{r} \psi^*_k(\vec{r}) \vec{\nabla}_\nu u(\vec{r} - \vec{R}_\nu) \psi_k(\vec{r}) \\
&= \left\langle k \middle| \Omega^{(1)}_k \middle| k \right\rangle
\end{aligned}
\tag{5.4.26}
$$

In the same manner

$$
\begin{aligned}
\frac{1}{2} \sum_{\nu,\nu',i,j} u^i_\nu u^j_{\nu'} \frac{\partial^2 \epsilon_k([\vec{R}^\nu])}{\partial r^\nu_i \partial r^{\nu'}_j} &= \frac{1}{2} \sum_{\nu,i,j} u^i_\nu u^j_\nu \cdot \int d\vec{r} \psi^*_k(\vec{r}) \frac{\partial^2 u(\vec{r} - \vec{R}_\nu)}{\partial r^i_\nu \partial r^j_\nu} \psi_k(\vec{r}) \\
&= \left\langle k \middle| \Omega^{(2)}_k \middle| k \right\rangle
\end{aligned}
\tag{5.4.27}
$$

The only difference from the expression appearing in reference (Wallace, 1998) corresponding to the term which is first order in the ion displacement, Eq.(25.7), is that here the terms are purely adiabatic. The fourth term now becomes

$$\sum_k \frac{e^{-\beta\epsilon_k([\vec{R}^\alpha])}}{Z_E} \prod_{\nu=1,\cdots,N} \frac{d\vec{r}^\nu d\vec{p}^\nu}{(2\pi\hbar)^{3\nu}} \frac{e^{-\beta H^C_{Ions}}}{Z_{Ions}} \left(\left\langle k \middle| \Omega^{(1)}_k \middle| k \right\rangle + \left\langle k \middle| \Omega^{(2)}_k \middle| k \right\rangle \right).$$

This term gives the adiabatic contribution, $\Omega_1^{(na)}$, found with the electron-phonon interaction. The fifth term describes corrections due to quantum mechanical behavior of the ions as the temperature is lowered. This leads to weak corrections to the terms discussed above.

$$\begin{aligned} & \frac{\beta\hbar^2}{24M} \sum_\nu \sum_k \vec{\nabla}^2_\nu \left(\Phi_k([\vec{R}^\nu]) - \Phi_g([\vec{R}^\nu]) + \Phi_g([\vec{R}^\nu]) \right) \frac{e^{-\beta\epsilon_k([\vec{R}^\alpha])}}{Z_E} \\ &= \frac{\beta\hbar^2}{24M} \sum_\nu \vec{\nabla}^2_\nu \Phi_g([\vec{R}^\nu]) + \frac{\beta\hbar^2}{24M} \sum_\nu \sum_k \vec{\nabla}^2_\nu \epsilon_k([\vec{R}^\alpha]) \frac{e^{-\beta\epsilon_k([\vec{R}^\alpha])}}{Z_E} \\ &= \frac{\beta\hbar^2}{24M} \sum_\nu \vec{\nabla}^2_\nu \Phi_g([\vec{R}^\nu]) - \frac{\hbar^2}{24M} \sum_\nu \vec{\nabla}^2_\nu \ln Z_E. \end{aligned} \tag{5.4.28}$$

In this temperature regime the electronic free energy is $\propto T^2$ so that the fifth contains T^{-1} and a T^1 contributions. The magnitude of these terms is reduced by the ion mass as well as having weaker temperature dependence at $T > 100$ K.

5.5 Conclusions

The adiabatic T contribution to the entropy due to the interaction between electronic and lattice degrees of freedom can be thought of either as being due to the temperature dependence of the renormalization of the electrons states or of the lattice modes.

Previous authors missed this contribution and found that the contribution to the entropy from the electron–phonon interaction decreased with temperature as T^{-1} and was insensitive to the details of the phonon spectrum, completely missing this adiabatic contribution. In contrast we found that

the adiabatic contribution is larger than the non–adiabatic contribution at lower temperatures and the larger the atomic mass of the elemental metal. These crossover temperatures are less than or comparable to room temperatures in general.

We have shown that calculations based on the low temperature electron–phonon limit and on the the high temperature electron–ion limit give compatible results in the intermediate temperature regime.

Our treatment of the high temperature limit is based on the harmonic approximation about equilibrium locations for the ions. This is justified by the comparatively weak temperature dependence of phonon spectra once thermal expansion is taken into account. It is unknown if these temperature dependences also hold once the lattice has melted. This question can possibly only be answered by numerical simulations.

Chapter 6

Conclusions

In this thesis we have studied the effect of the interaction between electronic and lattice degrees of freedom on single–particle and transport properties in the superconducting state at low temperatures and on thermodynamic properties at temperatures greater than 100 K. Our model for the interaction is based on a pseudopotential approach used by previous authors and fits to neutron scattering data on the phonons of lead, aluminum and sodium.

We used a different formulation of the problem in the superconducting state from the conventional Eliashberg equations. By transforming the Hamiltonian for the system so that calculations are carried out in terms of superconducting quasiparticles it is possible to calculate single–particle properties perturbatively and avoid the self–consistent calculations of Eliashberg theory. This allowed us to study the effect of the two very different components of the Fermi surface in lead. By deriving and solving a gap equation for lead which incorporated the two bands crossing the Fermi surface we were able to account for the two values of the superconducting gap, 1.286 meV and 1.379 meV, found by Farnworth and Timusk in tin films. Calculations of the single–particle properties and of the $\alpha^2F(\omega)$ features in optical conductivity further brought out the importance of accurate models for band structure. In particular it is clear that the third band is responsible for the dominant contributions to these properties.

Calculations of the single quasiparticle propagator self–energy showed none of the structure, two peaks at 4 meV and 8 meV, present in α^2F terms. Instead it showed almost monotonic increase in magnitude of the real and imaginary parts up to an energy equal to $\Delta_0 + \hbar\omega_{max}$, the maximum

phonon energy. Beyond this energy the real part monotonically decreased while the imaginary part was essentially constant just as in the case in the normal state. Nonetheless the rapid increase in the imaginary part leads to a feature in the spectral density which, when averaged over different momenta, resembles the photoemission spectrum of Chainani *et al.* (2000). However, contrary to their claim, it is not possible to identify features in their data with the α^2F function. This absence of α^2F features is not surprising since α^2F are only recovered in conventional superconductors from derivatives of optical conductivity or the current voltage characteristics of superconductor–insulator–superconductor junctions. Even in this case the features are roughly 5% of the magnitude of the large bias values of the $\frac{dI}{dV}$ function. The use of an accurate model for the Fermi surface leads to a good agreement between the experimental α^2F features in $\sigma(\omega)$. Previously Allen (Allen, 1971) using Eliashberg theory found that the peak at 8 meV was considerably smaller in magnitude than that at 4 meV and this lead to speculations about a transport version of α^2F, $\alpha^2_{tr}F$, which could account for the difference with experiment. We found that the inclusion of the topology of the 3^{rd} band Fermi surface, missed in Allen's model, makes this uneccessary.

As we pointed out there is another many–body feature at $\omega = 4\Delta_0$ which can be identified with an analogous feature at $E = 3\Delta_0$ in the single–particle self–energy. At this time quantitatively accurate calculations of this feature for lead are not practical since extending our calculation of $\sigma(\omega)$ to higher orders in the strength of the electron–phonon coupling in the memory function formalism which we used involves a very large increase in the computational time needed for the calculations. It also requires a study of the vertex corrections as we pointed out in the thesis. Quasiparticle effects have also been identified in tunneling characteristics on the hi–T_c materials. It would be interesting to understand what controls their magnitude in lead where there is no controversy regarding the Hamiltonian to see what light can be shed on their origin in hi–T_c.

Turning our attention to the normal state, we studied the effects of the electron–phonon interaction on thermodynamic properties in sodium. Two different approaches can be taken starting from different ends of the temperature spectrum. The electron–phonon approach, which uses quantized lattice vibrations, the phonons, starts out from low temperatures and one expands the single–ion potentials in powers of their displacement with respect to their equilibrium positions. This is the approach taken in the first part of Chapter 5. The other approach starts out at high temperatures, in a regime in which one can treat the ion motion classically. We identified the dominant contribution to the thermodynamic functions from the electron–phonon interaction which goes as T in the entropy. Previous authors had claimed that the electron–phonon interaction leads to a contribution

to the entropy which goes as T^{-1}. This T contribution already dominates the T^{-1} contribution at room temperature. We showed in the second part of this chapter how the two approaches connect at intermediate temperatures.

Appendix A

Brief Account of Method of Calculation

A.1 Gaussian Integration

The method used in this work is based on the so called Gauß–Kronrod algorithm (Piessens and Branders, 1974a,b). In this method one approximates the integral with a sum over function values at certain specific points multiplied by a weighting factor. Given a function $g(x)$ one proceeds to

$$\int_a^b dx\ g(x) = \int_a^b dx\ W(x)f(x), \tag{A.1}$$

by splitting $g(x)$ into a product of two functions, $W(x)$ and $f(x)$. The function $f(x)$ is assumed to be polynomial to a large degree, and the function $W(x)$ will contain the non-polynomial part. In particular, one will want to put any singularities into $W(x)$. This integral can be approximated by a sum as

$$\int_a^b dx\ W(x)f(x) \approx \sum_{j=1}^{N} w_j f(x_j). \tag{A.2}$$

This approximation is exact if $f(x)$ is a polynomial. The calculation of the weights w_j and the abcisses x_j depends on the exact form of the weighting function $W(x)$. The Gauß–Kronrod algorithm is based on this approach and extends it as to allow to reuse already calculated values. This method can therefore be used as an adaptive method in which one calculates a relatively small number N of abcisses, checks for convergence, and if necessary increases N by adding a few more extra abcisses.

A.2 Monte Carlo – VEGAS

Monte Carlo methods are based on a fundamentally different idea than Gaußian methods. In Monte Carlo one takes samples of the function to evaluate at random points and calculates their sum. If we denote the mean and the standard deviation of the samples by $\langle f \rangle$ and $\left\langle f^2 \right\rangle$, then the integral can be approximated by

$$\int dV \;\; f(\vec{x}) \approx V \langle f \rangle \pm V \sqrt{\frac{\langle f^2 \rangle - \langle f \rangle^2}{N}}. \tag{A.1}$$

The average and the standard deviation are defined as

$$\langle f \rangle = \frac{1}{N} \sum_{i=1}^{N} f(x_i), \tag{A.2}$$

$$\left\langle f^2 \right\rangle = \frac{1}{N} \sum_{i=1}^{N} \left(f(x_i) \right)^2, \tag{A.3}$$

and define the variance

$$\mathrm{Var}(\langle f \rangle) = \left\langle f^2 \right\rangle - \langle f \rangle^2. \tag{A.4}$$

The accuracy of a Monte Carlo integration will increase with $\sqrt{N}$, independent of the number of dimensions in the integral. In low dimensions this is rather expensive compared to Gaußian methods. At roughly 3-4 dimensions, Monte Carlo starts to become faster convergent than Gaußian methods.

The error estimate, the second term in (A.1), can only be taken as a rough estimate, since it is in general not known, what the distribution of the samples will look like. It is also of great importance that the samples are taken at *random* points in the integration volume, a condition that is not trivially solved in a computer. Random number generators with very large periods should be used.

In order to make this technique more efficient, the variance has to be reduced. A very popular algorithm commonly used that achieves just this is the so called VEGAS algorithm invented my Lepage (1978, 1980). It tries to reduce the variance by employing two techinques.

A.2.1 Importance Sampling

Suppose that the integrand can be written in the form

$$\int dV\ \ f = \int dV\ \ \frac{f}{g} g dV = \int dV\ \ hg, \tag{A.5}$$

and that h can be chosen such that it is nearly constant over the integration volume. A change of variables will lead to

$$\int (gdV)\ \ g, \tag{A.6}$$

which is an integral that will converge rather quickly. In practice this change of variables is done by altering the distribution of the random samples.

A.2.2 Stratified Sampling

The true average of the integrand is given by

$$\langle\langle f\rangle\rangle = \frac{1}{V}\int dV\ \ f. \tag{A.7}$$

This is related to the variance of the random samples, eq. (A.4), by

$$\lim_{N\to\infty} \mathrm{Var}(\langle f\rangle) = \frac{\mathrm{Var}(f)}{N}. \tag{A.8}$$

The idea of stratified sampling is to divide the integration volume into subvolumes, chosen such as to reduce the overall variance. Suppose the integration volume V is divided into 2 subvolumes, a and b, then the average over the function, $\langle f\rangle'$, is given by

$$\langle f\rangle' = \frac{1}{2}\left(\langle f\rangle_a + \langle f\rangle_b\right). \tag{A.9}$$

The variance becomes

$$\begin{aligned} \mathrm{Var}(\langle f\rangle') &= \frac{1}{4}\left(\mathrm{Var}(\langle f\rangle_a) + \mathrm{Var}(\langle f\rangle_b)\right) \\ &= \frac{1}{2N}\left(\mathrm{Var}_a(f) + \mathrm{Var}_b(f)\right). \end{aligned} \tag{A.10}$$

The real variance of the function depends on the subregions

$$\mathrm{Var}(f) = \frac{1}{2}\left(\mathrm{Var}_a(f) + \mathrm{Var}_b(f)\right) + \frac{1}{4}\left(\langle\langle f\rangle\rangle_a - \langle\langle f\rangle\rangle_b\right)^2, \tag{A.11}$$

which is never larger than the variance of the simpler one region integration. If the subregions are chosen in such a fashion that their means, $\langle\langle f\rangle\rangle_a$, and $\langle\langle f\rangle\rangle_b$, is different, the overal variance will be reduced compared to the one-region integration. VEGAS combines these two approaches.

Appendix B

Derivation of the transformed Hamiltonian

Starting from the electron–phonon Hamiltonian,

$$\begin{aligned}\mathcal{H} &= \sum_{\vec{k}} \xi_{\vec{k}} \left[c^{\dagger}_{\vec{k}\uparrow} c_{\vec{k}\uparrow} + c^{\dagger}_{-\vec{k}\downarrow} c_{-\vec{k}\downarrow} \right] \\ &\quad + \sum_{\vec{k}} \sum_{\vec{q}\vec{Q}\lambda} \Big\{ g(\vec{q},\vec{Q},\lambda)(a_{\vec{q}\lambda} + a^{\dagger}_{\vec{q}\lambda}) c^{\dagger}_{\vec{k}+\vec{q}+\vec{Q}\uparrow} c_{\vec{k}\uparrow} \\ &\quad + g(-\vec{q},-\vec{Q},\lambda)(a_{\vec{q}\lambda} + a^{\dagger}_{\vec{q}\lambda})^{\dagger} c^{\dagger}_{-\vec{k}-\vec{q}-\vec{Q}\downarrow} c_{-\vec{k}\downarrow} \Big\}, \end{aligned} \tag{B.1}$$

we apply the Bogoliubov transformations. The kinetic energy piece of the original Hamiltonian is now written as

$$\begin{aligned}\mathcal{H}_1 &= \sum_{\vec{k}} \xi_{\vec{k}} \Big[\left(u^{*}_{\vec{k}} \gamma^{\dagger}_{\vec{k}\uparrow} + v_{-\vec{k}} \gamma_{-\vec{k}\downarrow} \right) \left(u_{\vec{k}} \gamma_{\vec{k}\uparrow} + v^{*}_{-\vec{k}} \gamma^{\dagger}_{-\vec{k}\downarrow} \right) \\ &\quad + \left(u^{*}_{-\vec{k}} \gamma^{\dagger}_{-\vec{k}\downarrow} - v_{\vec{k}} \gamma_{\vec{k}\uparrow} \right) \left(u_{-\vec{k}} \gamma_{-\vec{k}\downarrow} - v^{*}_{\vec{k}} \gamma^{\dagger}_{\vec{k}\uparrow} \right) \Big]. \end{aligned} \tag{B.2}$$

Multiplying out the parentheses leads to

$$\begin{aligned}\mathcal{H}_1 &= \sum_{\vec{k}} \xi_{\vec{k}} \Big[u^*_{\vec{k}} u_{\vec{k}} \gamma^\dagger_{\vec{k}\uparrow} \gamma_{\vec{k}\uparrow} + u^*_{\vec{k}} v^*_{-\vec{k}} \gamma^\dagger_{\vec{k}\uparrow} \gamma^\dagger_{-\vec{k}\downarrow} + v_{-\vec{k}} u_{\vec{k}} \gamma_{-\vec{k}\downarrow} \gamma_{\vec{k}\uparrow} + v_{-\vec{k}} v^*_{-\vec{k}} \gamma_{-\vec{k}\downarrow} \gamma^\dagger_{-\vec{k}\downarrow} \\ &\quad + u^*_{-\vec{k}} u_{-\vec{k}} \gamma^\dagger_{-\vec{k}\downarrow} \gamma_{-\vec{k}\downarrow} - u^*_{-\vec{k}} v^*_{\vec{k}} \gamma^\dagger_{-\vec{k}\downarrow} \gamma^\dagger_{\vec{k}\uparrow} - v_{\vec{k}} u_{-\vec{k}} \gamma_{\vec{k}\uparrow} \gamma_{-\vec{k}\downarrow} + v_{\vec{k}} v^*_{\vec{k}} \gamma_{\vec{k}\uparrow} \gamma^\dagger_{\vec{k}\uparrow} \Big] . \end{aligned} \tag{B.3}$$

In order to simplify this expression it will be assumed that the coherence factors are inversion symmetric. Since the γ–operators satisfy Fermi statistics, they anti–commute[B.1]. $\mathcal{H}_1$ can therefore be simplified to

$$\begin{aligned}\mathcal{H}_1 &= \sum_{\vec{k}} \xi_{\vec{k}} \Big\{ \Big[|u_{\vec{k}}|^2 - |v_{\vec{k}}|^2 \Big] \Big[\gamma^\dagger_{\vec{k}\uparrow} \gamma_{\vec{k}\uparrow} + \gamma^\dagger_{-\vec{k}\downarrow} \gamma_{-\vec{k}\downarrow} \Big] + 2 \, |v_{\vec{k}}|^2 \\ &\quad + 2 \, u^*_{\vec{k}} v^*_{\vec{k}} \gamma^\dagger_{\vec{k}\uparrow} \gamma^\dagger_{-\vec{k}\downarrow} + 2 \, u_{\vec{k}} v_{\vec{k}} \gamma_{-\vec{k}\downarrow} \gamma_{\vec{k}\uparrow} \Big\} . \end{aligned} \tag{B.7}$$

After replacing the coherence factors with eqs. (3.3.4), the Hamiltonian splits into the new unperturbed piece, $\mathcal{H}_0$, and a perturbation part.

[B.1] The anti–commutation rules for the γ–operators are

$$\left\{ \gamma_{\vec{k}\sigma}, \gamma_{\vec{k}'\sigma'} \right\} = 0 \tag{B.4}$$

$$\left\{ \gamma^\dagger_{\vec{k}\sigma}, \gamma^\dagger_{\vec{k}'\sigma'} \right\} = 0 \tag{B.5}$$

$$\left\{ \gamma_{\vec{k}\sigma}, \gamma^\dagger_{\vec{k}'\sigma'} \right\} = \delta_{\vec{k},\vec{k}'} \delta_{\sigma,\sigma'} , \tag{B.6}$$

where $\{A, B\} = AB + BA$, denotes the anti–commutator.

$$\mathcal{H}_1 = \overbrace{\sum_{\vec{k}} \left\{ E_{\vec{k}} \left[\gamma^\dagger_{\vec{k}\uparrow}\gamma_{\vec{k}\uparrow} + \gamma^\dagger_{-\vec{k}\downarrow}\gamma_{-\vec{k}\downarrow} \right] + 2\left|v_{\vec{k}}\right|^2 \xi_{\vec{k}} \right\}}^{\mathcal{H}_0}$$
$$+ \underbrace{\sum_{\vec{k}} \left[\frac{\xi_{\vec{k}}\Delta^*_{\vec{k}}}{E_{\vec{k}}} \gamma^\dagger_{\vec{k}\uparrow}\gamma^\dagger_{-\vec{k}\downarrow} + \frac{\xi_{\vec{k}}\Delta_{\vec{k}}}{E_{\vec{k}}} \gamma_{-\vec{k}\downarrow}\gamma_{\vec{k}\uparrow} \right]}_{\mathcal{V}^\dagger_A + \mathcal{V}_A} + \underbrace{\sum_{\vec{k}} \frac{-\left|\Delta_{\vec{k}}\right|^2}{E_{\vec{k}}} \left[\gamma^\dagger_{\vec{k}\uparrow}\gamma_{\vec{k}\uparrow} + \gamma^\dagger_{-\vec{k}\downarrow}\gamma_{-\vec{k}\downarrow} \right]}_{\mathcal{V}_{B\uparrow} + \mathcal{V}_{B\downarrow}}. \tag{B.8}$$

Note that the excitation spectrum of the γ–operators is given by the BCS result, $E_{\vec{k}}$. The second part of $\mathcal{H}_1$, $\mathcal{V}_B$, will renormalize the quasiparticle energies, but as it turns out, this renormalization is very small. The electron–phonon part of the original Hamiltonian splits into several terms also.

$$\begin{aligned}\mathcal{H}_2 = \sum_{\vec{k}} \sum_{\vec{q}\vec{Q}\lambda} \Big\{ & g(\vec{q},\vec{Q},\lambda)(a_{\vec{q}\lambda} + a^\dagger_{\vec{q}\lambda}) \left[\left(u^*_{\vec{k}+\vec{q}+\vec{Q}} \gamma^\dagger_{\vec{k}+\vec{q}+\vec{Q}\uparrow} + v_{-\vec{k}-\vec{q}-\vec{Q}} \gamma_{-\vec{k}-\vec{q}-\vec{Q}\downarrow} \right) \right. \\ & \left. \times \left(u_{\vec{k}}\gamma_{\vec{k}\uparrow} + v^*_{-\vec{k}}\gamma^\dagger_{-\vec{k}\downarrow} \right) \right] \\ & + g(-\vec{q},-\vec{Q},\lambda)(a_{\vec{q}\lambda} + a^\dagger_{\vec{q}\lambda})^\dagger \left[\left(u^*_{-\vec{k}-\vec{q}-\vec{Q}} \gamma^\dagger_{-\vec{k}-\vec{q}-\vec{Q}\downarrow} - v_{\vec{k}+\vec{q}+\vec{Q}} \gamma_{\vec{k}+\vec{q}+\vec{Q}\uparrow} \right) \right] \Big\} \\ & \times \left(u_{-\vec{k}}\gamma_{-\vec{k}\downarrow} - v^*_{\vec{k}}\gamma^\dagger_{\vec{k}\uparrow} \right) \Big\}. \end{aligned} \tag{B.9}$$

This expression can be simplified by multiplying out the parentheses,

$$\begin{aligned}\mathcal{H}_2 = \sum_{\vec{k}} \sum_{\vec{q}\vec{Q}\lambda} \Big\{ & g(\vec{q},\vec{Q},\lambda)(a_{\vec{q}\lambda} + a^\dagger_{\vec{q}\lambda}) \left[u^*_{\vec{k}+\vec{q}+\vec{Q}} u_{\vec{k}} \gamma^\dagger_{\vec{k}+\vec{q}+\vec{Q}\uparrow}\gamma_{\vec{k}\uparrow} + u^*_{\vec{k}+\vec{q}+\vec{Q}} v^*_{-\vec{k}} \gamma^\dagger_{\vec{k}+\vec{q}+\vec{Q}\uparrow}\gamma^\dagger_{-\vec{k}\downarrow} \right. \\ & \left. + v_{-\vec{k}-\vec{q}-\vec{Q}} u_{\vec{k}} \gamma_{-\vec{k}-\vec{q}-\vec{Q}\downarrow}\gamma_{\vec{k}\uparrow} + v_{-\vec{k}-\vec{q}-\vec{Q}} v^*_{-\vec{k}} \gamma_{-\vec{k}-\vec{q}-\vec{Q}\downarrow}\gamma^\dagger_{-\vec{k}\downarrow} \right] \\ & + g(-\vec{q},-\vec{Q},\lambda)(a_{\vec{q}\lambda} + a^\dagger_{\vec{q}\lambda})^\dagger \left[u^*_{-\vec{k}-\vec{q}-\vec{Q}} u_{-\vec{k}} \gamma^\dagger_{-\vec{k}-\vec{q}-\vec{Q}\downarrow}\gamma_{-\vec{k}\downarrow} - u^*_{-\vec{k}-\vec{q}-\vec{Q}} v^*_{\vec{k}} \gamma^\dagger_{-\vec{k}-\vec{q}-\vec{Q}\downarrow}\gamma^\dagger_{\vec{k}\uparrow} \right. \\ & \left. - v_{\vec{k}+\vec{q}+\vec{Q}} u_{-\vec{k}} \gamma_{\vec{k}+\vec{q}+\vec{Q}\uparrow}\gamma_{-\vec{k}\downarrow} + v_{\vec{k}+\vec{q}+\vec{Q}} v^*_{\vec{k}} \gamma_{\vec{k}+\vec{q}+\vec{Q}\uparrow}\gamma^\dagger_{\vec{k}\uparrow} \right] \Big\}. \end{aligned} \tag{B.10}$$

In order to further simplify this part of the Hamiltonian, the γ–operators need to be rearranged and the labeling needs to be changed. This can easily be done by using,

$$\begin{aligned} \vec{k}+\vec{q} &= \vec{k}' \\ \vec{k} &= \vec{k}'+\vec{q}' \\ \vec{q}' &= -\vec{q}. \end{aligned} \tag{B.11}$$

The Hamiltonian $\mathcal{H}_2$ then can be split into

$$\begin{aligned} \mathcal{V}_{C\uparrow} &= \sum_{\vec{k}}\sum_{\vec{q}\vec{Q}\lambda} g(\vec{q},\vec{Q},\lambda)A_{\vec{q}\lambda}\left[u_{\vec{k}}u^*_{\vec{k}+\vec{q}+\vec{Q}} - v_{\vec{k}}v^*_{\vec{k}+\vec{q}+\vec{Q}}\right]\gamma^\dagger_{\vec{k}+\vec{q}+\vec{Q}\uparrow}\gamma_{\vec{k}\uparrow} \\ \mathcal{V}_{C\downarrow} &= \sum_{\vec{k}}\sum_{\vec{q}\vec{Q}\lambda} g(-\vec{q},-\vec{Q},\lambda)A^\dagger_{\vec{q}\lambda}\left[u_{\vec{k}}u^*_{\vec{k}+\vec{q}+\vec{Q}} - v_{\vec{k}}v^*_{\vec{k}+\vec{q}+\vec{Q}}\right]\gamma^\dagger_{-\vec{k}-\vec{q}-\vec{Q}\downarrow}\gamma_{-\vec{k}\downarrow}, \\ \mathcal{V}_{D} &= \sum_{\vec{k}}\sum_{\vec{q}\vec{Q}\lambda} g(-\vec{q},-\vec{Q},\lambda)A^\dagger_{\vec{q}\lambda}\left[u_{\vec{k}}v_{\vec{k}+\vec{q}+\vec{Q}} + v_{\vec{k}}u_{\vec{k}+\vec{q}+\vec{Q}}\right]\gamma_{-\vec{k}\downarrow}\gamma_{\vec{k}+\vec{q}+\vec{Q}\uparrow}, \\ \mathcal{V}^\dagger_{D} &= \sum_{\vec{k}}\sum_{\vec{q}\vec{Q}\lambda} g(\vec{q},\vec{Q},\lambda)A_{\vec{q}\lambda}\left[u^*_{\vec{k}}v^*_{\vec{k}+\vec{q}+\vec{Q}} + v^*_{\vec{k}}u^*_{\vec{k}+\vec{q}+\vec{Q}}\right]\gamma^\dagger_{\vec{k}+\vec{q}+\vec{Q}\uparrow}\gamma^\dagger_{-\vec{k}\downarrow}. \end{aligned} \tag{B.12}$$

Appendix C

S–Matrix Expansion

C.1 In the BCS ground state

The S–Matrix expansion of the two propagators eqs. (3.3.12) and (3.3.14) are given by

$$\begin{aligned} \mathcal{G}_\gamma(\vec{k}\sigma, \tau_2 - \tau_1) &= -\sum_{n=0}^{\infty} \left(-\frac{1}{\hbar}\right)^n \int_0^{\hbar\beta} d\tau_1' \cdots d\tau_n' \\ &\quad \times \left\langle T_\tau \left[\gamma_{\vec{k}\sigma}(\tau_2)\, \gamma^\dagger_{\vec{k}\sigma}(\tau_1)\, \mathcal{V}(\tau_1')\, \mathcal{V}(\tau_2') \cdots \mathcal{V}(\tau_n')\right]\right\rangle_{\text{d. c.}}, \end{aligned} \tag{C.1}$$

where σ indicates the spin up or down, and the subscript "d. c." that only different connected diagrams are to be considered.

$$\begin{aligned} \mathcal{F}^\dagger_\gamma(\vec{k}, \tau_2 - \tau_1) &= -\sum_{n=0}^{\infty} \left(-\frac{1}{\hbar}\right)^n \int_0^{\hbar\beta} d\tau_1' \cdots d\tau_n' \\ &\quad \times \left\langle T_\tau \left[\gamma^\dagger_{-\vec{k}\downarrow}(\tau_2)\, \gamma^\dagger_{\vec{k}\uparrow}(\tau_1)\, \mathcal{V}(\tau_1')\, \mathcal{V}(\tau_2') \cdots \mathcal{V}(\tau_n')\right]\right\rangle_{\text{d. c.}}. \end{aligned} \tag{C.2}$$

The Hamiltonian is given by eq. (3.3.7),

$$\mathcal{H} = \mathcal{H}_0 + \mathcal{V}_A + \mathcal{V}_A^\dagger + \mathcal{V}_{B\uparrow} + \mathcal{V}_{B\downarrow} + \mathcal{V}_{C\uparrow} + \mathcal{V}_{C\downarrow} + \mathcal{V}_D + \mathcal{V}_D^\dagger. \tag{C.3}$$

We will start with $\mathcal{G}_\gamma$ first. In zeroth order we obtain the unperturbed propagator, $\mathcal{G}_{\gamma(0)}(\vec{k}\sigma,\tau_2-\tau_1)$. Its Fourier transform to the discrete Matsubara frequencies[C.1] is given by

$$\mathcal{G}_{\gamma(0)}(\vec{k}\sigma, ik_n) = \frac{1}{ik_n - \hbar^{-1}E_{\vec{k}}}, \tag{C.7}$$

where $E_{\vec{k}}$ is the quasiparticle excitation energy. In first order, only the perturbation term $\mathcal{V}_B$ contributes, and we find

$$\begin{aligned}\mathcal{G}_{\gamma(1)}(\vec{k}\sigma,\tau_2-\tau_1) &= -\left(\frac{-1}{\hbar}\right)\int_0^{\hbar\beta} d\tau_1' \left\langle T_\tau \left[\gamma_{\vec{k}\sigma}(\tau_2)\,\gamma^\dagger_{\vec{k}\sigma}(\tau_1)\right.\right. \\ &\quad \left.\left. \times \sum_{\vec{p}} \left[\frac{-|\Delta_{\vec{p}}|^2}{E_{\vec{p}}}\right] \gamma^\dagger_{\vec{p}\sigma}(\tau_1')\,\gamma_{\vec{p}\sigma}(\tau_1')\right]\right\rangle.\end{aligned} \tag{C.8}$$

[C.1] We recall the definition of the Matsubara frequencies and the Fourier transform of the complex time Greens functions from Chapter 3, eqs. (3.3.16, 3.3.17, and 3.3.18). The Fourier transform is given by

$$\mathcal{G}(\vec{k}\sigma,\tau_2-\tau_1) = \frac{1}{\hbar\beta}\sum_{ik_n} e^{-ik_n(\tau_2-\tau_1)}\mathcal{G}(\vec{k}\sigma, ik_n) \tag{C.4}$$

$$\int_0^{\hbar\beta} d\tau\; e^{-ik_n\tau} = \hbar\beta\delta_{ik_n} \tag{C.5}$$

The discrete Matsubara frequencies are defined as

$$ik_n = \begin{cases} \frac{(2n+1)\pi}{\hbar\beta} & \text{for Fermions} \\ \frac{2n\,\pi}{\hbar\beta} & \text{for Bosons} \end{cases} \tag{C.6}$$

Using Wick's theorem we will contract the operators. We have to conserve momentum and spin, which implies that the sum over $\vec{p}$ vanishes in the above expression.

$$\begin{aligned}\mathcal{G}_{\gamma(1)}(\vec{k}\sigma,\tau_2-\tau_1) &= -\left(\frac{-1}{\hbar}\right)\left[\frac{-\left|\Delta_{\vec{k}}\right|^2}{E_{\vec{k}}}\right]\int_0^{\hbar\beta}d\tau_1'\left\langle T_\tau\left[\gamma_{\vec{k}\sigma}(\tau_2)\,\gamma^\dagger_{\vec{k}\sigma}(\tau_1')\right]\right\rangle \\ &\quad\times\left\langle T_\tau\left[\gamma_{\vec{k}\sigma}(\tau_1')\,\gamma^\dagger_{\vec{k}\sigma}(\tau_1)\right]\right\rangle. \qquad \text{(C.9)}\end{aligned}$$

Replacing the propagators with their Fourier transforms,

$$\begin{aligned}\mathcal{G}_{\gamma(1)}(\vec{k}\sigma,\tau_2-\tau_1) &= -\left(\frac{-1}{\hbar}\right)\left[\frac{-\left|\Delta_{\vec{k}}\right|^2}{E_{\vec{k}}}\right] \\ &\quad\times\int_0^{\hbar\beta}d\tau_1'\frac{1}{\hbar\beta}\sum_{ik_n}e^{ik_n(\tau_2-\tau_1')}\mathcal{G}_{\gamma(0)}(\vec{k}\sigma,ik_n)\frac{1}{\hbar\beta}\sum_{ik_n'}e^{ik_n'(\tau_1'-\tau_1)}\mathcal{G}_{\gamma(0)}(\vec{k}\sigma,ik_n'), \qquad \text{(C.10)}\end{aligned}$$

we can eliminate one sum over Fermion frequencies by calculating the τ–integral. This step leads to

$$\begin{aligned}\mathcal{G}_{\gamma(1)}(\vec{k}\sigma,\tau_2-\tau_1) &= -\left(\frac{-1}{\hbar}\right)\left[\frac{-\left|\Delta_{\vec{k}}\right|^2}{E_{\vec{k}}}\right]\frac{1}{\hbar\beta}\sum_{ik_n}e^{ik_n(\tau_2-\tau_1)} \\ &\quad\times\mathcal{G}_{\gamma(0)}(\vec{k}\sigma,ik_n)\,\mathcal{G}_{\gamma(0)}(\vec{k}\sigma,ik_n). \qquad \text{(C.11)}\end{aligned}$$

The Fourier transform of this propagator is therefore given by

$$\mathcal{G}_{\gamma(1)}(\vec{k}\sigma,ik_n) = -\left(\frac{-1}{\hbar}\right)\left[\frac{-\left|\Delta_{\vec{k}}\right|^2}{E_{\vec{k}}}\right]\mathcal{G}_{\gamma(0)}(\vec{k}\sigma,ik_n)^2. \qquad \text{(C.12)}$$

In second order, we find three contributions to the propagator.

$$-\left(-\frac{1}{\hbar}\right)^2 \int_0^{\hbar\beta} d\tau_1' d\tau_2' \left\langle T_\tau \left[\right.\right.$$

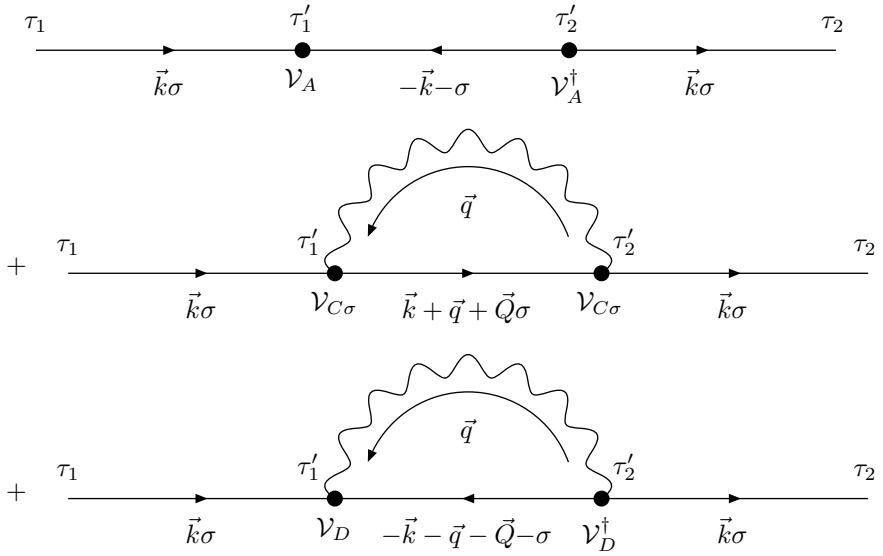

(C.13)

We will calculated these terms now one by one. The first one written out in terms of the Greens functions is given by

$$-\left(-\frac{1}{\hbar}\right)^2 \int_0^{\hbar\beta} d\tau_1' d\tau_2' \frac{\xi_{\vec{k}}^2 \left|\Delta_{\vec{k}}\right|^2}{E_{\vec{k}}^2} \left\langle T_\tau \left[\gamma_{\vec{k}\sigma}(\tau_2)\, \gamma_{\vec{k}\sigma}^\dagger(\tau_1) \right.\right.$$
$$\left.\left. \times\ \gamma_{-\vec{k}-\sigma}(\tau_1')\, \gamma_{\vec{k}\sigma}(\tau_1')\, \gamma_{\vec{k}\sigma}^\dagger(\tau_2')\, \gamma^\dagger{}_{-\vec{k}-\sigma}(\tau_2') \right] \right\rangle, \tag{C.14}$$

where we have conserved momentum and removed the sum over $\vec{p}$. We will apply Wick's theorem and Fourier transform this expression to Matsubara frequencies. Rearranging the γ–operators requires an odd number of permutations, we will therefore pick up an additional negative sign. Due to the definition of the Greens function however, we will have to add another negative sign.

$$-\left(-\frac{1}{\hbar}\right)^2 \frac{\xi_{\vec{k}}^2 \left|\Delta_{\vec{k}}\right|^2}{E_{\vec{k}}^2} \mathcal{G}_{\gamma(0)}(\vec{k}\sigma, ik_n)^2\, \mathcal{G}_{\gamma(0)}(-\vec{k}-\sigma, -ik_n). \tag{C.15}$$

The second and third terms are very similar. Written out in terms of the γ–operators, the first electron–phonon contribution reads

$$
\begin{aligned}
-\left(-\frac{1}{\hbar}\right)^2 \int_0^{\hbar\beta} d\tau_1' d\tau_2' \Big\langle T_\tau \Big[& \gamma_{\vec{k}\sigma}(\tau_2)\, \gamma^\dagger_{\vec{k}\sigma}(\tau_1) \\
& \times \sum_{\vec{p}} \sum_{\vec{q}\vec{Q}\lambda} g(\vec{q},\vec{Q},\lambda) A_{\vec{q}\lambda} \left[u_{\vec{p}} u^*_{\vec{p}+\vec{q}+\vec{Q}} - v_{\vec{p}} v^*_{\vec{p}+\vec{q}+\vec{Q}} \right] \gamma^\dagger_{\vec{p}+\vec{q}+\vec{Q}\sigma}(\tau_1')\, \gamma_{\vec{p}\sigma}(\tau_1') \\
& \times \sum_{\vec{p}'} \sum_{\vec{q}'\vec{Q}'\lambda'} g(\vec{q}',\vec{Q}',\lambda') A_{\vec{q}'\lambda'} \left[u_{\vec{p}'} u^*_{\vec{p}'+\vec{q}'+\vec{Q}'} - v_{\vec{p}'} v^*_{\vec{p}'+\vec{q}'+\vec{Q}'} \right] \\
& \times \gamma^\dagger_{\vec{p}'+\vec{q}'+\vec{Q}'\sigma}(\tau_2')\, \gamma_{\vec{p}'\sigma}(\tau_2') \Big] \Big\rangle .
\end{aligned}
\tag{C.16}
$$

Momentum conservation requires that we set $\vec{p} = \vec{k}$, $\vec{p}' + \vec{q}' + \vec{Q}' = \vec{k}$, $\vec{p}' = \vec{p} + \vec{q} + \vec{Q}$, and $\vec{q}' = -\vec{q}$. We also need to set $\lambda' = \lambda$ since the perturbation term conserves the phonon polarization.

$$
\begin{aligned}
-\left(-\frac{1}{\hbar}\right)^2 & \sum_{\vec{q}\vec{Q}\lambda} \left| g(\vec{q},\vec{Q},\lambda) \right|^2 \left| u_{\vec{k}} u^*_{\vec{k}+\vec{q}+\vec{Q}} - v_{\vec{k}} v^*_{\vec{k}+\vec{q}+\vec{Q}} \right|^2 \int_0^{\hbar\beta} d\tau_1' d\tau_2' \\
& \times \left\langle T_\tau \left[A_{\vec{q}\lambda}(\tau_1')\, A^\dagger_{\vec{q}\lambda}(\tau_2') \right] \right\rangle \left\langle T_\tau \left[\gamma_{\vec{k}\sigma}(\tau_1')\, \gamma^\dagger_{\vec{k}\sigma}(\tau_1) \right] \right\rangle \\
& \times \left\langle T_\tau \left[\gamma_{\vec{k}+\vec{q}+\vec{Q}\sigma}(\tau_2')\, \gamma^\dagger_{\vec{k}+\vec{q}+\vec{Q}\sigma}(\tau_1') \right] \right\rangle \left\langle T_\tau \left[\gamma_{\vec{k}\sigma}(\tau_2)\, \gamma^\dagger_{\vec{k}\sigma}(\tau_2') \right] \right\rangle ,
\end{aligned}
\tag{C.17}
$$

where we made use of the definition of the electron–phonon interaction, $g(\vec{q},\vec{Q},\lambda) = g(-\vec{q},-\vec{Q},\lambda)^*$, and the fact that $A_{\vec{q}\lambda} = A^\dagger_{-\vec{q}\lambda}$. The Fourier transform to Matsubara frequencies is given by

$$
\begin{aligned}
& -\left(-\frac{1}{\hbar}\right)^2 \sum_{\vec{q}\vec{Q}\lambda} \left| g(\vec{q},\vec{Q},\lambda) \right|^2 \left| u_{\vec{k}} u^*_{\vec{k}+\vec{q}+\vec{Q}} - v_{\vec{k}} v^*_{\vec{k}+\vec{q}+\vec{Q}} \right|^2 \\
& \times \mathcal{G}_{\gamma(0)}(\vec{k}\sigma, ik_n)^2\, \frac{1}{\hbar\beta} \sum_{iq_n} \mathcal{D}_{(0)}(\vec{q}\lambda, iq_n)\, \mathcal{G}_{\gamma(0)}(\vec{k}+\vec{q}+\vec{Q}\sigma, ik_n + iq_n).
\end{aligned}
\tag{C.18}
$$

The last term written out in terms of quasiparticle Greens functions it is given by

$$
\begin{aligned}
&-\left(-\frac{1}{\hbar}\right)^2 \int_0^{\hbar\beta} d\tau_1' d\tau_2' \left\langle T_\tau \left[\gamma_{\vec{k}\sigma}(\tau_2)\,\gamma^\dagger_{\vec{k}\sigma}(\tau_1)\right.\right. \\
&\quad \times \sum_{\vec{p}} \sum_{\vec{q}\vec{Q}\lambda} g(-\vec{q},-\vec{Q},\lambda) A^\dagger_{\vec{q}\lambda} \left[u_{\vec{p}} v_{\vec{p}+\vec{q}+\vec{Q}} + v_{\vec{p}} u_{\vec{p}+\vec{q}+\vec{Q}}\right] \gamma_{-\vec{p}-\sigma}(\tau_1')\,\gamma_{\vec{p}+\vec{q}+\vec{Q}\sigma}(\tau_1') \\
&\quad \times \sum_{\vec{p}'} \sum_{\vec{q}'\vec{Q}'\lambda'} g(\vec{q}',\vec{Q}',\lambda') A_{\vec{q}'\lambda'} \left[u^*_{\vec{p}'} v^*_{\vec{k}'+\vec{q}'+\vec{Q}'} + v^*_{\vec{p}'} u^*_{\vec{p}'+\vec{q}'+\vec{Q}'}\right] \\
&\quad \left.\left. \times\ \gamma^\dagger_{\vec{p}'+\vec{q}'+\vec{Q}'\sigma}(\tau_2')\,\gamma^\dagger_{-\vec{p}'-\sigma}(\tau_2')\right]\right\rangle . \qquad \text{(C.19)}
\end{aligned}
$$

As before, momentum conservation requires us to set $\lambda' = \lambda$, $\vec{p}+\vec{q}+\vec{Q} = \vec{k}$, $\vec{p} = \vec{p}'$, $\vec{p}'+\vec{q}'+\vec{Q}' = \vec{k}$, and $\vec{q} = \vec{q}'$. Noting that we pick up an additional negative sign due to the permutations, we arrive at

$$
\begin{aligned}
&\left(-\frac{1}{\hbar}\right)^2 \sum_{\vec{q}\vec{Q}\lambda} \left|g(\vec{q},\vec{Q},\lambda)\right|^2 \left|u_{\vec{k}} v_{\vec{k}+\vec{q}+\vec{Q}} + v_{\vec{k}} u_{\vec{k}+\vec{q}+\vec{Q}}\right|^2 \\
&\quad \times \mathcal{G}_{\gamma(0)}(\vec{k}\sigma, ik_n)^2\, \frac{1}{\hbar\beta} \sum_{iq_n} \mathcal{D}_{(0)}(\vec{q}\lambda, iq_n)\,\mathcal{G}_{\gamma(0)}(-\vec{k}-\vec{q}-\vec{Q}-\sigma, -ik_n - iq_n). \qquad \text{(C.20)}
\end{aligned}
$$

The sum over Boson frequencies, $\sum_{iq_n}$, is calculated by integrating a contour integral around the entire complex plane. We will use the function,

$$
\mathcal{D}_{(0)}(\vec{q}\lambda, z)\ \mathcal{G}_{\gamma(0)}(\vec{k}+\vec{q}+\vec{Q}\sigma, ik_n + z) n(z), \qquad \text{(C.21)}
$$

of complex argument z. The function $n(z)$ represents the Bose–Einstein distribution function,

$$
n(z) = \frac{1}{e^{\beta\hbar z} - 1}. \qquad \text{(C.22)}
$$

The contour integral,

$$\oint_{R\to\infty} \frac{dz}{2\pi i} \underbrace{\mathcal{D}_{(0)}(\vec{q}\lambda, z)\ \mathcal{G}_{\gamma(0)}(\vec{k}+\vec{q}+\vec{Q}\sigma, ik_n+z)n(z)}_{f(z)} = 0, \tag{C.23}$$

will vanish in the limit of the radius of the contour going to infinity. The solution of a contour integral of an analytic function is given by the sum of its residues inside the contour, according to Cauchy's theorem. Since we are integration around the whole complex plane, we need to include all of the residues. The Bose–Einstein distribution function has poles at the imaginary Matsubara frequencies, iq_n with residues[C.2] of $1/(\hbar\beta)$. The unperturbed propagators are given by

$$\mathcal{D}_{(0)}(\vec{q}\lambda, iq_n) = \frac{2\omega_{\vec{q}\lambda}}{(iq_n)^2 - \omega^2_{\vec{q}\lambda}}, \tag{C.25}$$

and

$$\mathcal{G}_{\gamma(0)}(\vec{k}\sigma, ik_n) = \frac{1}{ik_n - \hbar^{-1}E_{\vec{k}}}. \tag{C.26}$$

The residues of this integrand in eq. (C.23) are,

[C.2]The residues are defined as the coefficients of the Laurent series expansion of the complex function. A pole of order m at $z = z_0$ will have a residue of

$$a_{-1} = \operatorname*{Res}_{z=z_0}(f(z)) = \frac{1}{(m-1)!}\frac{d^{m-1}}{dz^{m-1}}\left[(z-z_0)^m f(z)\right]_{z=z_0}. \tag{C.24}$$

$$
\begin{aligned}
\operatorname*{Res}_{z=iq_n}(f(z)) &= \frac{1}{\hbar\beta}\,\mathcal{D}_{(0)}(\vec{q}\lambda, iq_n)\;\mathcal{G}_{\gamma(0)}(\vec{k}+\vec{q}+\vec{Q}\sigma, ik_n+iq_n) \\
\operatorname*{Res}_{z=\omega_{\vec{q}\lambda}}(f(z)) &= \frac{n(\omega_{\vec{q}\lambda})}{ik_n+\omega_{\vec{q}\lambda}-\hbar^{-1}E_{\vec{k}+\vec{q}+\vec{Q}}} \\
\operatorname*{Res}_{z=-\omega_{\vec{q}\lambda}}(f(z)) &= -\frac{n(-\omega_{\vec{q}\lambda})}{ik_n-\omega_{\vec{q}\lambda}-\hbar^{-1}E_{\vec{k}+\vec{q}+\vec{Q}}} \\
\operatorname*{Res}_{z=-ik_n+\hbar^{-1}E_{\vec{k}+\vec{q}+\vec{Q}}}(f(z)) &= \frac{2\omega_{\vec{q}\lambda}\;n(-ik_n+\hbar^{-1}E_{\vec{k}+\vec{q}+\vec{Q}})}{(ik_n-\hbar^{-1}E_{\vec{k}+\vec{q}+\vec{Q}})^2-\omega_{\vec{q}\lambda}^2}.
\end{aligned}
\tag{C.27}
$$

Since the sum is equal to zero, the solution to eq. (C.23) is found to be

$$
\begin{aligned}
&\frac{1}{\hbar\beta}\sum_{iq_n}\mathcal{D}_{(0)}(\vec{q}\lambda, iq_n)\;\mathcal{G}_{\gamma(0)}(\vec{k}+\vec{q}+\vec{Q}\sigma, ik_n+iq_n) = \\
&\quad -\frac{n(\omega_{\vec{q}\lambda})}{ik_n+\omega_{\vec{q}\lambda}-\hbar^{-1}E_{\vec{k}+\vec{q}+\vec{Q}}}+\frac{n(-\omega_{\vec{q}\lambda})}{ik_n-\omega_{\vec{q}\lambda}-\hbar^{-1}E_{\vec{k}+\vec{q}+\vec{Q}}} \\
&\quad -n(-ik_n+\hbar^{-1}E_{\vec{k}+\vec{q}+\vec{Q}})\left(\frac{1}{ik_n-\omega_{\vec{q}\lambda}-\hbar^{-1}E_{\vec{k}+\vec{q}+\vec{Q}}}-\frac{1}{ik_n+\omega_{\vec{q}\lambda}-\hbar^{-1}E_{\vec{k}+\vec{q}+\vec{Q}}}\right).
\end{aligned}
\tag{C.28}
$$

We can now combine terms with the same denominator and obtain,

$$
\frac{-n(\omega_{\vec{q}\lambda})+n(-ik_n+\hbar^{-1}E_{\vec{k}+\vec{q}+\vec{Q}})}{ik_n+\omega_{\vec{q}\lambda}-\hbar^{-1}E_{\vec{k}+\vec{q}+\vec{Q}}}+\frac{n(-\omega_{\vec{q}\lambda})-n(-ik_n+\hbar^{-1}E_{\vec{k}+\vec{q}+\vec{Q}})}{ik_n-\omega_{\vec{q}\lambda}-\hbar^{-1}E_{\vec{k}+\vec{q}+\vec{Q}}}
\tag{C.29}
$$

The thermal distribution functions can be simplified, since

$$
n(-\omega_{\vec{q}\lambda})=\frac{1}{e^{-\beta\hbar\omega_{\vec{q}\lambda}}-1}=-\frac{e^{\beta\hbar\omega_{\vec{q}\lambda}}-1+1}{e^{\beta\hbar\omega_{\vec{q}\lambda}}-1}=-\left[1+n(\omega_{\vec{q}\lambda})\right],
\tag{C.30}
$$

and

$$
n(-ik_n+\hbar^{-1}E_{\vec{k}+\vec{q}+\vec{Q}})=\frac{1}{-e^{\beta E_{\vec{k}+\vec{q}+\vec{Q}}}-1}=-f(E_{\vec{k}+\vec{q}+\vec{Q}}).
\tag{C.31}
$$

We have introduced another thermal distribution function, $f(E_{\vec{k}})$, which represents the Fermi–Dirac distribution for Fermions. This leads us to

$$\begin{aligned}\frac{1}{\hbar\beta}\sum_{iq_n}\mathcal{D}_{(0)}(\vec{q}\lambda,iq_n)\;\mathcal{G}_{\gamma(0)}(\vec{k}+\vec{q}+\vec{Q}\sigma,ik_n+iq_n)=\\ -\frac{n(\omega_{\vec{q}\lambda})+f(\vec{k}+\vec{q}+\vec{Q})}{ik_n+\omega_{\vec{q}\lambda}-\hbar^{-1}E_{\vec{k}+\vec{q}+\vec{Q}}}-\frac{1+n(\omega_{\vec{q}\lambda})-f(E_{\vec{k}+\vec{q}+\vec{Q}})}{ik_n-\omega_{\vec{q}\lambda}-\hbar^{-1}E_{\vec{k}+\vec{q}+\vec{Q}}}.\end{aligned} \tag{C.32}$$

In order to simplify notation, we will introduce the following function,

$$\hbar\,g(ik_n)=\frac{n(\omega_{\vec{q}\lambda})+f(E_{\vec{k}+\vec{q}+\vec{Q}})}{ik_n+\omega_{\vec{q}\lambda}-\hbar^{-1}E_{\vec{k}+\vec{q}+\vec{Q}}}+\frac{1+n(\omega_{\vec{q}\lambda})-f(E_{\vec{k}+\vec{q}+\vec{Q}})}{ik_n-\omega_{\vec{q}\lambda}-\hbar^{-1}E_{\vec{k}+\vec{q}+\vec{Q}}}. \tag{C.33}$$

The Matsubara frequency sum in terms of this function is given by

$$\frac{1}{\hbar\beta}\sum_{iq_n}\mathcal{D}_{(0)}(\vec{q}\lambda,iq_n)\,\mathcal{G}_{\gamma(0)}(\vec{k}+\vec{q}+\vec{Q}\sigma,ik_n+iq_n) \;=\; -\hbar\,g(ik_n) \tag{C.34}$$

$$\frac{1}{\hbar\beta}\sum_{iq_n}\mathcal{D}_{(0)}(\vec{q}\lambda,iq_n)\,\mathcal{G}_{\gamma(0)}(-\vec{k}-\vec{q}-\vec{Q}-\sigma,-ik_n-iq_n) \;=\; -\hbar\,g(-ik_n). \tag{C.35}$$

Using the above expressions for the sum over Matsubara frequencies, $\sum_{iq_n}$, the complete expression for the second order contribution to the quasiparticle Greens function $\mathcal{G}_\gamma$ is therefore,

$$\begin{aligned}\mathcal{G}_{\gamma(2)}(\vec{k}\sigma,ik_n) \;=\; &\left(-\frac{1}{\hbar}\right)^2\;\mathcal{G}_{\gamma(0)}(\vec{k}\sigma,ik_n)^2\left\{\frac{\xi_{\vec{k}}^2\left|\Delta_{\vec{k}}\right|^2}{E_{\vec{k}}^2}\frac{1}{ik_n+\hbar^{-1}E_{\vec{k}}}\right.\\ &+\sum_{\vec{q}\vec{Q}\lambda}\left|g(\vec{q},\vec{Q},\lambda)\right|^2\left[\left|u_{\vec{k}}u^*_{\vec{k}+\vec{q}+\vec{Q}}-v_{\vec{k}}v^*_{\vec{k}+\vec{q}+\vec{Q}}\right|^2\hbar\,g(ik_n)\right.\\ &\left.\left.-\left|u_{\vec{k}}v_{\vec{k}+\vec{q}+\vec{Q}}+v_{\vec{k}}u_{\vec{k}+\vec{q}+\vec{Q}}\right|^2\hbar\,g(-ik_n)\right\}.\end{aligned}$$

The coherence factors can be further simplified,

$$\left|u_{\vec{k}}v_{\vec{k}+\vec{q}+\vec{Q}}+v_{\vec{k}}u_{\vec{k}+\vec{q}+\vec{Q}}\right|^2 = \frac{1}{2}\left(1-\frac{\xi_{\vec{k}}}{E_{\vec{k}}}\frac{\xi_{\vec{k}+\vec{q}+\vec{Q}}}{E_{\vec{k}+\vec{q}+\vec{Q}}}+\Re\left\{\frac{\Delta_{\vec{k}}}{E_{\vec{k}}}\frac{\Delta_{\vec{k}+\vec{q}+\vec{Q}}}{E_{\vec{k}+\vec{q}+\vec{Q}}}\right\}\right) \tag{C.36}$$

$$\left|u_{\vec{k}}u^*_{\vec{k}+\vec{q}+\vec{Q}}-v_{\vec{k}}v^*_{\vec{k}+\vec{q}+\vec{Q}}\right|^2 = \frac{1}{2}\left(1+\frac{\xi_{\vec{k}}}{E_{\vec{k}}}\frac{\xi_{\vec{k}+\vec{q}+\vec{Q}}}{E_{\vec{k}+\vec{q}+\vec{Q}}}-\Re\left\{\frac{\Delta_{\vec{k}}}{E_{\vec{k}}}\frac{\Delta_{\vec{k}+\vec{q}+\vec{Q}}}{E_{\vec{k}+\vec{q}+\vec{Q}}}\right\}\right). \tag{C.37}$$

We want to turn our attention now to finding the propagator, $\mathcal{F}^\dagger_\gamma(\vec{k},ik_n)$. In zeroth order, the propagator is identically zero, due to our definition. In first order there will be contributions from the perturbation term $\mathcal{V}_A$ only. An odd number of permutations yields

$$\mathcal{F}^\dagger_{\gamma(1)}(\vec{k},ik_n) = \left(-\frac{1}{\hbar}\right)\frac{\xi_{\vec{k}}\Delta_{\vec{k}}}{E_{\vec{k}}}\,\mathcal{G}_{\gamma(0)}(\vec{k}\uparrow,ik_n)\,\mathcal{G}_{\gamma(0)}(-\vec{k}\downarrow,-ik_n). \tag{C.38}$$

The propagator $\mathcal{F}_{\gamma(1)}(\vec{k},ik_n)$ is given by the complex conjugate,

$$\mathcal{F}_{\gamma(1)}(\vec{k},ik_n) = \left(-\frac{1}{\hbar}\right)\frac{\xi_{\vec{k}}\Delta^*_{\vec{k}}}{E_{\vec{k}}}\,\mathcal{G}_{\gamma(0)}(\vec{k}\uparrow,ik_n)\,\mathcal{G}_{\gamma(0)}(-\vec{k}\downarrow,-ik_n). \tag{C.39}$$

In second order, four contributions are possible. The first two are due to the perturbation term $\mathcal{V}_B$, and the last two are electron–phonon contributions. The two terms out of each contribution differ only in one quasiparticle line which either propagates forward or backward in time. Their contributions will be different, necessitating the calculation of all four terms. The first two terms can be represented using Feynman diagrams in the following way,

$$-\left(-\frac{1}{\hbar}\right)^2 \int_0^{\hbar\beta} d\tau_1' d\tau_2' \left\langle T_\tau \left[\right.\right.$$

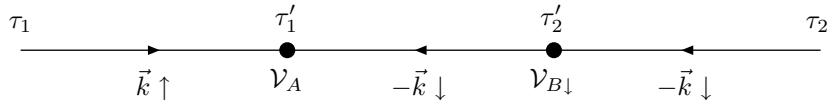

(C.40) $+$

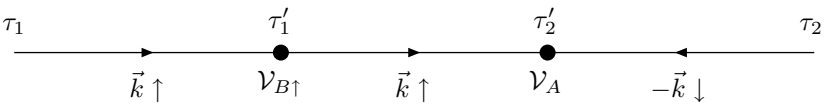

$$\left.\left.\right]\right\}.$$

Due to momentum and spin conservation at the vertices, the sums in the two perturbation terms collapse and those two contributions can be written as

$$\begin{aligned} &-\left(-\frac{1}{\hbar}\right)^2 \int_0^{\hbar\beta} d\tau_1' d\tau_2' \left[\frac{\xi_{\vec{k}}\Delta_{\vec{k}}}{E_{\vec{k}}}\right]\left[\frac{-\left|\Delta_{\vec{k}}\right|^2}{E_{\vec{k}}}\right] \\ &\quad\times\left\{\left\langle T_\tau\left[\gamma^\dagger_{-\vec{k}\downarrow}(\tau_2)\,\gamma^\dagger_{\vec{k}\uparrow}(\tau_1)\,\gamma_{-\vec{k}\downarrow}(\tau_1')\,\gamma_{\vec{k}\uparrow}(\tau_1')\,\gamma^\dagger_{-\vec{k}\downarrow}(\tau_2')\,\gamma_{-\vec{k}\downarrow}(\tau_2')\right]\right\rangle\right. \\ &\qquad\left.+\left\langle T_\tau\left[\gamma^\dagger_{-\vec{k}\downarrow}(\tau_2)\,\gamma^\dagger_{\vec{k}\uparrow}(\tau_1)\,\gamma^\dagger_{\vec{k}\uparrow}(\tau_1')\,\gamma_{\vec{k}\uparrow}(\tau_1')\,\gamma_{-\vec{k}\downarrow}(\tau_2')\,\gamma_{\vec{k}\uparrow}(\tau_2')\right]\right\rangle\right\}. \end{aligned} \tag{C.41}$$

Rearranging the operators introduces an overall negative sign, since we need an odd number of permutations in order to bring them into normal order. Wick's theorem separates the operators into unperturbed Greens functions and owing to the defintion of the Greens function we add another negative sign and obtain,

$$\begin{aligned} &-\left(-\frac{1}{\hbar}\right)^2 \left[\frac{\xi_{\vec{k}}\Delta_{\vec{k}}}{E_{\vec{k}}}\right]\left[\frac{-\left|\Delta_{\vec{k}}\right|^2}{E_{\vec{k}}}\right] \mathcal{G}_{\gamma(0)}(\vec{k}\uparrow, ik_n)\,\mathcal{G}_{\gamma(0)}(-\vec{k}\downarrow, -ik_n) \\ &\qquad\times\left\{\mathcal{G}_{\gamma(0)}(-\vec{k}\downarrow, -ik_n) + \mathcal{G}_{\gamma(0)}(\vec{k}\uparrow, ik_n)\right\}. \end{aligned} \tag{C.42}$$

The two electron–phonon contributions are given diagrammatically by the following two diagrams,

$$-\left(-\frac{1}{\hbar}\right)^2 \int_0^{\hbar\beta} d\tau_1' d\tau_2' \left\langle T_\tau \left[\right.\right.$$

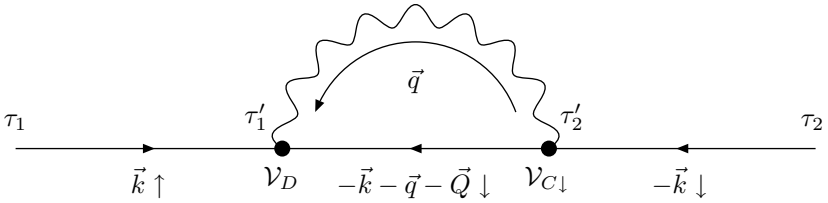

$$+$$

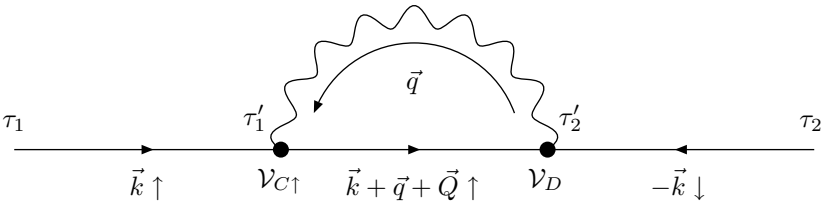

$$\left.\left.\right]\right\rangle\Bigg\}. \tag{C.43}$$

The full expressions before contraction are given by

$$\begin{aligned}
&-\left(-\frac{1}{\hbar}\right)^2 \int_0^{\hbar\beta} d\tau_1' d\tau_2' \Bigg\{ \Big\langle T_\tau \Big[\gamma^\dagger_{-\vec{k}\downarrow}(\tau_2)\, \gamma^\dagger_{\vec{k}\uparrow}(\tau_1) \\
&\quad \times \sum_{\vec{p}} \sum_{\vec{q}\vec{Q}\lambda} g(-\vec{q}, -\vec{Q}, \lambda) A^\dagger_{\vec{q}\lambda} \left[u_{\vec{p}} v_{\vec{p}+\vec{q}+\vec{Q}} + v_{\vec{p}} u_{\vec{p}+\vec{q}+\vec{Q}} \right] \gamma_{-\vec{p}\downarrow}(\tau_1')\, \gamma_{\vec{p}+\vec{q}+\vec{Q}\uparrow}(\tau_1') \\
&\quad \times \sum_{\vec{p}'} \sum_{\vec{q}'\vec{Q}'\lambda'} g(-\vec{q}', -\vec{Q}', \lambda') A^\dagger_{\vec{q}'\lambda'} \left[u_{\vec{p}'} u^*_{\vec{p}'+\vec{q}'+\vec{Q}'} - v_{\vec{p}'} v^*_{\vec{p}'+\vec{q}'+\vec{Q}'} \right] \\
&\qquad\qquad \times\ \gamma^\dagger_{-\vec{p}'-\vec{q}'-\vec{Q}'\downarrow}(\tau_2')\, \gamma_{-\vec{p}'\downarrow}(\tau_2') \Big] \Big\rangle \\
&\quad + \Big\langle T_\tau \Big[\gamma^\dagger_{-\vec{k}\downarrow}(\tau_2)\, \gamma^\dagger_{\vec{k}\uparrow}(\tau_1) \sum_{\vec{p}} \sum_{\vec{q}\vec{Q}\lambda} g(\vec{q}, \vec{Q}, \lambda) A_{\vec{q}\lambda} \left[u_{\vec{p}} u^*_{\vec{p}+\vec{q}-\vec{Q}} - v_{\vec{p}} v^*_{\vec{p}+\vec{q}+\vec{Q}} \right] \gamma^\dagger_{\vec{p}+\vec{q}+\vec{Q}\uparrow}(\tau_1')\, \gamma_{\vec{p}\uparrow}(\tau_1') \\
&\quad \times \sum_{\vec{p}'} \sum_{\vec{q}'\vec{Q}'\lambda'} g(-\vec{q}', -\vec{Q}', \lambda') A^\dagger_{\vec{q}'\lambda'} \left[u_{\vec{p}'} v_{\vec{p}'+\vec{q}'+\vec{Q}'} + v_{\vec{p}'} u_{\vec{p}'+\vec{q}'+\vec{Q}'} \right] \gamma_{-\vec{p}'\uparrow}(\tau_2')\, \gamma_{\vec{p}'+\vec{q}'+\vec{Q}'\uparrow}(\tau_2') \Big] \Big\rangle \Bigg\}.
\end{aligned} \tag{C.44}$$

Again, momentum has to be conserved at the vertices which reduces the sums. In addition to momentum conservation, we need to also conserve the phonon polarization direction, since our

interaction Hamiltonian conserves it. With the aid of Wick's theorem, we contract the operators and rearrange them in normal order. An odd number of permutations is necessary again, which introduces an overall negative sign. We replace contracted operators with unperturbed Greens functions and obtain,

$$\left(-\frac{1}{\hbar}\right)^2 \sum_{\vec{q}\vec{Q}\lambda} \left|g(\vec{q},\vec{Q},\lambda)\right|^2 \left[u_{\vec{k}}v_{\vec{k}+\vec{q}+\vec{Q}} + v_{\vec{k}}u_{\vec{k}+\vec{q}+\vec{Q}}\right]\left[u_{\vec{k}}u^*_{\vec{k}+\vec{q}+\vec{Q}} - v_{\vec{k}}v^*_{\vec{k}+\vec{q}+\vec{Q}}\right]$$
$$\mathcal{G}_{\gamma(0)}(\vec{k}\uparrow, ik_n)\,\mathcal{G}_{\gamma(0)}(-\vec{k}\downarrow, -ik_n)\,\frac{1}{\hbar\beta}\sum_{iq_n}\mathcal{D}^{(0)}(\vec{q}\lambda, iq_n)$$
$$\times\left[\mathcal{G}_{\gamma(0)}(-\vec{k}-\vec{q}-\vec{Q}\downarrow, -ik_n-iq_n) + \mathcal{G}_{\gamma(0)}(\vec{k}+\vec{q}+\vec{Q}\uparrow, ik_n+iq_n)\right]. \tag{C.45}$$

With the results of eqs. (C.34) and (C.35), the second order contribution to the quasiparticle propagator, $\mathcal{F}^\dagger_\gamma$ is given by

$$\mathcal{F}^\dagger_{\gamma(2)}(\vec{k}, ik_n) = \left(-\frac{1}{\hbar}\right)^2 \mathcal{G}_{\gamma(0)}(\vec{k}\uparrow, ik_n)\,\mathcal{G}_{\gamma(0)}(-\vec{k}\downarrow, -ik_n)$$
$$\times\left\{\frac{\xi_{\vec{k}}\Delta_{\vec{k}}\left|\Delta_{\vec{k}}\right|^2}{E^2_{\vec{k}}}\left[\frac{1}{ik_n-\hbar^{-1}E_{\vec{k}}} - \frac{1}{ik_n+\hbar^{-1}E_{\vec{k}}}\right]\right.$$
$$\left. - \sum_{\vec{q}\vec{Q}\lambda}\left|g(\vec{q},\vec{Q},\lambda)\right|^2\left[u_{\vec{k}}v_{\vec{k}+\vec{q}+\vec{Q}} + v_{\vec{k}}u_{\vec{k}+\vec{q}+\vec{Q}}\right]\left[u_{\vec{k}}u^*_{\vec{k}+\vec{q}+\vec{Q}} - v_{\vec{k}}v^*_{\vec{k}+\vec{q}+\vec{Q}}\right]\left[\hbar\,g(ik_n)+\hbar\,g(-ik_n)\right]\right\}. \tag{C.46}$$

The propagator $\mathcal{F}_{\gamma(2)}(\vec{k}, ik_n)$ is given by the complex conjugate,

$$\mathcal{F}_{\gamma(2)}(\vec{k}, ik_n) = \left(-\frac{1}{\hbar}\right)^2 \mathcal{G}_{\gamma(0)}(\vec{k}\uparrow, ik_n)\,\mathcal{G}_{\gamma(0)}(-\vec{k}\downarrow, -ik_n)$$
$$\times\left\{\frac{\xi_{\vec{k}}\Delta^*_{\vec{k}}\left|\Delta_{\vec{k}}\right|^2}{E^2_{\vec{k}}}\left[\frac{1}{ik_n-\hbar^{-1}E_{\vec{k}}} - \frac{1}{ik_n+\hbar^{-1}E_{\vec{k}}}\right]\right.$$
$$\left. - \sum_{\vec{q}\vec{Q}\lambda}\left|g(\vec{q},\vec{Q},\lambda)\right|^2\left[u^*_{\vec{k}}v^*_{\vec{k}+\vec{q}+\vec{Q}} + v^*_{\vec{k}}u^*_{\vec{k}+\vec{q}+\vec{Q}}\right]\left[u^*_{\vec{k}}u_{\vec{k}+\vec{q}+\vec{Q}} - v^*_{\vec{k}}v_{\vec{k}+\vec{q}+\vec{Q}}\right]\left[\hbar\,g(ik_n)+\hbar\,g(-ik_n)\right]\right\}. \tag{C.47}$$

We will now make the simplifying assumption that the coherence factors are real. This implies that the gap itself will be real valued. The coherence factors in $\mathcal{F}^\dagger(\vec{k}, ik_n)$ and $\mathcal{F}^\dagger(\vec{k}, ik_n)$ are given by

$$\left[u_{\vec{k}}v_{\vec{k}+\vec{q}+\vec{Q}} + v_{\vec{k}}u_{\vec{k}+\vec{q}+\vec{Q}}\right]\left[u_{\vec{k}}u_{\vec{k}+\vec{q}+\vec{Q}} - v_{\vec{k}}v_{\vec{k}+\vec{q}+\vec{Q}}\right] = \frac{\xi_{\vec{k}}\Delta_{\vec{k}+\vec{q}+\vec{Q}}}{2E_{\vec{k}}E_{\vec{k}+\vec{q}+\vec{Q}}} + \frac{\Delta_{\vec{k}}\xi_{\vec{k}+\vec{q}+\vec{Q}}}{2E_{\vec{k}}E_{\vec{k}+\vec{q}+\vec{Q}}} \tag{C.48}$$

There are a few points we would like to make regarding the self–energy at this point. Firstly, the factor

$$\frac{\xi_{\vec{k}}\Delta_{\vec{k}}^3}{E_{\vec{k}}^2} \tag{C.49}$$

is very small compared to the rest of the expression. This can be seen from the fact that the energy scales of the gap function and the quasiparticle excitations are very different. The gap function is of order meV, whereas the quasiparticle energies are essentially given by the electronic energies which are of order eV. The factor in eq. (C.49) is therefore of order Δ^3/ξ, the factors in

$$\frac{\xi_{\vec{k}}\Delta_{\vec{k}+\vec{q}+\vec{Q}}}{2E_{\vec{k}}E_{\vec{k}+\vec{q}+\vec{Q}}} + \frac{\Delta_{\vec{k}}\xi_{\vec{k}+\vec{q}+\vec{Q}}}{2E_{\vec{k}}E_{\vec{k}+\vec{q}+\vec{Q}}} \tag{C.50}$$

are of order Δ/ξ and are roughly 10^6 times larger. Secondly, the second term in eq. (C.50) is nearly an odd function of $\sum_{\vec{q}\vec{Q}\lambda}$. After integration, it will contribute only very little. Due to these arguments, we will neglect the factor (C.49) entirely and drop the second factor in (C.50). The self–energy then is approximately given by

$$\Sigma^{(2)}_{\gamma^\dagger\gamma^\dagger}(\vec{k}, ik_n) = \left(-\frac{1}{\hbar}\right)\frac{\xi_{\vec{k}}\Delta_{\vec{k}}}{E_{\vec{k}}} - \left(-\frac{1}{\hbar}\right)^2 \sum_{\vec{q}\vec{Q}\lambda}\left|g(\vec{q},\vec{Q},\lambda)\right|^2 \frac{\xi_{\vec{k}}\Delta_{\vec{k}+\vec{q}+\vec{Q}}}{2E_{\vec{k}}E_{\vec{k}+\vec{q}+\vec{Q}}}\left[\hbar\, g(ik_n) + \hbar\, g(-ik_n)\right]. \tag{C.51}$$

The self energy $\Sigma^{(2)}_{\gamma\gamma^\dagger}$ due to the Greens function $\mathcal{G}_\gamma$ is given by

$$\begin{aligned}\Sigma^{(2)}_{\gamma\gamma^\dagger}(\vec{k}, ik_n) &= -\frac{1}{\hbar}\frac{\Delta^2_{\vec{k}}}{E_{\vec{k}}} + \left(\frac{1}{\hbar}\right)^2 \left(\frac{\xi_{\vec{k}}\Delta_{\vec{k}}}{E_{\vec{k}}}\right)^2 \frac{1}{ik_n + \hbar^{-1}E_{\vec{k}}} \\ &\quad + \frac{1}{2}\left(\frac{1}{\hbar}\right)^2 \sum_{\vec{q}\vec{Q}\lambda} \left|g(\vec{q},\vec{Q},\lambda)\right|^2 \Bigg[\left(\hbar\, g(ik_n) - \hbar\, g(-ik_n)\right) \\ &\quad - \frac{\Delta_{\vec{k}}}{E_{\vec{k}}}\frac{\Delta_{\vec{k}+\vec{q}+\vec{Q}}}{E_{\vec{k}+\vec{q}+\vec{Q}}} \left(\hbar\, g(ik_n) + \hbar\, g(-ik_n)\right) \\ &\quad + \frac{\xi_{\vec{k}}}{E_{\vec{k}}}\frac{\xi_{\vec{k}+\vec{q}+\vec{Q}}}{E_{\vec{k}+\vec{q}+\vec{Q}}} \left(\hbar\, g(ik_n) + \hbar\, g(-ik_n)\right) \Bigg]. \end{aligned} \tag{C.52}$$

The argument can be made that the last term in the above is nearly odd in $\sum_{\vec{q}\vec{Q}\lambda}$ and therefore will be small compared to the other terms. We will neglect this term. The second term,

$$\left(\frac{1}{\hbar}\right)^2 \left(\frac{\xi_{\vec{k}}\Delta_{\vec{k}}}{E_{\vec{k}}}\right)^2 \frac{1}{ik_n + \hbar^{-1}E_{\vec{k}}}, \tag{C.53}$$

does not contain any phonon–related features. In addition, the energy pole is at negative energies, $-E_{\vec{k}}$, but our quasi–particle excitation spectrum is positive definite. We do not expect a large contribution from this term and will neglect it. The final expression we will use henceforth is given by

$$\begin{aligned}\Sigma^{(2)}_{\gamma\gamma^\dagger}(\vec{k}, ik_n) &= -\frac{1}{\hbar}\frac{\Delta^2_{\vec{k}}}{E_{\vec{k}}} + \frac{1}{2}\left(\frac{1}{\hbar}\right)^2 \sum_{\vec{q}\vec{Q}\lambda} \left|g(\vec{q},\vec{Q},\lambda)\right|^2 \left(\hbar\, g(ik_n) - \hbar\, g(-ik_n)\right) \\ &\quad - \frac{1}{2}\left(\frac{1}{\hbar}\right)^2 \sum_{\vec{q}\vec{Q}\lambda} \left|g(\vec{q},\vec{Q},\lambda)\right|^2 \frac{\Delta_{\vec{k}}}{E_{\vec{k}}}\frac{\Delta_{\vec{k}+\vec{q}+\vec{Q}}}{E_{\vec{k}+\vec{q}+\vec{Q}}} \left(\hbar\, g(ik_n) + \hbar\, g(-ik_n)\right). \end{aligned} \tag{C.54}$$

We wish to calculate the retarded versions of the self–energies given above now. Up to second order in the electron–phonon interaction the self–energy of $\mathcal{F}^\dagger_\gamma$ was given by eq. (C.51),

(C.55)
$$\Sigma^{(2)}_{\gamma^\dagger\gamma^\dagger}(\vec{k}, ik_n) = \left(-\frac{1}{\hbar}\right)\frac{\xi_{\vec{k}}\Delta_{\vec{k}}}{E_{\vec{k}}} - \left(-\frac{1}{\hbar}\right)^2 \sum_{\vec{q}\vec{Q}\lambda} \left|g(\vec{q},\vec{Q},\lambda)\right|^2 \frac{\xi_{\vec{k}}}{E_{\vec{k}}}\frac{\Delta_{\vec{k}+\vec{q}+\vec{Q}}}{2E_{\vec{k}+\vec{q}+\vec{Q}}}\left[\hbar\, g(ik_n) + \hbar\, g(-ik_n)\right],$$

where the function $g(ik_n)$ is given by eqs. (C.33). Through analytic continuation to the real energy axis, we get the retarded self–energy, $\Sigma^{ret}_{\gamma^\dagger\gamma^\dagger}(\vec{k}, E)$. We replace factors if ik_n in the self–energy expressions with $E + i\delta$, where $\delta \ll 1$ and positive. The thermal functions $g(ik_n)$ will then have real and imaginary parts given by the identity

(C.56)
$$\frac{1}{x \pm i\delta} = \mathcal{P}\frac{1}{x} \mp i\pi\delta(x),$$

where $\mathcal{P}$ indicates the principal value. The retarded version of $g(ik_n)$ is given by

(C.57)
$$\hbar\, g^{ret}(\pm E) = \frac{n_{\vec{q}\lambda} + f_{\vec{k}+\vec{q}+\vec{Q}}}{\pm\hbar^{-1}E + \omega_{\vec{q}\lambda} - \hbar^{-1}E_{\vec{k}+\vec{q}+\vec{Q}} \pm i\delta} + \frac{1 + n_{\vec{q}\lambda} - f_{\vec{k}+\vec{q}+\vec{Q}}}{\pm\hbar^{-1}E - \omega_{\vec{q}\lambda} - \hbar^{-1}E_{\vec{k}+\vec{q}+\vec{Q}} \pm i\delta}.$$

For the real part we find

(C.58)
$$\Re\left(\hbar\, g^{ret}(\pm E)\right) = \mathcal{P}\left[\frac{n_{\vec{q}\lambda} + f_{\vec{k}+\vec{q}+\vec{Q}}}{\pm\hbar^{-1}E + \omega_{\vec{q}\lambda} - \hbar^{-1}E_{\vec{k}+\vec{q}+\vec{Q}}} + \frac{1 + n_{\vec{q}\lambda} - f_{\vec{k}+\vec{q}+\vec{Q}}}{\pm\hbar^{-1}E - \omega_{\vec{q}\lambda} - \hbar^{-1}E_{\vec{k}+\vec{q}+\vec{Q}}}\right],$$

and for the imaginary part

(C.59)
$$\begin{aligned}\Im\left(\hbar\, g^{ret}(\pm E)\right) &= \mp\pi\left[n_{\vec{q}\lambda} + f_{\vec{k}+\vec{q}+\vec{Q}}\right]\delta(\pm\hbar^{-1}E + \omega_{\vec{q}\lambda} - \hbar^{-1}E_{\vec{k}+\vec{q}+\vec{Q}}) \\ &\quad \mp\pi\left[1 + n_{\vec{q}\lambda} - f_{\vec{k}+\vec{q}+\vec{Q}}\right]\delta(\pm\hbar^{-1}E - \omega_{\vec{q}\lambda} - \hbar^{-1}E_{\vec{k}+\vec{q}+\vec{Q}}).\end{aligned}$$

C.2 In the Normal State

The S–Matrix expansion of the electron creation and annihilation operators, $c_{\vec{k}\sigma}$ and $c^{\dagger}_{\vec{k}\sigma}$, is given by

$$\begin{aligned}\mathcal{G}(\vec{k}\sigma,\tau_2-\tau_1) &= -\sum_{n=0}^{\infty}\left(-\frac{1}{\hbar}\right)^n\int_0^{\hbar\beta}d\tau_1'\cdots d\tau_n' \\ &\times\left\langle T_\tau\left[c_{\vec{k}\sigma}(\tau_2)\,c^{\dagger}_{\vec{k}\sigma}(\tau_1)\,\mathcal{V}(\tau_1')\,\mathcal{V}(\tau_2')\cdots\mathcal{V}(\tau_n')\right]\right\rangle_{\text{different connected}},\end{aligned} \tag{C.60}$$

where σ indicates the spin. The interaction Hamiltonian is given by eqs. (2.1.26) and (2.1.29),

$$\mathcal{H}=\mathcal{H}_0+\mathcal{H}_{ep}^{(0)}+\mathcal{H}_{ep}^{(1)}+\mathcal{H}_{ep}^{(2)}. \tag{C.61}$$

We are only interested in expanding up to second order in the electron phonon interaction. The term $\mathcal{H}_{ep}^{(1)}$ is first order in the interaction, the term $\mathcal{H}_{ep}^{(2)}$ is second order. In zeroth order the S–Matrix expansion is given by the unperturbed single particle Greens function. In first order there are two contributions, namely

$$\mathcal{G}^{(1)}(\vec{k}\sigma,\tau_2-\tau_1)=-\left(\frac{-1}{\hbar}\right)\int_0^{\hbar\beta}d\tau_1'\;\left\langle T_\tau\left[c_{\vec{k}\sigma}(\tau_2)c^{\dagger}_{\vec{k}\sigma}(\tau_1)\left\{\mathcal{H}_{ep}^{(0)}(\tau_1')+\mathcal{H}_{ep}^{(2)}(\tau_1')\right\}\right]\right\rangle, \tag{C.62}$$

which are given by

$$\begin{aligned}\mathcal{G}^{(1)}(\vec{k}\sigma,\tau_2-\tau_1)=-\left(\frac{-1}{\hbar}\right)\int_0^{\hbar\beta}d\tau_1'\;\Bigg\langle T_\tau\Bigg[&c_{\vec{k}\sigma}(\tau_2)c^{\dagger}_{\vec{k}\sigma}(\tau_1)\sum_{\kappa\vec{Q}}U(\vec{Q})c^{\dagger}_{\kappa+\vec{Q}}c_\kappa \\ &+\frac{1}{2}\sum_{\kappa}\sum_{\vec{q}\vec{q}'\vec{Q}}\sum_{\lambda\lambda'}h(\vec{q},\vec{q}',\vec{Q},\lambda,\lambda')A_{\vec{q}\lambda}(\tau_1')A_{\vec{q}'\lambda'}(\tau_1')c^{\dagger}_{\kappa+\vec{q}+\vec{q}'+\vec{Q}}(\tau_1')c_\kappa(\tau_1')\Bigg]\Bigg\rangle.\end{aligned} \tag{C.63}$$

Because of momentum conservation at the vertex, we need to set $\vec{q} = -\vec{q}'$, $\vec{Q} = 0$, and $\lambda = \lambda'$ in both contributions. A subsequent Fourier transformation to Matsubara frequencies yields

$$\Sigma^{(1)}(\vec{k}\sigma, ik_n) = \frac{1}{\hbar}U(0) - \frac{1}{2\hbar}\sum_{\vec{q}\lambda} h(\vec{q}, -\vec{q}, 0, \lambda, \lambda)\frac{1}{\hbar\beta}\sum_{iq_n}\mathcal{D}^0(\vec{q}\lambda, iq_n). \tag{C.64}$$

The sum $\sum_{iq_n}$ can easily be done and yields,

$$\frac{1}{\hbar\beta}\sum_{iq_n}\mathcal{D}^0(\vec{q}\lambda, iq_n) = -2\left(n_{\vec{q}} + \frac{1}{2}\right). \tag{C.65}$$

The first order contribution to the single–particle self–energy therefore is given by

$$\Sigma^{(1)}(\vec{k}\sigma, ik_n) = \frac{1}{\hbar}U(0) + \frac{1}{\hbar}\sum_{\vec{q}\lambda} h(\vec{q}, -\vec{q}, 0, \lambda, \lambda)\left(n_{\vec{q}} + \frac{1}{2}\right). \tag{C.66}$$

The matrix elements, $h(\vec{q}, -\vec{q}, 0, \lambda, \lambda)$, vanish and we write,

$$\Sigma^{(1)}(\vec{k}\sigma, ik_n) = \frac{U(0)}{\hbar}. \tag{C.67}$$

In second order, we will have to consider all three terms in eq. (C.61). The second order term in the S–Matrix expansion is given by

$$\begin{aligned}\mathcal{G}^{(2)}(\vec{k}\sigma, \tau_2 - \tau_1) &= -\left(-\frac{1}{\hbar}\right)^2\frac{1}{2}\int_0^{\hbar\beta} d\tau_1' d\tau_2' \left\langle T_\tau\left[c_{\vec{k}\sigma}(\tau_2)c^\dagger_{\vec{k}\sigma}(\tau_1)\right.\right. \\ &\left.\left. \times\left\{\mathcal{H}^{(0)}_{ep}(\tau_1') + \mathcal{H}^{(1)}_{ep}(\tau_1') + \mathcal{H}^{(2)}_{ep}(\tau_1')\right\}\left\{\mathcal{H}^{(0)}_{ep}(\tau_2') + \mathcal{H}^{(1)}_{ep}(\tau_2') + \mathcal{H}^{(2)}_{ep}(\tau_2')\right\}\right]\right\rangle.\end{aligned} \tag{C.68}$$

We added a factor of 1/2 to the Greens function since not all of the above contributions are "different" in the sense of eq. (C.60). Multiplying out the terms in the curly brackets will give us three terms, but as it turns out, two of them are identical and cancel with the additional factor of 1/2 we added. The three terms are $\mathcal{H}_{ep}^{(0)}(\tau_1')\mathcal{H}_{ep}^{(2)}(\tau_2')$, $\mathcal{H}_{ep}^{(1)}(\tau_1')\mathcal{H}_{ep}^{(1)}(\tau_2')$, and $\mathcal{H}_{ep}^{(2)}(\tau_1')\mathcal{H}_{ep}^{(0)}(\tau_2')$. The identical pair is the first and the last term. We will calculate the two terms now. Since there are two possible time–orderings for each of the two contributions, another factor of 2 needs to be added. The middle term is given by

$$\begin{aligned}\mathcal{G}_A^{(2)}(\vec{k}\sigma,\tau_2-\tau_1) &= -\left(-\frac{1}{\hbar}\right)^2\int_0^{\hbar\beta}d\tau_1'd\tau_2'\ \Big\langle T_\tau\Big[c_{\vec{k}\sigma}(\tau_2)c_{\vec{k}\sigma}^\dagger(\tau_1)\\ &\quad\times\sum_{\vec{p}}\sum_{\vec{q}\vec{Q}\lambda}g(\vec{q},\vec{Q},\lambda)A_{\vec{q}\lambda}(\tau_1')c_{\vec{p}+\vec{q}+\vec{Q}\sigma}(\tau_1')c_{\vec{p}\sigma}^\dagger(\tau_1')\\ &\quad\times\sum_{\vec{p}'}\sum_{\vec{q}'\vec{Q}'\lambda'}g(\vec{q}',\vec{Q}',\lambda')A_{\vec{q}'\lambda'}(\tau_2')c_{\vec{p}'+\vec{q}'+\vec{Q}'\sigma'}(\tau_2')c_{\vec{p}'\sigma'}^\dagger(\tau_2')\Big]\Big\rangle,\end{aligned}\tag{C.69}$$

where the factor of 1/2 has already been canceled. Contracting the operators requires an even number of permutations. The Fourier transform of this expression is given by

$$\mathcal{G}_A^{(2)}(\vec{k}\sigma,ik_n)=-\left(\frac{1}{\hbar}\right)^2\sum_{\vec{q}\vec{Q}\lambda}\Big|g(\vec{q},\vec{Q},\lambda)\Big|^2\mathcal{G}^0(\vec{k}\sigma,ik_n)^2\frac{1}{\hbar\beta}\sum_{iq_n}\mathcal{D}^0(\vec{q}\lambda,iq_n)\mathcal{G}^0(\vec{k}+\vec{q}+\vec{Q}\sigma,ik_n+iq_n).\tag{C.70}$$

With the result from eq. (C.32) we find for the self–energy

$$\Sigma_A^{(2)}(\vec{k}\sigma,ik_n)=\left(\frac{1}{\hbar}\right)^2\sum_{\vec{q}\vec{Q}\lambda}\Big|g(\vec{q},\vec{Q},\lambda)\Big|^2\left\{\frac{n_{\vec{q}\lambda}+f_{\vec{k}+\vec{q}+\vec{Q}}}{ik_n+\omega_{\vec{q}\lambda}-\hbar^{-1}\xi_{\vec{k}\vec{q}\vec{Q}}}+\frac{1+n_{\vec{q}\lambda}-f_{\vec{k}+\vec{q}+\vec{Q}}}{ik_n-\omega_{\vec{q}\lambda}-\hbar^{-1}\xi_{\vec{k}\vec{q}\vec{Q}}}\right\}.\tag{C.71}$$

The other term written out is given by

$$\begin{aligned}\mathcal{G}_B^{(2)}(\vec{k}\sigma,\tau_2-\tau_1) = &-\left(-\frac{1}{\hbar}\right)^2\int_0^{\hbar\beta} d\tau_1' d\tau_2' \ \Big\langle T_\tau\Big[c_{\vec{k}\sigma}(\tau_2)c^\dagger_{\vec{k}\sigma}(\tau_1)\\ &\times 2\sum_{\vec{p}\vec{Q}\sigma} U(\vec{Q})c^\dagger_{\vec{p}+\vec{Q}\sigma}(\tau_1')c_{\vec{p}\sigma}(\tau_1')\\ &\times\frac{1}{2}\sum_{\vec{p}'\sigma}\sum_{\vec{q}\vec{q}'\vec{Q}'}\sum_{\lambda\lambda'} h(\vec{q},\vec{q}',\vec{Q},\lambda,\lambda')A_{\vec{q}\lambda}(\tau_2')A_{\vec{q}'\lambda'}(\tau_2')c^\dagger_{\vec{p}'+\vec{q}+\vec{q}'+\vec{Q}'\sigma}(\tau_2')c_{\vec{p}'\sigma}(\tau_2')\Big]\Big\rangle .\end{aligned} \tag{C.72}$$

Contraction requires an even number of permutations and momentum conservation at the vertices yields,

$$\Sigma_B^{(2)}(\vec{k}\sigma,ik_n) = 2\left(\frac{1}{\hbar}\right)^2\sum_{\vec{q}\vec{Q}\lambda} U(\vec{Q})h(\vec{q},-\vec{q},\vec{Q},\lambda,\lambda)\mathcal{G}^0(\vec{k}\sigma,ik_n)\left[\frac{1}{2}+n_{\vec{q}\lambda}\right]. \tag{C.73}$$

The self energy up in second order is therefore given by

$$\begin{aligned}\Sigma^{(2)}(\vec{k}\sigma,ik_n) = &\left(\frac{1}{\hbar}\right)^2\sum_{\vec{q}\vec{Q}\lambda}\Bigg[2\ U(\vec{Q})h(\vec{q},-\vec{q},\vec{Q},\lambda,\lambda)\mathcal{G}^0(\vec{k}+\vec{Q}\sigma,ik_n)\left[\frac{1}{2}+n_{\vec{q}\lambda}\right]\\ &+\Big|g(\vec{q},\vec{Q},\lambda)\Big|^2\left\{\frac{n_{\vec{q}\lambda}+f_{\vec{k}+\vec{q}+\vec{Q}}}{ik_n+\omega_{\vec{q}\lambda}-\hbar^{-1}\xi_{\vec{k}\vec{q}\vec{Q}}}+\frac{1+n_{\vec{q}\lambda}-f_{\vec{k}+\vec{q}+\vec{Q}}}{ik_n-\omega_{\vec{q}\lambda}-\hbar^{-1}\xi_{\vec{k}\vec{q}\vec{Q}}}\right\}\Bigg].\end{aligned} \tag{C.74}$$

Appendix D

Calculation of $M_{ij}(\omega)$ to higher orders in g^2

The memory function is defined by

$$M(\omega) = \frac{\omega\chi(\omega)}{\chi(0) - \chi(\omega)}, \tag{D.1}$$

where

$$\chi(\omega) = \langle\langle j; j\rangle\rangle = \frac{\langle\langle [j,H]\,;[j,H]\rangle\rangle_\omega - \langle\langle [j,H]\,;[j,H]\rangle\rangle_{\omega=0}}{\omega^2}. \tag{D.2}$$

The assumption is that $M(\omega)$ can be calculated by expanding $\chi(\omega)$ in powers of g^2. The equations for the real and imaginary parts are,

$$\begin{aligned} \Re\left(M(\omega)\right) &= \omega\frac{\Re\left(\chi(\omega)\right)\left[\chi(0) - \Re\left(\chi(\omega)\right)\right] - \Im\left(\chi(\omega)\right)^2}{\left[\chi(0) - \Re\left(\chi(\omega)\right)\right]^2 + \Im\left(\chi(\omega)\right)^2} \\ \Im\left(M(\omega)\right) &= \omega\frac{\Im\left(\chi(\omega)\right)}{\left[1 - \Im\left(\chi(\omega)\right)\right]^2 + \Im\left(\chi(\omega)\right)^2}. \end{aligned} \tag{D.3}$$

Denoting the contributions to $M(\omega)$ and $\chi(\omega)$ of order g^k by $M_k(\omega)$ and $\chi_k(\omega)$, the leading term is

$$\Re\left(M_2(\omega)\right) + i\Im\left(M_2(\omega)\right) = \frac{\omega}{\chi(0)}\left[\Re\left(\chi_2'(\omega)\right) + i\Im\left(\chi_2(\omega)\right)\right]. \tag{D.4}$$

Explicit expressions were given in the text for the real and imaginary parts of $M_2(\omega)$. This can be regarded as an integration over non–interacting $\gamma^\dagger\gamma$ propagators, coherence factors and matrix elements.

The contributions of order g^4 are

$$\begin{aligned}
\Re\left(M_4(\omega)\right) &= \omega\left[\frac{\Re\left(\chi_4(\omega)\right)}{\chi(0)} + \left(\frac{\Re\left(\chi_2(\omega)\right)^2 - \Im\left(\chi_2(\omega)\right)^2}{\chi^2(0)}\right)\right] \\
\Im\left(M_4(\omega)\right) &= \omega\left[\frac{\Im\left(\chi_4(\omega)\right)}{\chi(0)} + 2\frac{\Im\left(\chi_2(\omega)\right)\Re\left(\chi_2(\omega)\right)}{\chi^2(0)}\right].
\end{aligned} \tag{D.5}$$

$\chi_4(\omega)$ can be thought of as made up of self–energy terms, which dress the free propagators in $\chi_2(\omega)$, and vertex corrections. Equations for higher order contributions to $M(\omega)$ beyond $\mathcal{O}(g^4)$ can be easily derived with the same division between self–energy and vertex corrections.

Considering the contribution to the correlation which survives as $T \to 0$, explicit expression for the $\chi_k(\omega)$ are found by expanding the time evolution operator in the correlation function.

$$\begin{aligned}
\langle\langle [j,H]\,;[j,H]\rangle\rangle_\omega = -i\int_0^\infty PT\; e^{i\omega t} \sum_{\vec{k}_1,\vec{q}_1,\vec{k}_2,\vec{q}_2} \mathcal{M}^*(\vec{k}_1,\vec{q}_1\lambda)\mathcal{M}(\vec{k}_2,\vec{q}_2\lambda) \\
\times \Big\langle\Big\langle T\, e^{i\int_{-\infty}^{\infty} dt'\; \mathcal{H}_{ep}} \Big(B_{\vec{q}_1}(t)B_{\vec{q}_2}(0)c^\dagger_{\vec{k}_1+\vec{q}_1}(t)c_{\vec{k}_1}(t)c^\dagger_{\vec{k}_2+\vec{q}_2}(0)c_{\vec{k}_2}(0) \\
- B_{\vec{q}_2}(0)B_{\vec{q}_1}(t)c^\dagger_{\vec{k}_2+\vec{q}_2}(0)c_{\vec{k}_2}(0)c^\dagger_{\vec{k}_1+\vec{q}_1}(t)c_{\vec{k}_1}(t)\Big)\Big\rangle\Big\rangle,
\end{aligned} \tag{D.6}$$

where $B_{\vec{q}}(t) = b_{\vec{q}}(t) + b^\dagger_{-\vec{q}}(t)$.

First considering the lowest order $T\; e^{i\int dt'\; \mathcal{H}_{ep}} = 1$ the correlation function to order g^2 is

$$\begin{aligned}
\langle\langle [j,H]\,;[j,H]\rangle\rangle^{(S)}_\omega = -i\int_0^\infty dt\; e^{i\omega t} \sum_{\vec{k},\vec{q}} \left[u^2_{\vec{k}}v^2_{\vec{k}+\vec{q}} + v^2_{\vec{k}}u^2_{\vec{k}+\vec{q}} - 2u_{\vec{k}}v_{\vec{k}}u_{\vec{k}+\vec{q}}u_{\vec{k}+\vec{q}}\right]\left|\mathcal{M}(\vec{k},\vec{\lambda})\right|^2 \\
\times \left(e^{-i\omega_{\vec{q}}t}G^>_{\gamma^\dagger\gamma}(-\vec{k}+\vec{q},t)G^>_{\gamma^\dagger\gamma}(\vec{k},t) - e^{i\omega_{\vec{q}}t}G^>_{\gamma^\dagger\gamma}(-\vec{k}+\vec{q},-t)G^>_{\gamma^\dagger\gamma}(\vec{k},-t)\right),
\end{aligned} \tag{D.7}$$

where $G^{>}_{\gamma^\dagger\gamma}(\vec{k},t) = i\left\langle \gamma_{\vec{k}}(t)\gamma^\dagger_{\vec{k}}(0)\right\rangle = ie^{-iE_{\vec{k}}t}$ with $t>0$.

Integrating over t gives $\langle\langle [j,H]\,;[j,H]\rangle\rangle^{(S)}_{\omega}$ and the expression for $\chi_2(\omega)$ given in Chapter 4. The correlation function to order g^4 is

$$\begin{aligned}\langle\langle [j,H]\,;[j,H]\rangle\rangle_{\omega} = i\int_0^\infty dt\ e^{i\omega t} \sum_{\vec{k}_1,\vec{q}_1,\vec{k}_2,\vec{q}_2} \mathcal{M}^*(\vec{k}_1,\vec{q}_1\lambda)\mathcal{M}(\vec{k}_2,\vec{q}_2\lambda) \\ \times\left\langle\left\langle T\left[\int_{-\infty}^{\infty} dt_1\ \mathcal{H}_{ep}(t_1)\int_{-\infty}^{\infty} dt_2\ \mathcal{H}_{ep}(t_2)\left(B_{\vec{q}_1}(t)B_{\vec{q}_2}(0)c^\dagger_{\vec{k}_1+\vec{q}_1}(t)c_{\vec{k}_1}(t)c^\dagger_{\vec{k}_2+\vec{q}_2}(0)c_{\vec{k}_2}(0)\right.\right.\right. \\ \left.\left.\left. - B_{\vec{q}_2}(0)B_{\vec{q}_1}(t)c^\dagger_{\vec{k}_2+\vec{q}_2}(0)c_{\vec{k}_2}(0)c^\dagger_{\vec{k}_1+\vec{q}_1}(t)c_{\vec{k}_1}(t)\right)\right]\right\rangle\right\rangle. \end{aligned} \tag{D.8}$$

This term generates a large number of contributions because of the large number of contractions which can be considered as either self–energy or vertex corrections. Since the pole at $\omega=0$ in $\sigma(\omega)$ has been taken care of explicitly in the memory function formalism the vertex corrections should not introduce additional qualitative effects.

Collecting the self–energy corrections in each order of g^2 the unrenormalized propagators in $\chi_2(\omega)$ can be replaced with fully renormalized ones and the correlation to all orders can be written as

$$\begin{aligned}\langle\langle [j,H]\,;[j,H]\rangle\rangle^{(S)}_{\omega} = \sum_{\vec{k},\vec{q}}\left[u^2_{\vec{k}}v^2_{\vec{k}+\vec{q}} + v^2_{\vec{k}}u^2_{\vec{k}+\vec{q}} - 2u_{\vec{k}}v_{\vec{k}}u_{\vec{k}+\vec{q}}u_{\vec{k}+\vec{q}}\right]\left|\tilde{\mathcal{M}}(\vec{k},\vec{q},\lambda)\right|^2 \\ \times\int dz_1\int dz_2\ A(\vec{k},z_1)A(-\vec{k}+\vec{q},z_2)\frac{z_1+z_2+\omega_{\vec{q}}}{\omega^2-(z_1+z_2+\omega_{\vec{q}})^2}, \end{aligned} \tag{D.9}$$

where $A(\vec{k},z)$ is the spectral density of quasiparticle propagator and $\left|\tilde{\mathcal{M}}(\vec{k},\vec{q},\lambda)\right|^2$ includes all vertex corrections. Quantitatively accurate evaluations of $M(\omega)$ beyond order g^2 will require the evaluation of the vertex corrections which will be difficult if the experimentally determined details of the Fermi surface are to be included.

Bibliography

A. A. Abrikosov, L. P. Gorkov, and I. E. Dzyaloshinskii. "Methods of Quantum Field Theory in Statistical Physics". Prentic–Hall, Inc., Englewood Cliffs, NJ, 1963.

P. B. Allen. *Phys. Rev. B*, **3**, 305, 1971.

J. R. Anderson and A. V. Gold. *Phys. Rev.*, **139**, A1459, 1965.

A. O. E. Animalu and V. Heine. *Phil. Mag.*, **12**, 1249, 1965.

N. W. Ashcroft and J. W. Wilkins. *Phys. Lett.*, **14**, 285, 1965.

Neil W. Ashcroft and N. David Mermin. "Solid State Physics". Saunders College, 1976.

B. J. Austin, V. Heine, and L. J. Sham. *Phys. Rev.*, **127**, 276, 1962.

J. Bardeen, L. N. Cooper, and J. R. Schrieffer. *Phys. Rev.*, **105**, 162, 1957a.

J. Bardeen, L. N. Cooper, and J. R. Schrieffer. *Phys. Rev.*, **108**, 1175, 1957b.

N. N. Bogoliubov. *Nuovo Cimento*, **7**, 794, 1958.

N. N. Bogoliubov, V. V. Tolmachev, and D. V. Shirkov. "A New Method in the Theory of Superconductivity". Consultants Bureau, New York, 1959.

M. Born and K. Huang. "Dynamical Theory of Crystal Lattices". Clarendon Press, Oxford, 1954.

G. Brändli. *Phys. Rev. Lett.*, **28**, 159, 1972.

G. Brändli and A. J. Sievers. *Phys. Rev. B*, **5**, 3550, 1972.

S. L. Bud'ko, G. Lapertot, C. Petrovic, C. E. Cunningham, N. Anderson, and P. C. Canfield. *Phys. Rev. Lett.*, **86**, 1877, 2001.

A. Chainani, T. Yokoya, T. Kiss, and S. Shin. *Phys. Rev. Lett.*, **85**, 1966, 2000.

R. G. Chambers. *Proc. Roy. Soc. (London). Series A*, **215**, 481, 1952.

D. Coffey. *Europhys. Lett.*, **40**(5), 563, 1997.

D. Coffey. *Physica C*, **305**, 139, 1998.

E. R. Cowley. *Sol. State Comm.*, **15**, 587, 1974a.

E. R. Cowley. *Can. J. Phys.*, **52**, 1714, 1974b.

D. L. Cox, C. Tannous, and J. W. Wilkins. *Phys. Rev. B*, **33**, 2132, 1986.

Andrea Damascelli, Zahid Hussain, and Zhi-Xun Shen. "Angle-resolved photoemission studies of the cuprate superconductors". *Rev. Mod. Phys.*, **75**, 473, 2003.

F. Doğan and F. Marsiglio. *cond-mat*, **0309075**, 2003.

S. Doniach and S. Engelsberg. *Phys. Rev. Lett.*, **17**, 1750, 1966.

G. M. Eliashberg. *Zh. Eksp. Teor. Fiz.*, **38**, 966, 1960a.

G. M. Eliashberg. *Soviet Phys. – JETP*, **11**, 696, 1960b.

B. Farnworth. "Phonon–Induced Far Infrared Absorption in Superconductors". PhD thesis, McMaster University (Canada), 1976.

B. Farnworth and T. Timusk. *Phys. Rev. B*, **10**, 2799, 1974.

B. Farnworth and T. Timusk. *Phys. Rev. B*, **14**, 5119, 1976.

Alexander L. Fetter and John Dirk Walecka. "Quantum Theory of Many–Particle Systems". McGraw–Hill Inc, 1971.

Richard P. Feynman. "Statistical Mechanics". Addison–Wesley, Reading, Mass., 1972.

D. Forster. "Hydrodynamic fluctuations, broken symmetry, and correlation functions". Addison Wesley Publishing Company Inc., Advanced Book Program, 1983.

H. Fröhlich. *Phys. Rev.*, **79**, 845, 1950.

A. Gavini and T. Timusk. *Phys. Rev. B*, **3**, 1049, 1971.

Karl A. Geschneidner. "Solid State Physics: Advances in Research and Applications", volume 16. Academic Press, New York, 1964.

W. Götze and P. Wölfle. *Phys. Rev. B*, **6**, 1226, 1972.

G. Grimvall. *Physica Scripta*, **14**, 63, 1976.

G. Grimvall. "The Electron–Phonon Interaction in Metals". North–Holland Publishing Company, 1981.

Walter A. Harrison. *Phys. Rev.*, **118**, 1182, 1960.

Walter A. Harrison. "Pseudopotentials in the Theory of Metals". Benjamin, Reading, Mass., 1966.

V. Heine and I. V. Abarenkov. *Philos. Mag.*, **9**, 451, 1964.

V. Heine and I. V. Abarenkov. *Philos. Mag.*, **12**, 529, 1965.

C. Herring. *Phys. Rev.*, **57**, 1169, 1940.

T. Holstein. *Phys. Rev.*, **88**, 1427, 1952.

T. Holstein. *Ann. Phys.*, **29**, 410, 1964.

H. Jones. "The Theory of Brilluoin Zones and Electronic States in Crystals". North-Holland Publishing Company, 2nd edition, 1975.

R. R. Joyce and P. L. Richards. *Phys. Rev. Lett.*, **24**, 1007, 1970.

H. Kammerlingh-Onnes. *Comm. Phys. Lab. Univ. Leiden*, **119, 120, 122**, 1911.

J. G. Kirkwood. *Phys. Rev.*, **44**, 31, 1933.

J. Kortus, I. I. Mazin, K. D. Belashchenko, V. P. Antropov, and L. L. Boyer. *Phys. Rev. Lett.*, **86**, 4656, 2001.

G. P. Lepage. "A new algorithm for adaptive multidimensional integration". *Journal of Computational Physics*, **27**, 192–203, 1978.

G. P. Lepage. "Vegas: An adaptive multi-dimensional integration program". *Cornell preprint CLNS*, , 447, 1980.

J. K. Lindhard. *Dan. Vidensk. Selsk. Mat. Fys. Medd.*, **28**, 8, 1954.

Amy Y. Liu, I. I. Mazin, and Jens Kortus. *Phys. Rev. Lett.*, **87**, 087005, 2001.

F. London. *Phys. Rev.*, **47**, 562, 1948.

Gerald D. Mahan. "Many–Particle Physics". Plenum Press, New York, 1990.

D. C. Mattis and J. Bardeen. *Phys. Rev.*, **111**, 412, 1958.

E. Maxwell. *Phys. Rev.*, **78**, 477, 1950.

A. B. Migdal. *JETP*, **7**, 996, 1958.

E. Montroll. "Statictical Mechanics of Irreveribility", volume 3, p. 221 of *Lectures in Theoretical Physics*. Interscience, New York, 1961.

K. A. Müller and J. G. Bednorz. "The discovery of a class of high-temperature superconductors". *Science*, **237**, 1133, 1987.

J. C. Phillips and L. Kleinman. *Phys. Rev.*, **116**, 287,880, 1959.

Robert Piessens and Maria Branders. *Math. Comp.*, **28**, 135, 1974a.

Robert Piessens and Maria Branders. *Math. Comp.*, **28**, 344, 1974b.

A. B. Pippard. "Advances in Electronics and Electron Physics", volume 5. Academic Press, 1954.

R. E. Prange and L. P. Kadanoff. *Phys. Rev.*, **134**, A566, 1964.

G. E. Reuter and E. H. Sondheimer. *Proc. Roy. Soc. (London) Series A*, **195**, 336, 1948.

C. A. Reynolds, B. Serin, W. H. Wright, and L. B. Nesbitt. *Phys. Rev.*, **78**, 487, 1950.

G. Rubio-Bollinger, H. Suderow, and S. Vieira. *Phys. Rev. Lett.*, **86**, 5582, 2001.

Douglas J. Scalapino. "Superconductivity", volume 1. Marcel Dekker, Inc., 1969.

H. Scher. *Phys. Rev. Lett.*, **25**, 759, 1970.

Herbert Schmidt, J. F. Zasadzinski, K. E. Gray, and D. G. Hinks. *Phys. Rev. B*, **63**, 220504(R), 2001.

J. R. Schrieffer, D. J. Scalapino, and J. W. Wilkins. *Phys. Rev. Lett.*, **10**, 336, 1963.

R. Stedman, L. Almqvist, and G. Nillson. *Phys. Rev.*, **162**, 549, 1967.

M. Tinkham. "Introduction to Superconductivity". Robert E. Krieger Publishing Company, Florida, 1980.

Michael Tinkham. "Group Theory and Quantum Mechanics". McGraw-Hill Book Company, 1964.

J. Valatin. *Nuovo Cimento*, **7**, 843, 1958.

Duane C. Wallace. *Phys. Rev. E*, **56**, 1981, 1997.

Duane C. Wallace. "Thermodynamics of Crystals". Dover Publications Inc., 1998.

D. N. Zubarev. *Usp. Fiz. Nauk*, **71**, 71, 1960.

R. Zwanzig. "Statistical Mechanics of Irreveribility", volume 3, p. 106 of *Lectures in Theoretical Physics*. Interscience, New York, 1961.

R. W. Zwanzig. *Phys. Rev.*, **106**, 13, 1957.